Modeling, Simulation, and Optimization of Cancer Chemotherapies

Michael Engelhart

RUPRECHT-KARLS-UNIVERSITÄT HEIDELBERG
FAKULTÄT FÜR MATHEMATIK UND INFORMATIK

Modeling, Simulation, and Optimization of Cancer Chemotherapies

Diplomarbeit

vorgelegt von cand. math. Michael Engelhart

im August 2009

betreut durch Dr. Sebastian Sager

Abstract

It is still an open question, even among physicians and oncologists, how much potential good timing of a chemotherapy yields. Systematic approaches from scientific computing can provide additional insight, even though available mathematical models are far from an exact description of reality due to patient-, cancer-, and therapy-specific components. In this diploma thesis, different mathematical models of cancer and cancer chemotherapy presented in the literature are investigated with scientific computing methods.

We present five models based on ordinary differential equations which all contain some kind of drug treatment, such as chemotherapy, immunotherapy, anti-angiogenic therapy and combinations of these. Optimal control problem formulations corresponding to these models are presented, proposed, and compared.

The optimal control problems are solved numerically with Bock's direct multiple shooting method, which is explained in the work. As the resulting optimal controls may not be realizable in medical practice, also mixed-integer optimal control problems are considered. Mixed-integer solutions are computed with the MS MINTOC approach. To overcome problems with chattering behavior of optimal solutions, a new approach is introduced, where a mixed-integer linear program is solved to approximate the continuous control with a limited number of switches.

Optimal control results are presented for six different parameter sets. Four of them have been solved to optimality for the first time. Where no optimal control problems have been published yet, we formulate some. In particular, we show that an optimally controlled therapy can be the reason for the difference between a growing and a totally vanishing tumor in a comparison to standard schemes and untreated or wrongly treated tumors. We consider different objective functions and show that the obvious one, a minimization of the tumor at the end time of a treatment, is not always adequate. The new mixed-integer method is tested and it is shown that this technique may provide practicable treatments. The continuous treatments are also compared to the more practicable mixed-integer ones.

The work shows that there is a high potential for the optimization of chemotherapies, although the current models have not yet been appropriate for taking the optimal therapies into medical practice. Here, patient- and tumor-specific parameter estimation on well-understood mathematical models, together with an intensified collaboration of mathematicians, biologists, and physicians could lead to significant improvements.

Zusammenfassung

Auch unter Medizinern und Onkologen ist es nach wie vor eine offene Frage, wie viel Potential im richtigen Timing von Chemotherapien steckt. Systematische Ansätze aus dem wissenschaftlichen Rechnen können hier zusätzliche Einsichten liefern, auch wenn die vorhandenen mathematischen Modelle aufgrund von Patienten-, Krebs- und Therapie-spezifischen Komponenten noch weit von einer akkuraten Beschreibung der Realität entfernt sind. In dieser Diplomarbeit werden verschiedene mathematische Modelle aus der Literatur für Krebs und die zugehörige Chemotherapie mit Methoden des wissenschaftlichen Rechnens untersucht.

Wir stellen fünf verschiedene Modelle mit gewöhnlichen Differentialgleichungen vor, in denen allen eine Art medikamentöser Behandlung wie Chemotherapie, Immuntherapie, Anti-Angiogenese oder eine Kombination aus diesen enthalten ist. Vorhandene Optimalsteuerungsprobleme zu diesen Modellen werden dargestellt.

Die Optimalsteuerungsprobleme werden mit Bocks direkter Mehrzielmethode gelöst, die in dieser Arbeit erläutert wird. Da die resultierenden Optimalsteuerungen möglicherweise in der medizinischen Praxis nicht umsetzbar sind, betrachten wir auch gemischt-ganzzahlige Optimalsteuerungsprobleme. Die entsprechenden Steuerungen werden mit dem in der Arbeit beschriebenen MS MINTOC Algorithmus berechnet. Hierbei wird eine neue Heuristik eingeführt, in der ein gemischt-ganzzahliges lineares Programm gelöst wird, um die kontinuierliche Steuerung mit einer beschränkten Anzahl an Schaltvorgängen zu approximieren.

Ergebnisse der Optimalsteuerung werden für sechs verschiedene Parametersätze vorgestellt, wobei für vier davon erstmals Optimallösungen berechnet wurden. Sofern es bisher keine publizierten Optimalsteuerungsprobleme zu den Parametersätzen bzw. Modellen gibt, formulieren wir solche. Insbesondere zeigen wir, dass eine optimalgesteuerte Therapie zu einem vollständig verschwindenden Tumor führen kann im Gegensatz zu einem wachsenden Tumor bei nicht-optimaler Behandlung, indem die Ergebnisse unter optimalen Steuerungen mit denen unter Standardbehandlungen, sowie falsch oder gar nicht behandelten Tumoren verglichen werden. Wir betrachten verschiedene Zielfunktionen und zeigen dabei, dass die naheliegendste, die Minimierung des Tumors am Ende des Behandlungszeitraums, nicht immer geeignet ist. Unsere neue Heuristik für gemischt-ganzzahlige Probleme wird auf die beschriebenen Modelle angewandt und es wird gezeigt, dass sich mit diesem Verfahren in einigen Szenarien praktikable Therapien ergeben. Die kontinuierlichen Behandlungen werden ebenfalls mit den praxisnäheren gemischt-ganzzahligen Gegenstücken verglichen.

Die Arbeit zeigt, dass es ein möglicherweise großes Potential für die Optimierung von Chemotherapien gibt, wenn auch die derzeitigen Modelle es noch nicht erlauben, die mit ihnen errechneten optimalgesteuerten Therapien in der Realität anzuwenden. Hier könnte patienten- und tumorspezifische Parameterschätzung auf gut verstandenen mathematischen Modellen, zusammen mit einer intensiven Zusammenarbeit zwischen Mathematikern, Biologen und Medizinern, zu signifikanten Verbesserungen führen.

Acknowledgements

Notation

Symbols

$\mathbb{R}$ real numbers
$\mathbb{N}$ natural numbers

Names

δ	delta distribution
D	Domain
f	right hand side of an ODE
Φ	objective function, objective function value
Φ_M	mayer term of objective function
Φ_L	lagrangian term of objective function
$\mathcal{G}, \mathcal{G}^k$	time grids
h_k	switching interval lengths
I_i	partial time intervals
n_i, n_e	number of inequality/equality constraints
n_u	number of controls (dimension of control vector)
n_x	number of states (dimension of state vector)
N	maximum number of switches (decomposed MILP)
$p_0, p_1, \ldots$	parameters (in objective function)
p	parameter vector, different parameter sets
q_i	continuous discretized control value
r_i, r_e	inequality/equality boundary conditions
s	different initial value sets
s_i	additional initial values at multiple shooting nodes
s_j	slack variables
t	time, different time scenarios
t_0	start time (of a problem, treatment, ...)
t_f	end time
$[t_0, t_f]$	time interval
t^k	step size in SQP method
$\tau_0, \ldots, \tau_m$	time grid points
$\mathcal{T}, \mathcal{T}^k$	trajectories
u	control (vector)
$u_0, u_1, \ldots$	controls
v	binary parameter vector
w	integer or binary control (vector)
w_i	discretized control parameter, integer/binary control value
$x_0, x_1, \ldots$	states
x	state vector
$\dot{x}$	time derivative of x

$\hat{x}_0$	initial value for state vector
Δx^k	step in SQP method

Abbreviations

BDF	backward differentiation formula
DAE	differential algebraic equation
MILP	mixed-integer linear program/problem
MINLP	mixed-integer nonlinear program/problem
MIOC	mixed-integer optimal control
MIOCP	mixed-integer optimal control problem
NLP	nonlinear programming problem
NMPC	nonlinear model predictive control
ODE	ordinary differential equation
QP	quadratic program/problem
SOS1	special ordered set, type 1
SQP	sequential quadratic programming

Different lower an upper case letters, both latin and greek, are used for parameters in the models. In general, these symbols are chosen to be consistent with the corresponding references, if this did not conflict with the overall notation in this work.

Contents

Chapter 1

Introduction

Cancer and Chemotherapy

Today, cancer is one of the major diseases of humanity. In Germany, one in four cases of death is caused by cancer and every year about 400,000 new affections are detected. Whereas the exact causes of cancer have not been fully known until today, there is the consensus that cancer arises from a mutation of genes which are responsible for the correct reproduction of cells. The final result is a malignancy, a tumor, which grows uncontrolled, invasive, and sometimes builds metastases. Thereby, generally all tissues and organs can be affected, although incidence and the chance of a cure vary a lot.

Classic treatments contain the removal by surgery, radiotherapy, and also chemotherapy, which means the admission of drugs which inhibit or stop the growth of tumor cells. A chemotherapy, however, in general affects also non-tumor cells, a negative side effect, which has to be kept under control. Such therapies may be combined with additional medicamentous therapies, like anti-angiogenesis, which has an effect on the blood vessel in the neighbourhood of the tumor, or immunotherapy which aims at a stimulation of the patients' immune system. Particularly for medical treatments such as chemotherapy, immunotherapy, anti-angiogenic therapy, and a combination of them, time and amount of drug admission may be crucial, since the cell populations underly complex processes.

Mathematical Modelling, Simulation, and Optimization

While Scientific Computing has become an indispensable ingredient of research and every-day-practice in robotics and mechanics, chemical engineering, aerospace, transport, and many other areas, the application of numerical methods to find answers to open questions in medicine has not yet been as evolved.

Scientific Computing, and in particular the modeling, simulation, and optimization of processes, is often regarded as the third pillar of science, complementary to theory and experiment. In medicine however, experiments are not so easily reproducable as in mechanics, and the theoretic interpretation of drug influence is not as well understood as e.g. Newton's equations of motion.

Especially the influence of medicaments and drugs is often not fully understood, and of course highly patient-dependent. Hence it cannot be expected that currently available models in ordinary differential equations are a good match to clinical reality. A patient- and tumor-specific parameter estimation on well-understood mathematical models, possibly also taking into account spatial effects, will hopefully lead the way in the future.

This work is meant to be another small step in this direction. The basic mathematical models that have been proposed in the literature over the last years should already capture several important dynamic effects of chemotherapy treatments. Having in mind that the gap between simulated and real-world data will still be large, we focus in this work on

general insights that can already be gained by optimization of available mathematical models. Examples for basic questions are

- What similarities and what differences arise for the different mathematical models? We present five mathematical models for cancer and cancer chemotherapy. Although they all contain some kind of chemotherapy, they differ in the kind of additional treatments and in type and amount of cell types they include. For the five models, there are eight parameter sets. We present optimal control results for six of them, whereas to the best of our knowledge four sets were not solved to optimality before.

- How much potential for the right timing of drug delivery is there? In general the aim of a therapy, no matter what kind, is to *minimize* the tumor size, i.e. the tumor volume or the amount of tumor cells. To answer this question, we consider also therapies which, with a fixed amount of drugs, *maximize* the tumor size on a certain time horizon. The result, a therapy, which makes the tumor grow as big as possible under these constraints, can be considered the *worst* treatment one could apply. Together with the optimal control for a minimal tumor, the *best* treatment, we compare these results to standard treatments or untreated tumors, e.g. in figures 5.9, 5.17, 5.47, and 5.60. It turns out that there are scenarios where the differences between worst and best treatments are small, but we also show scenarios where the same amount of drugs leads to a growing tumor on the one hand and a total disappearance on the other hand (figure 5.25).

- How sensitive are optimal control strategies against the choice of the objective function? The formulation of an objective function is crucial for the optimal control result. We formulate new optimal control problems with different objective functions for models for which such problems have not been published yet. Results for different objectives are shown in sections 5.3, 5.4, and 5.5 (e.g. see figures 5.13 and 5.14, 5.32 and 5.35).

- How much of our objective do we lose because of practical restrictions, e.g. a discrete and not continuous therapy plan? Optimal controls may consist of so-called *singular arcs*, which are parts where the control is not at its lower or upper bound. A treatment with a singular arc may not be realizable in medical practice. Therefore we also have a look at corresponding practicable therapies, which are computed as mixed-integer controls, and compare the results under these treatments to the optimal ones. This is shown in figures 5.11, 5.42, and 5.44, for example. For this part, we implemented and tested a new heuristic for the solution of the arising mixed-integer optimal control problems.

Contributions

This diploma thesis gives an extensive overview of existing mathematical models for cancer and cancer chemotherapy. Multiple corrections are given and mistakes are revealed. We apply state-of-the-art optimal control methods to these models. In particular, we use Bock's direct multiple shooting for continuous optimal control and MS MINTOC for mixed-integer optimal control.

The existing mixed-integer algorithms are extended with a new rounding heuristic. Therefore, the methodic proposal of the advisor has been implemented and is applied successfully. Optimal solutions for four models are computed, whereas a part of these problems are solved

to optimality for the first time. Optimal control results from the literature are partly verified, partly falsified. For the first time in this context, a focus is set on integer respectively binary controls. The numerical results of both continuous and mixed-integer optimal control are analysed, compared and explained.

Note that not all mechanisms of cancer are well understood yet. Some, e.g. anti-angiogenesis, are still controversial, but a discussion of such processes is not an aim of this work. These processes are described from a layman point of view while the focus is set on the resulting mathematical models and the application of methods from scientific computing.

Structure

The work is structured as follows. In the next chapter, we present the five different models that have been investigated in this work including the eight different parameter sets. We also introduce some optimal control problems – readers who are totally unfamiliar with optimal control problems are referred to section 3.1 where we give an abstract problem formulation. Chapter 3 explains the techniques we used to solve the arising continuous optimal control problems, direct multiple shooting, while Chapter 4 contains a mixed-integer optimal control approach together with a new rounding heuristic, where a decomposed mixed-integer linear program is solved. The optimal control results can be found in chapter 5, where also interpretations and comparisons between the different scenarios are given. Our work concludes with a summary of our results and an outlook on possible future work.

Chapter 2

Modeling Cancer and Treatments

In this work, five different models of cancer and cancer chemotherapy respectively immuno-therapy with a total of eight different parameter sets have been investigated. The models are all based on a set of ordinary differential equations and feature some kind of medical treatment. In this section, an overview over the models is given and differences between them are highlighted. We also present their scientific context and give a survey of adjacent approaches we did not consider in detail.

2.1 Hahnfeldt et al. 1999

In *Hahnfeldt et al.* [24], a model with two states and one control is given. The states are the volume of the tumor x_0 on the one hand and the volume of blood vessels in the neighborhood of the tumor x_1 on the other hand. This is due to the fact that the therapy u_0 applied in this model is an *anti-angiogenic* therapy.

Optimal control techniques have not been applied to this model, but as the model presented in the next section is derived from *Hahnfeldt et al.*, it is useful to verify implementation results and to give an introduction to *Anti-Angiogenesis*.

The model has been implemented in the *chemo1* application.

Anti-angiogenesis

Anti-angiogenesis is a concept introduced in the 1970s by *Folkman* [20], who is also one of the co-authors of [24]. As a tumor needs proliferating blood vessels to survive and to grow, the basic idea is to administer a drug u_0 that supresses *Angiogenesis*, the process of blood vessels growing from existing vessels. While the killing agents applied by classic chemotherapy attack the tumor cells directly, this drugs—TNP-470, Endostatin, and Angiostatin in [24]—inhibit the growth of endothelial cells which provide the tumor with necessary nutrition. According to [20], without this *neovascularization*, most tumors cannot exceed a diameter of 2–3 mm so an *anti-angiogenic* therapy may be interesting in particular as a combination therapy with classic chemotherapy when the tumor is attacked directly in addition.

Model Equations

The tumor volume equation consists of a *Gompertz*-term

$$-\zeta\, x_0(t) \log\left(\frac{x_0(t)}{x_1(t)}\right) \tag{2.1}$$

in which the limit has been replaced by the endothelial volume. *Gompertz growth* beside *logistic growth* is one of the two types of growth chosen in all models that have been investigated.

The classic *Gompertz growth* equation reads

$$\dot{N}(t) = -\zeta N(t) \log \left(\frac{N(t)}{K} \right) \tag{2.2}$$

where K—the limit for the population $N(t)$—is called *carrying capacity*. Inserting the blood vessel volume as *carrying capacity* instead of a fixed value means that the growth of the tumor is limited by the vasculature volume. Thus to grow in the long-term, the tumor needs the blood vessels to grow. Note that log refers to the *natural logarithm*—at least, we could only reproduce the results perfectly using natural logarithm, see chapter 5.

The equation for blood vessel volume is a bit more complex. There is a term

$$-\mu \, x_1(t) \tag{2.3}$$

that represents the spontaneous loss of vasculature and one that represents the stimulation of *neovascularization* by the tumor (e.g. by VEGF, *vascular endothelial growth factor*),

$$b \, x_0(t). \tag{2.4}$$

The third term,

$$-d \, x_0(t)^{\frac{2}{3}} x_1(t), \tag{2.5}$$

comes from the endogeneous inhibition of the vasculature previously generated. Finally, with

$$-G \, g(t) \, x_1(t) \tag{2.6}$$

the response to the *anti-angiogenic* drug is modeled. $g(t)$ is the concentration of the drug at the tumor site and contains the effect from partially cleared drug amounts from prior adminstrations:

$$g(t) = \int_0^t u_0(t') \exp \left(-\gamma \left(t - t' \right) \right) dt' \tag{2.7}$$

For reasonable results of course, we have to require all populations as well as the drug administration to be ≥ 0, so we have to add

$$0 \leq u_0(t), x_0(t), x_1(t). \tag{2.8}$$

Parameters and Optimal Control

The parameters G, b, d, μ, ζ, γ in [24] are derived by about 1,000,000 runs of a monte-carlo-algorithm based on data from experiments with mice that have been injected Lewis lung carcinoma cells.

In *Hahnfeldt et al.*, neither any optimization of treatment schemes is done nor an optimization problem is formulated. However, different fixed scenarios with the three different drugs mentioned above are evaluated. The whole model is described by the following equations. Initial values used in the article are listed in Table 2.1, parameters compared to the ones from *d'Onofrio et al.* [17] can be found in Table 2.3.

$x_0(t_0)$	$x_1(t_0)$	Description
~200	625	Control
~170	625	TNP-470, low
12, 300	625	TNP-470, middle
17, 300	625	TNP-470, high
177	625	Endostatin
170	625	Angiostatin, low
240	625	Angiostatin, middle
400	625	Angiostatin, high

Table 2.1: Initial values used in *Hahnfeldt et al.*

$$\dot{x}_0(t) = -\zeta\, x_0(t) \log\left(\frac{x_0(t)}{x_1(t)}\right), \tag{2.9a}$$

$$\dot{x}_1(t) = b\, x_0(t) - \mu\, x_1(t) - d\, x_0(t)^{\frac{2}{3}} x_1(t) - G\, g(t)\, x_1(t), \tag{2.9b}$$

$$g(t) = \int_0^t u_0(t') \exp\left(-\gamma\left(t - t'\right)\right) dt', \tag{2.9c}$$

$$0 \leq u_0(t), x_0(t), x_1(t), \tag{2.9d}$$

$$t \in [t_0, t_f]. \tag{2.9e}$$

2.2 d'Onofrio et al. 2009

The model in *d'Onofrio et al.* [17] is based on the work in [24] (section 2.1) and especially on a modification of the *Hahnfeldt*-model by *d'Onofrio and Gandolfi* [15, 16]. Therefore we implemented it also in the *chemo1* application. A major modification is the identification of drug concentration and dosage. Hence, there is no concentration equation like (2.9c) in section 2.1. Furthermore, a classic chemotherapy treatment has been added, so that now there are two controls: u_0 representing anti-angiogenic treatment, and u_1 representing chemotherapy.

Model Equations and Parameters

The chemotherapeutic drug influences both tumor and vasculature, so the blood vessel equation now reads

$$\dot{x}_1(t) = b\, x_0(t) - \mu\, x_1(t) - d\, x_0(t)^{\frac{2}{3}} x_1(t) - G\, u_0(t)\, x_1(t) - \eta\, x_1(t)\, u_1(t). \tag{2.10}$$

If the chemotherapeutic drug is effective, the killing effect on tumor cells should be higher than on other cells. At least one has to assume that the effect on blood vessel cells and tumor cells is different, so a different parameter F for the chemotherapy killing term in the tumor equation is used. Finally, they replace log by ln, although our computation results of the

Hahnfeldt model suggest that log in [24] already means *natural logarithm*. However this results in an corresponding transformation of ζ (see table 2.3). The modified tumor equation is

$$\dot{x}_0(t) = -\zeta\, x_0(t) \ln\left(\frac{x_0(t)}{x_1(t)}\right) - F\, x_0(t)\, u_1(t). \tag{2.11}$$

In *d'Onofrio et al.*, the total amount of drug applied is limited. To be able to treat this constraints easily in `MUSCOD-II` (see chapter 3 and 5), we add two auxiliary states which sum up the amounts of given drugs:

$$\dot{x}_2(t) = u_0(t), \tag{2.12}$$
$$\dot{x}_3(t) = u_1(t). \tag{2.13}$$

Now the constraints on the total amount can be written as

$$x_2(t_f) \leq A, \tag{2.14}$$
$$x_3(t_f) \leq C, \tag{2.15}$$

and the additional constraints on the controls are

$$u_0(t) \leq a, \tag{2.16}$$
$$u_1(t) \leq c. \tag{2.17}$$

Thus, with slight transformations the total model with constraints is described by the system

$$\dot{x}_0(t) = -\zeta\, x_0(t) \ln\left(\frac{x_0(t)}{x_1(t)}\right) - F\, x_0(t)\, u_1(t), \tag{2.18a}$$

$$\begin{aligned} \dot{x}_1(t) = b\, x_0(t) - \mu\, x_1(t) - d\, x_0(t)^{\frac{2}{3}} x_1(t) \\ - G\, u_0(t)\, x_1(t) - \eta\, x_1(t)\, u_1(t), \end{aligned} \tag{2.18b}$$

$$\dot{x}_2(t) = u_0(t), \tag{2.18c}$$
$$\dot{x}_3(t) = u_1(t), \tag{2.18d}$$
$$0 \leq a - u_0(t), \tag{2.18e}$$
$$0 \leq c - u_1(t), \tag{2.18f}$$
$$0 \leq A - x_2(t_f), \tag{2.18g}$$
$$0 \leq C - x_3(t_f), \tag{2.18h}$$
$$0 \leq u_0(t), u_1(t), x_0(t), x_1(t), \tag{2.18i}$$
$$t \in [t_0, t_f]. \tag{2.18j}$$

The values of the parameters can be found in table 2.3, initial values are listed in table 2.2. Note that the parameters F, η, A, a, C, c, which are not taken from [24], are not based on experimental data. These values have just been used for numerical experiments.

Optimal Control Problem and Initial Values

In the numerical analysis section, an optimal control problem is posed. The objective function, which should be minimized, is

$$x_0\left(t_f\right) + \alpha \int_{t_0}^{t_f} u_0(t)^2 \quad dt, \tag{2.19}$$

$x_0(t_0)$	$x_1(t_0)$	$x_2(t_0)$	$x_3(t_0)$	Description
12,000	15,000	0	0	u_{max}—sing—0
14,000	5,000	0	0	0—sing—0

Table 2.2: Initial values used in *d'Onofrio et al.*

Parameter	d'Onofrio et al.	Hahnfeldt et al.	Description
F	0.1	—	tumor killing by chemotherapy
G	0.15	0.15/0.66/1.3	vasculature killing by *Anti-Angiogenesis*
b	5.85	5.85	birth parameter
d	0.00873	0.00873	death parameter
μ	0.02	0.0	natural inhibition parameter
ζ	0.084 (ln)	0.192 (log)	tumor growth parameter
γ	—	0.13/0.39/0.39	drug clearance rate
η	0.0–0.1	—	vasculature killing by chemotherapy
A	300	—	maximum inhibitor available
a	75	—	maximum dosage of inhibitor
C	2/10	—	maximum killing agent available
c	1/2	—	maximum dosage of killing agent

Table 2.3: Parameters in *Hahnfeldt et al.* and *d'Onofrio et al.*

while the end time t_f is free. This means that we minimize the tumor volume at the end time of the treatment and penalize the angiogenic drug dosage. Hence, the value for α should be chosen such that the penalty does not dominate the tumor volume part. In the numerical experiments in the article $\alpha = 0.005$ is chosen.

Combining (2.18) and (2.19) we finally get the optimization problem

$$\min \quad x_0\left(t_f\right) + \alpha \int_{t_0}^{t_f} u_0(t)^2 \quad dt \tag{2.20a}$$

$$\text{subject to} \quad (2.18). \tag{2.20b}$$

The initial values have been chosen such that the solution of the optimal control problem (2.20) has different structures. With the initial values $x_0(t_0) = 12,000$, $x_1(t_0) = 15,000$ the structure is maximum—singular—minimum (note that here minimum means 0), while the structure with $x_0(t_0) = 14,000$, $x_1(t_0) = 5,000$ is minimum—singular—minimum.

2.3 De Pillis et al. 2006

While the first two models were relatively small, the model by *de Pillis et al. (2006)* [10] is a little bigger, especially concerning the number of parameters. It consists of five respectively

Name	Description
x_0	number of tumor cells
x_1	number of NK cells
x_2	number CD8+ T cells
x_3	number of circulating lymphocytes
x_4	chemotherapeutic drug concentration
x_5	immunotherapeutic drug concentration
u_0	chemotherapeutic drug dosage
u_1	immunotherapeutic drug dosage (IL-2)
u_2	cytolytic immune cell dosage (TIL)

Table 2.4: Overview of states and controls in *de Pillis et al. 2006*

six states, up to three controls and 29 parameters in three parameter sets. The work is based on previous work by the same or similar authors [11, 12, 13].

As a major difference to the models above, this one contains a combination of *chemotherapy* and *immunotherapy*. Thus, one of the five states is still the tumor population x_0, but in absolute cell count. Instead of the blood vessel volume, this model features three types of immune cell populations (all in absolute cell count):

- NK cells x_1—unspecific immune cells which are also present in a healthy body, "natural killer" cells

- CD8+ T cells x_2—tumor-specific immune cells

- circulating lymphocytes x_3—white blood cells

The fifth and the sixth state represent the chemotherapeutic drug concentration x_4 respectively *interleukin-2* concentration x_5. *Interleukin-2*, which is one of the two *immunotherapeutic* controls, is a cytokine that stimulates the production of CD8+ T cells and is used "to boost immune system function" [10]. In addition, there is a control for a classic *chemotherapeutic drug* u_0 and one for a *tumor infiltrating lymphocyte* injection (*TIL*) u_2. The latter means an injection of CD8+ T cells that have been highly stimulated against tumor cells outside the body. See table 2.4 for an overview of states and controls.

The model has been implemented in the *chemo3* `MUSCOD-II`-application.

Parameter Sets

There are three parameter sets given: *mouse*, *human 9*, and *human 10*. As the name suggests, the *mouse* parameter set contains parameters derived from murine experiments.

In fact, the parameters come from different papers treating different types of cancer and different types of mice. For example the *tumor growth parameter a* has been fitted to data from a paper by *Diefenbach et al.* [14]. In that article, *EL4* thymoma, *RMA* lymphoma and *B16-BL6* melanoma have been implanted into *B6-Rag$^{-/-}$* mice. On the other hand, e.g. the death rate

of NK cells f is derived from *Kuznetsov et al.* [28], where a mathematical model is used to describe the kinetics of growth and regression of a BCL_1 lymphoma in *BALB/c* mice. For the parameters r_2 and v, there is no source.

For the *human* parameter set, the authors refer to an article by *Dudley et al.*[18]. This publication contains real proband data of 13 melanoma patients. The data of the ones numbered 9 and 10 has been used in *de Pillis et al. 2006* for fitting seven of the parameters. Again, for r_2 and v, there is no source. Actually, there are eight more references for the *human* parameter set, e.g. the two murine papers from the *mouse* parameter set. Another source [27] refers among others to *Kuznetsov et al.* Note that this means that about one third of the *human* parameters comes from *murine* experiments.

In [27] it is stated that the value of a certain parameter in their model "(...) varies greatly from patient to patient and cancer to cancer." So this model may not be adequate for generating exact treatment schedules [1]—in particular for humans since there is only little human data used and the values may highly depend on the patient and the type of cancer. But it still may be useful for making general qualitative statements.

Table 2.5 gives an overview of the different parameter sets.

Model Equations

The model features a *logistic growth* term in the tumor equation, here

$$a\, x_0(t)\, (1 - b\, x_0(t)).\tag{2.21}$$

As already mentioned above, NK cells x_1 and CD8+ T cells x_2 both kill tumor cells. The interaction between NK and tumor cells is modeled with a bilinear term, while the effect of CD8+ T cells introduces a quotient also used in other equations:

$$-c\, x_1(t)\, x_0(t) - D\, x_0(t) \quad \text{with} \quad D = d\, \frac{(x_2(t)/x_0(t))^l}{s + (x_2(t)/x_0(t))^l}.\tag{2.22}$$

Both terms are taken from *de Pillis et al. 2003* [12]. The last summand in the tumor equation represents the effect of chemotherapy on the tumor where a saturation term $(1 - \mathrm{e}^{-x_4(t)})$ is used. This term with different parameters is contained in the immune cell equations, too:

$$\text{tumor } x_0: \quad -K_T \left(1 - \mathrm{e}^{-x_4(t)}\right) x_0(t),\tag{2.23a}$$

$$\text{NK cells } x_1: \quad -K_N \left(1 - \mathrm{e}^{-x_4(t)}\right) x_1(t),\tag{2.23b}$$

$$\text{CD8+ T cells } x_2: \quad -K_L \left(1 - \mathrm{e}^{-x_4(t)}\right) x_2(t),\tag{2.23c}$$

$$\text{circ. lymphocytes } x_3: \quad -K_C \left(1 - \mathrm{e}^{-x_4(t)}\right) x_3(t).\tag{2.23d}$$

The equation for NK cells contains a recruitment term of circulating lymphocytes $e\, x_3(t)$ and an exponential decay term $-f\, x_1(t)$ representing the limited natural lifespan of each cell. Additionally, there is a term for recruitment of NK cells,

$$g\, \frac{x_0(t)^2}{h + x_0(t)^2} x_1(t),\tag{2.24}$$

---

[1] except for Mickey Mouse. . .

Parameter	Mouse	Human 9	Human 10	Description
a	$4.31 \cdot 10^{-1}$	$4.31 \cdot 10^{-1}$	$4.31 \cdot 10^{-1}$	tumor growth rate
b	$2.17 \cdot 10^{-8}$	$1.02 \cdot 10^{-9}$	$1.02 \cdot 10^{-9}$	reciprocal of tumor carrying capacity
c	$7.13 \cdot 10^{-10}$	$6.41 \cdot 10^{-11}$	$6.41 \cdot 10^{-11}$	fractional tumor cell kill by NK cells
d	8.17	2.34	1.88	saturation level of frac. tumor cell kill by CD8+ cells
l	$6.57 \cdot 10^{-1}$	2.09	1.81	exponent of fractional tumor cell kill by CD8+ cells
s	$6.18 \cdot 10^{-1}$	$8.39 \cdot 10^{-2}$	$5.12 \cdot 10^{-1}$	steepness coefficient of the tumor-CD8+-lysis term
e	$1.29 \cdot 10^{-3}$	$2.08 \cdot 10^{-7}$	$2.08 \cdot 10^{-7}$	fraction of circ. lymphocytes becoming NK cells
f	$4.12 \cdot 10^{-2}$	$4.12 \cdot 10^{-2}$	$4.12 \cdot 10^{-2}$	death rate of NK cells
g	$4.98 \cdot 10^{-1}$	$1.25 \cdot 10^{-2}$	$1.25 \cdot 10^{-2}$	maximum NK cell recruitment rate
h	$2.02 \cdot 10^{7}$	$2.02 \cdot 10^{7}$	$2.02 \cdot 10^{7}$	steepness coeff. of the NK cell recruitment curve
p	$1.0 \cdot 10^{-7}$	$3.42 \cdot 10^{-6}$	$3.59 \cdot 10^{-6}$	NK cell inactivation rate
m	$2.0 \cdot 10^{-2}$	$2.04 \cdot 10^{-1}$	9.12	death rate of CD8+ cells
j	$9.96 \cdot 10^{-1}$	$2.49 \cdot 10^{-2}$	$2.49 \cdot 10^{-2}$	maximum CD8+ cell recruitment rate
k	$3.03 \cdot 10^{5}$	$3.66 \cdot 10^{7}$	$5.66 \cdot 10^{7}$	steepness coeff. of the CD8+ cell recruitment curve
q	$3.42 \cdot 10^{-10}$	$1.42 \cdot 10^{-6}$	$1.59 \cdot 10^{-6}$	CD8+ cell inactivation rate
r_1	$1.10 \cdot 10^{-7}$	$1.10 \cdot 10^{-7}$	$1.10 \cdot 10^{-7}$	CD8+ cell production stimulation rate by NK cells
r_2	$3.0 \cdot 10^{-11}$	$6.50 \cdot 10^{-11}$	$6.50 \cdot 10^{-11}$	CD8+ cell production stimulation rate by circulating lymphocytes
v	$1.80 \cdot 10^{-8}$	$3.00 \cdot 10^{-10}$	$3.00 \cdot 10^{-10}$	regulatory function by NK cells on CD8+ cells
K_T	$9.00 \cdot 10^{-1}$	$9.00 \cdot 10^{-1}$	$9.00 \cdot 10^{-1}$	fractional tumor cell kill by chemotherapy
K_N	$6.00 \cdot 10^{-1}$	$6.00 \cdot 10^{-1}$	$6.00 \cdot 10^{-1}$	fractional NK cell kill by chemotherapy
K_L	$6.00 \cdot 10^{-1}$	$6.00 \cdot 10^{-1}$	$6.00 \cdot 10^{-1}$	fractional CD8+ cell kill by chemotherapy
K_C	$6.00 \cdot 10^{-1}$	$6.00 \cdot 10^{-1}$	$6.00 \cdot 10^{-1}$	fractional circulating lymphocytes cell kill by chemotherapy
α	$1.21 \cdot 10^{5}$	$7.50 \cdot 10^{8}$	$5.00 \cdot 10^{8}$	constant source of circulating lymphocytes
β	$1.20 \cdot 10^{-2}$	$1.20 \cdot 10^{-2}$	$8.00 \cdot 10^{-3}$	natural death and differentiation of circulating lymphocytes
γ	$9.00 \cdot 10^{-1}$	$9.00 \cdot 10^{-1}$	$9.00 \cdot 10^{-1}$	rate of chemotherapy drug decay
p_I	—	$1.25 \cdot 10^{-1}$	$1.25 \cdot 10^{-1}$	maxmimum CD8+ cell recruitment rate by IL-2
g_I	—	$2.00 \cdot 10^{7}$	$2.00 \cdot 10^{7}$	steepness of CD8+ cell recruitment curve by IL-2
μ_I	—	$1.00 \cdot 10^{1}$	$1.00 \cdot 10^{1}$	rate of IL-2 drug decay

Table 2.5: Parameter sets of *de Pillis et al. 2006*

$x_0(t_0)$	$x_1(t_0)$	$x_2(t_0)$	$x_3(t_0)$	$x_4(t_0)$	$x_5(t_0)$	**Parameter set**
$1 \cdot 10^6$	$5 \cdot 10^4$	$1 \cdot 10^2$	$1.1 \cdot 10^7$	0	0	Mouse
$1 \cdot 10^6$	$1 \cdot 10^5$	$1 \cdot 10^2$	$6 \cdot 10^{10}$	0	0	Human 9/10
$1 \cdot 10^6$	$1 \cdot 10^3$	1	$6 \cdot 10^8$	0	0	Human 9
$2 \cdot 10^7$	$1 \cdot 10^3$	1	$6 \cdot 10^8$	0	0	Human 9
$1 \cdot 10^8$	$1 \cdot 10^3$	1	$6 \cdot 10^8$	0	0	Human 9
$1 \cdot 10^7$	$1 \cdot 10^3$	1	$6 \cdot 10^8$	0	0	Human 9/10
$1 \cdot 10^5$	$1 \cdot 10^5$	$1 \cdot 10^2$	$6 \cdot 10^{10}$	0	0	Human 10

Table 2.6: Initial values of *de Pillis et al. 2006*

and one for the inactivation of NK cells after interaction with tumor cells

$$-p\,x_1(t)\,x_0(t). \tag{2.25}$$

Matching the assumption that there are no CD8+ T cells present in the absence of a tumor, there is no growth term but an exponential decay $-m\,x_2$ in the corresponding equation. However, there are several recruitment terms. One for the recruitment by tumor-CD8+ T cell interaction, one for the recruitment by tumor cells killed by NK cells (*tumor debris*), and one for the recruitment by encounters between tumor cells and circulating lymphocytes:

$$j\,\frac{D^2\,x_0(t)^2}{k + D^2\,x_0(t)^2}x_2(t) + r_1\,x_1(t)\,x_0(t) + r_2\,x_3(t)\,x_0(t). \tag{2.26}$$

Similar to the inactivation of NK cells there is a summand $-q\,x_2\,x_0$ for the inactivation of CD8+ T cells after interacting with tumor cells. In addition, there is an inactivation term $-v\,x_1\,x_2{}^2$ describing the regulation and suppression of CD8+ T cell activity at high cell levels. In the CD8+ T cell equation there is also a *Michaelis-Menten-term* for the influence of IL-2 and a simple input of the TIL control,

$$\frac{p_I\,x_2(t)\,x_5(t)}{g_I + x_5(t)} + u_2(t) \tag{2.27}$$

Circulating lymphocytes are expected to have a constant source and again a limited natural lifespan which leads—together with chemotherapeutic influence—to

$$\dot{x}_3(t) = \alpha - \beta\,x_3(t) - K_C\left(1 - \mathrm{e}^{-x_4(t)}\right)x_3(t), \tag{2.28}$$

The last two equations—the ones for chemo- and immunotherapeutic drug concentration—are of simple exponential decay type with the corresponding controls as inputs:

$$\dot{x}_4(t) = -\gamma\,x_4(t) + u_0(t), \tag{2.29a}$$
$$\dot{x}_5(t) = -\mu_I\,x_5(t) + u_1(t). \tag{2.29b}$$

Again for reasonable results, it is necessary that all states and controls are ≥ 0. Therefore we add the constraints

$$x_0(t), x_1(t), x_2(t), x_3(t), x_4(t), x_5(t) \geq 0, \tag{2.30a}$$

$$u_0(t), u_1(t), u_2(t) \geq 0. \tag{2.30b}$$

Finally we get the whole model by the following set of ODEs. In favor of readability we omit the time dependence of states and controls. For more details on the equations we refer to [10, 12].

$$\dot{x}_0 = a\,x_0\,(1 - b\,x_0) - c\,x_1\,x_0 - D\,x_0 - K_T\left(1 - \mathrm{e}^{-x_4}\right)x_0, \tag{2.31a}$$

$$\dot{x}_1 = e\,x_3 - f\,x_1 + g\,\frac{x_0{}^2}{h + x_0{}^2}x_1 - p\,x_1\,x_0 - K_N\left(1 - \mathrm{e}^{-x_4}\right)x_1, \tag{2.31b}$$

$$\begin{aligned}
\dot{x}_2 = {}&-m\,x_2 + j\,\frac{D^2\,x_0{}^2}{k + D^2\,x_0{}^2}x_2 - q\,x_2\,x_0 + (r_1\,x_1 + r_2\,x_3)\,x_0 \\
&- v\,x_1\,x_2{}^2 - K_L\left(1 - \mathrm{e}^{-x_4}\right)x_2 + \frac{p_I\,x_2\,x_5}{g_I + x_5} + u_2,
\end{aligned} \tag{2.31c}$$

$$\dot{x}_3 = \alpha - \beta\,x_3 - K_C\left(1 - \mathrm{e}^{-x_4}\right)x_3, \tag{2.31d}$$

$$\dot{x}_4 = -\gamma\,x_4 + u_0, \tag{2.31e}$$

$$\dot{x}_5 = -\mu_I\,x_5 + u_1, \tag{2.31f}$$

$$D = d\,\frac{(x_2/x_0)^l}{s + (x_2/x_0)^l}, \tag{2.31g}$$

$$0 \leq x_0, x_1, x_2, x_3, x_4, x_5, \tag{2.31h}$$

$$0 \leq u_0, u_1, u_2, \tag{2.31i}$$

$$t \in [t_0, t_f] \tag{2.31j}$$

Initial Values and Optimal Control

There are nine different initial value sets given in the article: one for the *mouse* setting and eight for *human 9* respectively *human 10*. They are listed in table 2.6. In *de Pillis et al. 2006*, there is no optimal control problem given and no optimization done. Though there are many different scenarios investigated, e.g. big initial tumor size vs. small initial tumor size, combination therapy vs. monotherapy and so on.

The setting with nonlinear ODEs, multiple controls, three different parameter sets and lots of initial values looks interesting for an application of our optimal control techniques (chapters 3 and 4). Numerical results for different scenarios are presented and discussed in chapter 5. To the best of our knowledge, this model has not been solved to optimality before—except for the *NMPC* approach mentioned in 2.6.

2.4 De Pillis et al. 2008

Analog to *de Pillis et al. 2006* [10] being essentially derived from previous work by the authors, *de Pillis et al. 2008* [9] can be considered a descendant of *de Pillis et al. 2006* (section 2.3).

The model contains again three controls, namely a *chemotherapeutic* one u_0 and an *immunotherapeutic (IL-2)* one u_1 as well as *TIL* injections u_2. It includes one state for the tumor

cell population x_0, three for immune cell populations (NK cells x_1, CD8+ T cells x_2, circulating lymphocytes x_3) and two for chemotherapeutic drug concentration x_4 and IL-2 concentration x_5.

In contrast to the previous article, this one focuses on optimal control results. There are some modifications on the equations, but overall they are very similar. Most of the parameters have been adapted either from the *mouse* or the *human 9/human 10* sets.

The MUSCOD-II application *chemo3a* contains this model.

Model Equations

At least some of the changes in the model equations compared to [10] may be owed to the tractability with an *indirect optimal control approach*. These techniques are applied in *de Pillis et al. 2008*. Hence, the saturation term for the influence of chemotherapy $(1 - e^{-x_4(t)})$ has been simply replaced by the drug concentration x_4 resulting in the following transformations in the corresponding equations.

$$\text{tumor } x_0: \quad -K_T \left(1 - e^{-x_4(t)}\right) x_0(t) \longrightarrow -K_T \, x_4(t) \, x_0(t), \tag{2.32a}$$

$$\text{NK cells } x_1: \quad -K_N \left(1 - e^{-x_4(t)}\right) x_1(t) \longrightarrow -K_N \, x_4(t) \, x_1(t), \tag{2.32b}$$

$$\text{CD8+ T cells } x_2: \quad -K_L \left(1 - e^{-x_4(t)}\right) x_2(t) \longrightarrow -K_L \, x_4(t) \, x_2(t), \tag{2.32c}$$

$$\text{circ. lymphocytes } x_3: \quad -K_C \left(1 - e^{-x_4(t)}\right) x_3(t) \longrightarrow -K_C \, x_4(t) \, x_3(t). \tag{2.32d}$$

The production rate of NK cells is now constant α_1 like in [28], instead of proportionally linked to the circulating lymphocytes. In the CD8+ T cell equation, the terms

$$j \frac{D^2 \, x_0^2}{k + D^2 \, x_0^2} x_2 + r_1 \, x_1 \, x_0 \tag{2.33}$$

are omitted—the latter because of representing *tumor debris*, the activation of CD8+T cells, which is said to be still under discussion. For the first term the authors give no reasons.

They also assume now that the regulation of CD8+ T cells at high levels is a self-regulative process and does not involve NK cells, meaning $-v \, x_1 \, x_2^2$ becomes $-v \, x_2^2$. Completely new are the terms

$$\frac{p_T \, x_2 \, x_0}{g_T + x_0} - w \, x_2 \, x_5 \tag{2.34}$$

in the IL-2 concentration equation. While the first (*Michaelis-Menten-*)term is said to represent "the understanding that the interaction of tumor-specific T cells with tumor cells stimulates IL-2 production" [9], the second is referenced to *Abbas et al.* [3] where it is stated that all types of T cells produce IL-2. Note that in [3] there is no reason given for a linear interaction term, so it is not obvious why the author used $-w \, x_2 \, x_5$ instead of $-w \, x_2$ for example.

All the modifications result in the following set of ODEs describing the model. For expla-

Parameter	Value
g_T	$1.00 \cdot 10^5$
p_T	$6.00 \cdot 10^{-1}$
w	$2.00 \cdot 10^{-4}$
α_1	$1.30 \cdot 10^4$

Table 2.7: Additional parameters introduced in *de Pillis et al. 2008*

nations of the unmodified terms, please have a look at section 2.3.

$$\dot{x}_0 = a\, x_0\, (1 - b\, x_0) - c\, x_1\, x_0 - D\, x_0 - K_T\, x_4\, x_0, \tag{2.35a}$$

$$\dot{x}_1 = \alpha_1 - f\, x_1 + g\, \frac{x_0}{h + x_0}\, x_1 - p\, x_1\, x_0 - K_N\, x_4\, x_1, \tag{2.35b}$$

$$\dot{x}_2 = -m\, x_2 - q\, x_2\, x_0 + r_2\, x_3\, x_0$$
$$\qquad - v\, x_2{}^2 - K_L\, x_4\, x_2 + \frac{p_I\, x_2\, x_5}{g_I + x_5} + u_2, \tag{2.35c}$$

$$\dot{x}_3 = \alpha - \beta\, x_3 - K_C\, x_4\, x_3, \tag{2.35d}$$

$$\dot{x}_4 = -\gamma\, x_4 + u_0, \tag{2.35e}$$

$$\dot{x}_5 = \frac{p_T\, x_2\, x_0}{g_T + x_0} - w\, x_2\, x_5 - \mu_I\, x_5 + u_1, \tag{2.35f}$$

$$D = d\, \frac{(x_2/x_0)^l}{s + (x_2/x_0)^l}, \tag{2.35g}$$

$$0 \le x_0, x_1, x_2, x_3, x_4, x_5, \tag{2.35h}$$

$$0 \le u_0, u_1, u_2, \tag{2.35i}$$

$$t \in [t_0, t_f] \tag{2.35j}$$

Parameters and Initial Values

Unlike in section 2.3, only one parameter set is contained. The parameters are mainly referenced to [14, 18], so one would probably expect that they should be comparable to the *human* parameter sets in *de Pillis et al. 2006*. Actually it turns out that they are a mixture between the *human* and the *mouse* sets. A comparison is given in table 2.9.

About half of the parameters have changed a bit or are completely new. Of course this may be due to the changes in the model. Some of the parameters are subject of fluctuations of a couple of orders of magnitude. The newly introduced parameters can be found in table 2.7.

The authors use two sets of initial values. The first set has a small tumor cell population and is therefore called "small". The other set contains a "detectable" initial tumor population. See table 2.8 for the exact values of all states.

Optimal Control Problems

As already mentioned, this paper is mainly about optimal control of the model. Therefore, there are different objective functions given depending on treatment combinations. They all

$x_0(t_0)$	$x_1(t_0)$	$x_2(t_0)$	$x_3(t_0)$	$x_4(t_0)$	$x_5(t_0)$	**Parameter set**
$1 \cdot 10^2$	$3 \cdot 10^4$	$3 \cdot 10$	$5 \cdot 10^6$	0	0	small
$1 \cdot 10^7$	$5 \cdot 10^5$	$2 \cdot 10^3$	$4.17 \cdot 10^{10}$	0	0	detectable

Table 2.8: Initial values in *de Pillis et al. 2008*

can be written in the form

$$\int_{t_0}^{t_f} x_0(t) + \frac{p_0}{2} u_0(t)^2 + \frac{p_1}{2} u_1(t)^2 + \frac{p_2}{2} u_2(t)^2 \quad dt. \tag{2.36}$$

All optimal control problems in the paper aim to minimize these functions. The quadratic terms are penalties on the controls and of course it is reasonable to minimize the tumor population over the whole treatment time. The p_i are set to 10^7 or 10^5 depending on the scenario. If $u_i(t)$ is not considered in a calculation, the corresponding p_i is set to zero.

The three different treatment schemes which have been investigated are a combination of chemotherapy and immunotherapy, a combination of chemotherapy and TIL, and a combination of all of them. See table 2.10 for the corresponding objective functions.

Optimal control results, especially compared to the results in the paper, can be found in chapter 5.

2.5 AG Lebiedz, Freiburg 2009

The model presented in this section is work of our cooperation partner *Dirk Lebiedz* and his workgroup, in particular of *Marcel Rehberg* and *Melanie Franzem*, who we would like to thank for a pleasant and inspiring cooperation. Via a collaboration with medical scientists, they have access to human proband data with a combination of *chemotherapy* and *immunotherapy*. The chemotherapy u_0 is based on *methotrexat* (*MTX*) and the control u_1 consists of the application of *leucovorin*, which is used as a kind of a *rescue package* pushing up the depleted immune system and is not comparable to the *immunotherapy* applied in the previous models. Since it is subject of current work, this model has not yet been published, but publications are in preparation.

This model differs from all previous models in using *transit compartments* for immune cell populations. Additionally to states for the tumor x_0 and drug concentrations x_6 and x_7 there are stem cells x_1 on the one side which transfer partially through three compartments x_2, x_3, and x_4 to the circulating leucocytes x_5 on the other side (see table 2.11 for an overview). Circulating leucocytes themselves transfer partially to stem cells again. The idea behind this is that cells are less sensitive or not sensitive at all to specific drugs in some states. Further information especially on how circadian rhythms and appropriate drug timing impact the drug's effect can be found in a work by *Lévi and Schibler* [31].

There are two parameter sets used—one with testing values and one with values fitted from real proband data. The *chemo4* application is used for this model.

Parameter	New value$^\diamond$	Mouse*	Human 9*	Human 10*
a	$\mathbf{2.00 \cdot 10^{-3}}$	$4.31 \cdot 10^{-1}$	$4.31 \cdot 10^{-1}$	$4.31 \cdot 10^{-1}$
b	$\mathbf{1.02 \cdot 10^{-9}}$	$2.17 \cdot 10^{-8}$	$\mathbf{1.02 \cdot 10^{-9}}$	$\mathbf{1.02 \cdot 10^{-9}}$
c	$\mathbf{3.23 \cdot 10^{-7}}$	$7.13 \cdot 10^{-10}$	$6.41 \cdot 10^{-11}$	$6.41 \cdot 10^{-11}$
d	$\mathbf{5.00}$	8.17	2.34	1.88
l	$\mathbf{2/3}$	$6.57 \cdot 10^{-1}$	2.09	1.81
s	$\mathbf{3.00 \cdot 10^{-1}}$	$6.18 \cdot 10^{-1}$	$8.39 \cdot 10^{-2}$	$5.12 \cdot 10^{-1}$
e	—	$1.29 \cdot 10^{-3}$	$2.08 \cdot 10^{-7}$	$2.08 \cdot 10^{-7}$
f	$\mathbf{4.12 \cdot 10^{-2}}$	$\mathbf{4.12 \cdot 10^{-2}}$	$\mathbf{4.12 \cdot 10^{-2}}$	$\mathbf{4.12 \cdot 10^{-2}}$
g	$\mathbf{2.50 \cdot 10^{-2}}$	$4.98 \cdot 10^{-1}$	$1.25 \cdot 10^{-2}$	$1.25 \cdot 10^{-2}$
h	$\mathbf{6.00 \cdot 10^{2}}$	$2.02 \cdot 10^{7}$	$2.02 \cdot 10^{7}$	$2.02 \cdot 10^{7}$
p	$\mathbf{1.00 \cdot 10^{-7}}$	$\mathbf{1.0 \cdot 10^{-7}}$	$3.42 \cdot 10^{-6}$	$3.59 \cdot 10^{-6}$
m	$\mathbf{2.00 \cdot 10^{-2}}$	$\mathbf{2.0 \cdot 10^{-2}}$	$2.04 \cdot 10^{-1}$	9.12
j	—	$9.96 \cdot 10^{-1}$	$2.49 \cdot 10^{-2}$	$2.49 \cdot 10^{-2}$
k	—	$3.03 \cdot 10^{5}$	$3.66 \cdot 10^{7}$	$5.66 \cdot 10^{7}$
q	$\mathbf{3.42 \cdot 10^{-10}}$	$\mathbf{3.42 \cdot 10^{-10}}$	$1.42 \cdot 10^{-6}$	$1.59 \cdot 10^{-6}$
r_1	—	$1.10 \cdot 10^{-7}$	$1.10 \cdot 10^{-7}$	$1.10 \cdot 10^{-7}$
r_2	$\mathbf{3.0 \cdot 10^{-11}}$	$\mathbf{3.0 \cdot 10^{-11}}$	$6.50 \cdot 10^{-11}$	$6.50 \cdot 10^{-11}$
v	$\mathbf{3.00}$	$1.80 \cdot 10^{-8}$	$3.00 \cdot 10^{-10}$	$3.00 \cdot 10^{-10}$
K_T	$\mathbf{8.00 \cdot 10^{-1}}$	$9.00 \cdot 10^{-1}$	$9.00 \cdot 10^{-1}$	$9.00 \cdot 10^{-1}$
K_N	$\mathbf{6.00 \cdot 10^{-1}}$	$\mathbf{6.00 \cdot 10^{-1}}$	$\mathbf{6.00 \cdot 10^{-1}}$	$\mathbf{6.00 \cdot 10^{-1}}$
K_L	$\mathbf{6.00 \cdot 10^{-1}}$	$\mathbf{6.00 \cdot 10^{-1}}$	$\mathbf{6.00 \cdot 10^{-1}}$	$\mathbf{6.00 \cdot 10^{-1}}$
K_C	$\mathbf{6.00 \cdot 10^{-1}}$	$\mathbf{6.00 \cdot 10^{-1}}$	$\mathbf{6.00 \cdot 10^{-1}}$	$\mathbf{6.00 \cdot 10^{-1}}$
α	$\mathbf{5.00 \cdot 10^{8}}$	$1.21 \cdot 10^{5}$	$7.50 \cdot 10^{8}$	$5.00 \cdot 10^{8}$
β	$\mathbf{1.20 \cdot 10^{-2}}$	$\mathbf{1.20 \cdot 10^{-2}}$	$\mathbf{1.20 \cdot 10^{-2}}$	$8.00 \cdot 10^{-3}$
γ	$\mathbf{9.00 \cdot 10^{-1}}$	$\mathbf{9.00 \cdot 10^{-1}}$	$\mathbf{9.00 \cdot 10^{-1}}$	$\mathbf{9.00 \cdot 10^{-1}}$
p_I	$\mathbf{1.25 \cdot 10^{-1}}$	—	$\mathbf{1.25 \cdot 10^{-1}}$	$\mathbf{1.25 \cdot 10^{-1}}$
g_I	$\mathbf{2.00 \cdot 10^{7}}$	—	$\mathbf{2.00 \cdot 10^{7}}$	$\mathbf{2.00 \cdot 10^{7}}$
μ_I	$\mathbf{1.00 \cdot 10^{1}}$	—	$\mathbf{1.00 \cdot 10^{1}}$	$\mathbf{1.00 \cdot 10^{1}}$

Table 2.9: Parameters of *de Pillis et al. 2008*$^\diamond$ compared to the sets of *de Pillis et al. 2006**. Parameters that equal the new ones are printed in bold face.

p_0	p_1	p_2	Description
$1 \cdot 10^7$	$1 \cdot 10^7$	0	chemotherapy and immunotherapy
$1 \cdot 10^7$	0	$1 \cdot 10^7$	chemotherapy and TIL
$1 \cdot 10^7$	$1 \cdot 10^5$	$1 \cdot 10^5$	chemotherapy, immunotherapy, and TIL

Table 2.10: Objective functions in *de Pillis et al. 2008*

Name	Description
x_0	tumor cells
x_1	stem cells
x_2	leucocyte transit compartment 1
x_3	leucocyte transit compartment 2
x_4	leucocyte transit compartment 3
x_5	circulating leucocytes
x_6	MTX drug concentration
x_7	Leucovorin drug concentration
u_0	chemotherapeutic (MTX) drug dosage
u_1	immunotherapeutic (Leucovorin) drug dosage

Table 2.11: Overview of states and controls in the *AG Lebiedz* model

Model Equations

The tumor equation contains *logistic growth* and a linear interaction term for killing of tumor cells by chemotherapy:

$$\dot{x}_0(t) = \nu\, x_0(t) \left(1 - \frac{x_0(t)}{K}\right) - \mu_M\, x_6(t)\, x_0(t) \tag{2.37}$$

Leucocyte dynamics are based on work by *Friberg et al.* [22]. As mentioned above we use a compartment model with 5 compartments, namely stem cells, circulating leucocytes and three transit compartments. For simplicity, the same transfer rate k_t is used for all compartment transfers, while a part of the last compartment (circulating leucocytes) is transfered to the first (stem cells) again. The interaction between *leucovorin* and *MTX* in the influence on the tumor cells is modeled with a *hill-type* equation

$$-\alpha\, k_t \left(1 - \frac{x_7(t)^N}{k^N + x_7(t)^N}\right) x_6(t)\, x_1(t) \tag{2.38}$$

where $1 - \frac{x_7(t)^N}{k^N + x_7(t)^N}$ tends to zero for growing concentration of *leucovorin* x_7 and thus the influence of *MTX* diminishes. In the stem cell equation a growth term

$$k_t\, x_1(t) \left(\frac{B}{x_5(t)}\right)^{\gamma} \tag{2.39}$$

is included. It is chosen such that for no chemotherapy (meaning $x_6 = 0$) $x_j \longrightarrow B$ for $t \longrightarrow \infty$. This makes the leucocyte dynamics look like that:

$$\dot{x}_1(t) = k_t\, x_1(t) \left[\left(\frac{B}{x_5(t)}\right)^{\gamma} - \alpha \left(1 - \frac{x_7(t)^N}{k^N + x_7(t)^N}\right) x_6(t) - 1\right], \tag{2.40a}$$

$$\dot{x}_2(t) = k_t\, x_1(t) - k_t\, x_2(t), \tag{2.40b}$$

$$\dot{x}_3(t) = k_t\, x_2(t) - k_t\, x_3(t), \tag{2.40c}$$

$$\dot{x}_4(t) = k_t\, x_3(t) - k_t\, x_4(t), \tag{2.40d}$$

$$\dot{x}_5(t) = k_t\, x_4(t) - k_t\, x_5(t). \tag{2.40e}$$

For the pharmacokinetics, we use simple exponential decay and the corresponding controls as inputs.

$$\dot{x}_6(t) = -\alpha_M\, x_6(t) + \beta_M\, u_0(t), \tag{2.41a}$$

$$\dot{x}_7(t) = -\alpha_L\, x_7(t) + \beta_L\, u_1(t). \tag{2.41b}$$

As in all other models, states and controls have to be ≥ 0.

$$x_0(t), x_1(t), x_2(t), x_3(t), x_4(t), x_5(t), x_6(t), x_7(t) \geq 0, \tag{2.42a}$$

$$u_0(t), u_1(t) \geq 0. \tag{2.42b}$$

Taking together tumor dynamics, leucocyte dynamics, pharmacokinetics, and constraints, the whole model is described by the following set of ODEs.

$$\dot{x}_0(t) = \nu\, x_0(t) \left(1 - \frac{x_0(t)}{K}\right) - \mu_M\, x_6(t)\, x_0(t), \tag{2.43a}$$

$$\dot{x}_1(t) = k_t\, x_1(t) \left[\left(\frac{B}{x_5(t)}\right)^\gamma - \alpha \left(1 - \frac{x_7(t)^N}{k^N + x_7(t)^N}\right) x_6(t) - 1\right], \tag{2.43b}$$

$$\dot{x}_2(t) = k_t\, x_1(t) - k_t\, x_2(t), \tag{2.43c}$$

$$\dot{x}_3(t) = k_t\, x_2(t) - k_t\, x_3(t), \tag{2.43d}$$

$$\dot{x}_4(t) = k_t\, x_3(t) - k_t\, x_4(t), \tag{2.43e}$$

$$\dot{x}_5(t) = k_t\, x_4(t) - k_t\, x_5(t), \tag{2.43f}$$

$$\dot{x}_6(t) = -\alpha_M\, x_6(t) + \beta_M\, u_0(t), \tag{2.43g}$$

$$\dot{x}_7(t) = -\alpha_L\, x_7(t) + \beta_L\, u_1(t), \tag{2.43h}$$

$$0 \le x_0(t), x_1(t), x_2(t), x_3(t), x_4(t), x_5(t), x_6(t), x_7(t), \tag{2.43i}$$

$$0 \le u_0(t), u_1(t), \tag{2.43j}$$

$$t \in [t_0, t_f]. \tag{2.43k}$$

Parameters and Initial Values

While the parameter set with testing values contains values estimated for testing purposes, the fitted parameters are gained from a fit with human proband data. The 29 patients suffer from *non-hodgkin lymphoma of CNS* and are older than 65 years. Data is being collected since december 2007 and the observation period ends in the third quarter of 2009.

So this model is the only one of the investigated ones concerning a specific human cancer type. Unlike the *human* parameter sets in *de Pillis et al. 2006* [10], the fitted parameters are based completely on human proband data. Note that some parameters could not be fitted yet because of insufficient data. Both parameter sets are listed in table 2.12.

As initial values we currently only use test values because we still have not enough data. The initial value test set is

$$x_0(t_0) = 3.0 \cdot 10^2, \qquad x_1(t_0) = 7.0, \qquad x_2(t_0) = 7.0, \tag{2.44a}$$

$$x_3(t_0) = 7.0, \qquad x_4(t_0) = 7.0, \qquad x_5(t_0) = 7.0, \tag{2.44b}$$

$$x_6(t_0) = 0.0, \qquad x_7(t_0) = 0.0. \tag{2.44c}$$

Optimal Control

Since this model is new work, neither corresponding optimal control problems nor any optimal control results have been published yet.

We present appropriate objective functions and some numerical optimal control results in this work in chapter 5 for both parameter sets. Together with the fitted parameters and prospective new data, the setting looks promising for improvements in chemotherapy practice with (future) optimal control results.

Parameter	Test set	Fitted set	Description
ν	$1.0 \cdot 10^{-3}$	$1.0 \cdot 10^{-3}$	tumor growth rate $^\diamond$
K	$1.0 \cdot 10^{3}$	$1.0 \cdot 10^{3}$	tumor growth limit $^\diamond$
μ_M	$2.0 \cdot 10^{-3}$	$2.0 \cdot 10^{-3}$	tumor cell kill by MTX $^\diamond$
n_t	3	3	number of transit compartments
MIT	$9.0 \cdot 10^{1}$	$1.005802 \cdot 10^{2}$	mean-transit-time of leucocytes
k_t	$\frac{n_t+1}{MIT}$	$\frac{n_t+1}{MIT}^{\blacksquare}$	transit and growth rate of leucocytes
B	7.0	$2.758 \cdot 10^{-1}$	base value for circulating leucocytes
γ	$1.0 \cdot 10^{-1}$	$2.652 \cdot 10^{-1}$	exponential for feedback factor
α	$5.0 \cdot 10^{-2}$	$2.63 \cdot 10^{-2}$	influence of MTX and hill parameter
N	4.0	$9.888 \cdot 10^{-1}$	influence of MTX and hill parameter
k	2.0	5.0780	influence of MTX and hill parameter
α_M	$2.0 \cdot 10^{-1}$	$2.545 \cdot 10^{-1}$	first order elimination rate of MTX drug
α_L	$1.0 \cdot 10^{-2}$	$\frac{\log 2}{6.2}^{\blacksquare}$	first order elimination rate of Leucovorin drug
β_M	1.0	$3.617 \cdot 10^{-5}$	factor for MTX drug dosage
β_L	1.0	1.0	factor for Leucovorin drug dosage $^\diamond$

Table 2.12: Parameters in the *AG Lebiedz* model
$^\diamond$: these parameters have not yet been fitted to experimental data
$^\blacksquare$: values are not results of numerical fit, but defined like that respectively representing the drug half-life

2.6 Other Approaches

Finally we give a short survey on approaches we did not consider in detail. There are lots of different mathematical modelling approaches in cancer chemotherapy context, so we restrict ourselves to some that are neighboring the ones presented above.

Ergun et al. 2001

The model in *Ergun et al.* [19] is—similar to the one in section 2.2—a modification of the *Hahnfeldt*-model [24]. In this article, a combination of radiotherapy and anti-angiogenic therapy is investigated. The major difference in the model is the decoupling of the vasculature equation from tumor volume by simply replacing tumor volume by vasculatur volume. For the radiotherapy an *LQ* (*linear quadratic*) model is used. The authors present several optimal control results.

Chareyron and Alamir 2008

The work by *Chareyron and Alamir* [8] is based on the work by *de Pillis et al.* [11, 12, 13, 10]. The authors use the model presented in section 2.3 to apply *nonlinear model predictive control* (*NMPC*) techniques.

However, only the chemotherapy control is subject of the NMPC scheme while both the immunotherapy and the TIL are derived by *indirect methods* independently from the chemotherapy. The chemotherapy itself is fixed to a finite set of values (0%, 20%, 40%, 60%, 80%, and 100% of maximum). This means chemotherapy in this results is not a continuous control but a mixed-integer one.

The authors propose two optimal control problems. The first one aims to minimize tumor size at the end time while keeping the circulating lymphocyte above a lower bound. The second one maximizes the minimum of circulating lymphocytes over the whole treatment time keeping the tumor size at the end time under a certain fraction of the tumor size at start time.

Since NMPC techniques are not part of this work and we also want to do optimal control of *continuous* chemotherapy, we did not pursue this approach.

De Pillis et al. 2001

De Pillis et al. 2001 [11] is one of the "ancestors" of *de Pillis et al. 2006*. It only includes a chemotherapy control. An optimal control problem is posed (minimize tumor size at end time subject to the number of "normal" cells is above some lower bound) and optimal control results are presented. With one control and the constraint on normal cells, surprising results are not to be expected and indeed the optimal schedules show a bang-bang-structure.

We wanted to verify these results in a `MUSCOD-II` application (chemo2), but some of the model's parameters are only given in relations or intervals (e.g. "$0 \leq s \leq 0.5$", "$a_3 \leq a_1 \leq a_2$"). Several attempts to contact the authors, to get to know the exact parameters they used in their numerical experiments, failed. So this approach was not subject of further investigations.

	Hahnfeldt	d'Onofrio	de Pill. 2006	de Pill. 2008	AG Lebiedz
states	2	2	5/6	6	6
controls	1	2	2/3	2/3	2
parameter sets	1	1	3	1	2
chemotherapy	□	■	■	■	■
immunotherapy	□	□	■	■	■
anti-angiogenesis	■	■	□	□	□
TIL	□	□	■	■	□
optimal control in paper	□	■	□	■	□*
optimal control in this work	□	■	■	■	■
application	chemo1	chemo1	chemo3	chemo3a	chemo4

Table 2.13: An overview over the models implemented and optimized in this work.
*: cooperation work, not published yet, ■: yes, □: no

Isaeva and Osipov 2008

At last, there is an article by *Isaeva and Osipov* [25] on *arXiv.org*. It is somewhat similar to *de Pillis et al. 2006* taking chemotherapy and two types of immunotherapy into account, but the model also has some differences. For example, they use *Gompertz growth* instead of *logistic growth* and just one state for immune cell populations.

Because of the similarities in the structure to *de Pillis et al. 2006*, we decided to investigate only one of the two approaches. Our choice was *de Pillis et al.*, because the scenario with multiple immune cell populations raised expectations for more interesting optimal control results.

Chapter 3

Optimal Control Methods

In the last chapter, within the model presentations, we already formulated some *optimal control problems*. Now we want to explain the methods that have been applied in this thesis to solve these problems, especially with continuous controls. These methods are the base for the *mixed-integer optimal control* approach presented in chapter 4, too. We start with an abstract formulation of the class of problems.

3.1 Problem Formulation

In general, a nonlinear optimization problem looks like

$$\min_{x} \quad f(x) \tag{3.1a}$$

$$\text{subject to} \quad g(x) = 0, \tag{3.1b}$$

$$h(x) \geq 0, \tag{3.1c}$$

with $f : \mathbb{R}^{n_x} \supset D \to \mathbb{R}$, $g : D \to \mathbb{R}^{n_e}$, and $h : D \to \mathbb{R}^{n_i}$. f is called *objective function*, g are the *equality constraints* and h the *inequality constraints*. Obviously, the restriction to min and $h(x) \geq 0$ is no limitation of generality, since $\max f(x)$ is the same as $\min -f(x)$ and so on.

An optimal control problem is a nonlinear optimization problem in some way, but there are also some differences. First of all, in this work, we only consider optimal control problems based on an ODE model. This means, that some variables, the *states*

$$x_i : [t_0, t_f] \to \mathbb{R}, t \mapsto x_i(t), \qquad i \in \{0, \ldots, n_x - 1\}, \tag{3.2}$$

are determined by a set of ODEs (let x be the vector of states x_i),

$$\dot{x}(t) = f(t, x(t), u(t), p), \tag{3.3}$$

depending on the time $t \in [t_0, t_f]$, some free or fixed *parameters* $p \in \mathbb{R}^{n_p}$ and the *controls*

$$u_i : [t_0, t_f] \to \mathbb{R}, t \mapsto u_i(t), \qquad i \in \{0, \ldots, n_u - 1\}, \tag{3.4}$$

which are functions that can be chosen freely (let u be the vector of controls u_i). In addition, we could have some boundary conditions

$$r_e(x(t_0), x(t_f)) = 0, \tag{3.5a}$$

$$r_i(x(t_0), x(t_f)) \geq 0, \tag{3.5b}$$

some control and path constraints

$$g(t, x(t), u(t), p) \geq 0, \tag{3.6}$$

and initial values for the states

$$x(t_0) = \hat{x}_0. \tag{3.7}$$

In the context of cancer chemotherapy, as already described in each model in chapter 2, states are usually tumor volume or population, vasculature volume (with *anti-angiogenesis*) or some kinds of immune cell populations, because their dynamics are given by growth, decay, interaction terms and so on. Drug dosages are generally the controls as they can be influenced directly, e.g. by physicians applying the drugs.

The aim is again to minimize (or maximize) an objective function Φ which is usually written as a sum of a *Mayer term* Φ_M and a *Lagrangian term* Φ_L,

$$\Phi = \Phi_M + \Phi_L \tag{3.8a}$$

$$\text{with } \Phi_M = \Phi_M(t_f, x(t_f), p) \tag{3.8b}$$

$$\text{and } \Phi_L = \int_{t_0}^{t_f} L(t, x(t), u(t), p) \quad dt. \tag{3.8c}$$

Φ is then called *Bolza functional*.

Equations (3.2)–(3.8) together give the following *optimal control problem*, which represents the class of problems we want to solve in this thesis:

$$\min_{x,u,p} \quad \Phi(x, u, p) \tag{3.9a}$$

$$\text{subject to} \quad \dot{x}(t) = f(t, x(t), u(t), p), \tag{3.9b}$$

$$x(t_0) = \hat{x}_0, \tag{3.9c}$$

$$0 = r_e(x(t_0), x(t_f)), \tag{3.9d}$$

$$0 \leq r_i(x(t_0), x(t_f)), \tag{3.9e}$$

$$0 \leq g(t, x(t), u(t), p), \tag{3.9f}$$

$$t \in [t_0, t_f]. \tag{3.9g}$$

Transformations of Time and Objective Functions

Of course, in a general problem, one could wish to have a free end time t_f (or free start time t_0). Especially in the context of our models, we could use a free end time of the treatment while minimizing the tumor population at end time, to let the treatment end when the tumor population is as small as possible. In section 2.2 for example, a problem with free end time is formulated. However, for the description of our methods, we want to restrict the class of problems for simplicity to autonomous problems (no explicit time dependence) with fixed end time and an objective function only consisting of a lagrangian term. This is no restriction to generality since there are simple transformations.

First, we want to ensure the equivalence of Mayer and Lagrangian terms. For the transformation of a lagrangian term into a mayer term, we simply define a new state

$$\dot{x}_{n_x}(t) := L(t, x(t), u(t), p), \tag{3.10}$$

and redefine the corresponding variables $\tilde{x}(t) = (x_0(t), \ldots, x_{n_x-1}(t), x_{n_x}(t))^T$, $\tilde{n}_x = n_x + 1$, and so on. Now with

$$\Phi_M := x_{n_x}(t_f) \tag{3.11}$$

we have transformed the Lagrangian into a Mayer term. For the other direction, we define

$$L(t, x(t), u(t), p) := \frac{\partial \Phi_M}{\partial x}(t, x(t), p) f(t, x(t), u(t), p) + \frac{\partial \Phi_M}{\partial t}(t, x(t), p) \tag{3.12}$$

and hence get

$$\Phi_M(t_f, x(t_f), p) = \Phi_M(t_0, x_0, p) + \int_{t_0}^{t_f} L(t, x(t), u(t), p) \quad dt. \tag{3.13}$$

Because $\Phi_M(t_0, x_0, p)$ is constant, we can omit this part in an objective function and get a Lagrangian functional.

A problem with explicit time-dependence can be transformed into an autonomous problem by adding an ODE for the time,

$$\dot{x}_{n_x} = 1, \qquad x_{n_x}(t_0) = t_0, \tag{3.14}$$

meaning $x_{n_x}(t) = t$. Free end time problems can be transformed by introducing a normed time $\tau \in [0, 1]$ with

$$\tau = \frac{t - t_0}{t_f - t_0} \tag{3.15a}$$

$$\Rightarrow \quad t(\tau) = t_0 + \tau \left(t_f - t_0 \right) \tag{3.15b}$$

$$\Rightarrow \quad d\tau = dt \cdot \left(t_f - t_0 \right), \quad \frac{\partial}{\partial \tau} = \frac{\partial}{\partial t} \left(t_f - t_0 \right). \tag{3.15c}$$

Now, $\hat{t} := (t_f - t_0)$ is introduced as a free parameter and with the transformations

$$\tilde{x}(\tau) := x(t(\tau)), \tag{3.16a}$$
$$\tilde{u}(\tau) := x(t(\tau)), \tag{3.16b}$$
$$\tilde{p} := (p, \hat{t}), \tag{3.16c}$$
$$\frac{\partial \tilde{x}}{\partial \tau} = f(t(\tau), \tilde{x}(\tau), \tilde{u}(\tau), \tilde{p}) \cdot \hat{t} \tag{3.16d}$$
$$=: \tilde{f}(\tau, \tilde{x}(\tau), \tilde{u}(\tau), \tilde{p}), \tag{3.16e}$$
$$\tilde{L} := L(\tau, \tilde{x}(\tau), \tilde{u}(\tau), \tilde{p}), \tag{3.16f}$$
$$\tilde{r}_e(\tilde{x}(0), \tilde{x}(1)) := r_e(\tilde{x}(0), \tilde{x}(1)), \tag{3.16g}$$
$$\tilde{r}_i(\tilde{x}(0), \tilde{x}(1)) := r_i(\tilde{x}(0), \tilde{x}(1)), \tag{3.16h}$$

we get an autonomous problem. For a free start time t_0, we can do the same.

3.2 Discretization with Bock's Direct Multiple Shooting Method

In this work, we use the *direct multiple shooting* method, developed by *Bock and Plitt* [6] in the 1980s, for the solution of optimal control problems. The method is explained in this section. In the articles mentioned in chapter 2, mostly *indirect methods* have been used, in case optimal control was considered at all. These methods in general make use of *Pontryagin's maximum principle* (a *Hamilton-Jacobi-Bellman-equation* approach would be another possibility).

In contrast, with direct multiple shooting, we do not need to compute adjoint equations, which makes the class of problems that can be effectively treated larger.

The issue with the optimal control problem (3.9) is that it is of infinite dimension because the function spaces, where x and u lie in, are infinite-dimensional. Such a problem cannot be treated numerically. Therefore we need a discretization.

Free parameters p are treated as artificial constant states while the initial value is optimized. Thus, the parameter vector is omitted in the following.

Discretization of Controls

We start with the discretization of the controls. The continuous controls are replaced by local *base functions*, such as piecewise constant or piecewise linear functions (see figures 3.1 and 3.2 for examples). It is important that they have compact support. These functions can be described by finitely many parameters.

To do so, we select a time grid

$$t_0 = \tau_0 < \tau_1 < \cdots < \tau_m = t_f, \quad m \in \mathbb{N} \tag{3.17}$$

and with $I_i := [\tau_i, \tau_{i+1}] \; \forall \, i \in \{0, \ldots, m-1\}$ set

$$u(t)\Big|_{I_i} = \phi_i(t, w_i), \quad w_i \in \mathbb{R}^{\mu_i}, \tag{3.18}$$

where the ϕ_i are the base functions. Now we have transformed the infinite-dimensional control u into a finite parameter vector $w = (w_0, \ldots, w_{m-1})$.

Discretization of States

The states x are discretized with *multiple shooting* (see figure 3.3 for an illustration). So we have to choose a time grid again and for efficiency and simplicity we choose the same grid as for the controls. In theory, this is no limitation of generality, as we could refine the grids such that they match and add some constraints. Hence, we have again

$$t_0 = \tau_0 < \tau_1 < \cdots < \tau_m = t_f \quad \text{with } I_i = [\tau_i, \tau_{i+1}] \; \forall \, i \in \{0, \ldots, m-1\}. \tag{3.19}$$

We introduce $m + 1$ new variables $s_0, \ldots, s_m$ which represent the initial values of the ODE on each interval I_i respectively the final value s_m. Now we solve m independent *initial value problems* $\forall \, i \in \{0, \ldots, m-1\}$,

$$\dot{x}(t; \tau_i, s_i) = f(t, x_i(t), \phi_i(t, w_i)), \tag{3.20a}$$
$$x(\tau_i; \tau_i, s_i) = s_i, \tag{3.20b}$$
$$t \in [\tau_i, \tau_{i+1}]. \tag{3.20c}$$

In this work, a BDF-based DAE solver, *DAESOL* [5], has been used to solve the initial value problems. Note that the method is exact if the initial value problems are solved exactly.

Now we need to do some transformations to get a discretized optimal control problem. To ensure equivalence to the original problem, we have to add *matching conditions*, which are the equality constraints

$$s_{i+1} = x(\tau_{i+1}; \tau_i, s_i) \quad \forall \, i \in \{0, \ldots, m-1\}. \tag{3.21}$$
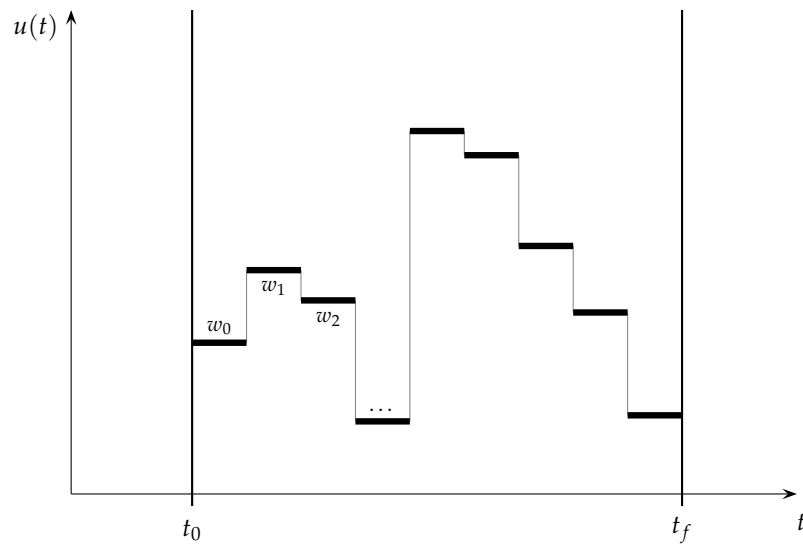
Figure 3.1: Piecewise constant control function
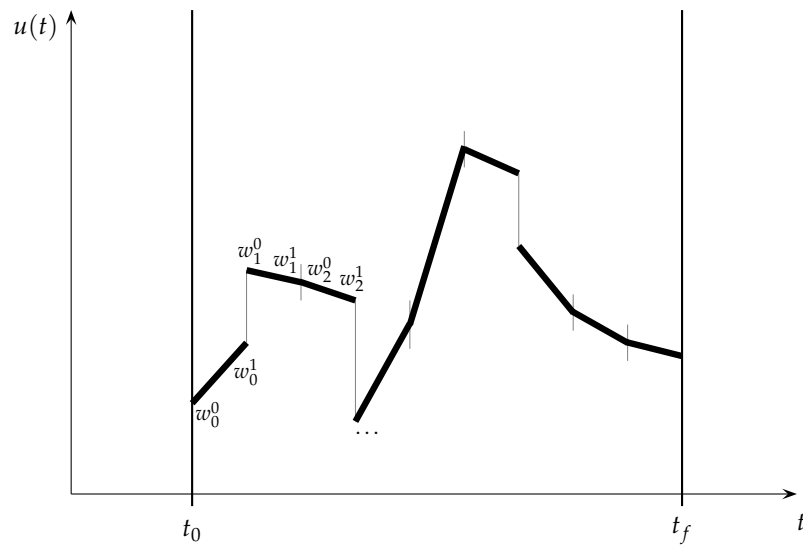
Figure 3.2: Piecewise linear control function

Additionally, the objective function is seperable, though it can be computed seperately on each interval by

$$\int_{t_0}^{t_f} L(t, x(t), \phi(t, w))\, dt = \sum_{i=0}^{m-1} L_i(\tau_{i+1})$$

$$\text{with } L_i(t) = \int_{\tau_i}^{t} L(t', x(t'; \tau_i, s_i), \phi_i(t', w_i))dt', \quad t \in I_i,$$

$$\text{and } \phi(t, w) := \phi_i(t, w_i) \text{ for } t \in I_i. \tag{3.22}$$

The continuous constraints $g(t, x(t), u(t), p) \geq 0$ are now evaluated pointwise on the grid (for the ease of notation, we write $x(\tau_m; \tau_m, s_m) := x(\tau_m; \tau_{m-1}, s_{m-1})$ and $\phi_m(\tau_m, w_m) := \phi_{m-1}(\tau_m, w_{m-1})$ from now on):

$$g(\tau_i, x(\tau_i; \tau_i, s_i), \phi_i(\tau_i, w_i)) \geq 0, \quad \forall\, i \in \{0, \dots, m\} \tag{3.23}$$

Finally, transformed boundary conditions and initial values read

$$r(s_0, s_m) = 0, \tag{3.24a}$$

$$s_0 = \hat{x}_0. \tag{3.24b}$$

Nonlinear Programming Problem

With the discretization above, we have transformed the infinite-dimensional optimal control problem (3.9) into a finite-dimensional *nonlinear programming problem* (NLP). By defining $y := (s_0, w_0, \dots, s_{m-1}, w_{m-1}, s_m)$, we get

$$\min_{y} \quad \sum_{i=0}^{m-1} L_i(\tau_{i+1}) \tag{3.25a}$$

$$\text{s.t.} \quad 0 = s_{i+1} - x(\tau_{i+1}; \tau_i, s_i) \qquad\qquad \forall\, i \in \{0, \dots, m-1\}, \tag{3.25b}$$

$$0 \leq g(\tau_i, x(\tau_i; \tau_i, s_i), \phi_i(\tau_i, w_i)), \qquad\qquad \forall\, i \in \{0, \dots, m\}, \tag{3.25c}$$

$$0 = r_e(s_0, s_m), \tag{3.25d}$$

$$0 \leq r_i(s_0, s_m), \tag{3.25e}$$

$$0 = s_0 - \hat{x}_0. \tag{3.25f}$$

3.3 Solution of the NLP with an SQP Method

After the discretization of the optimal control method in section 3.2, the resulting *nonlinear programming problem* (*NLP*) is solved with an *SQP* (*sequential quadratic programming*) method. This technique has been introduced by *Wilson* [41], *Han*, and *Powell* [34].

The result of section 3.2 is an NLP of the form

$$\min_{x} \quad f(x) \tag{3.26a}$$

$$\text{subject to} \quad g(x) = 0, \tag{3.26b}$$

$$h(x) \geq 0, \tag{3.26c}$$
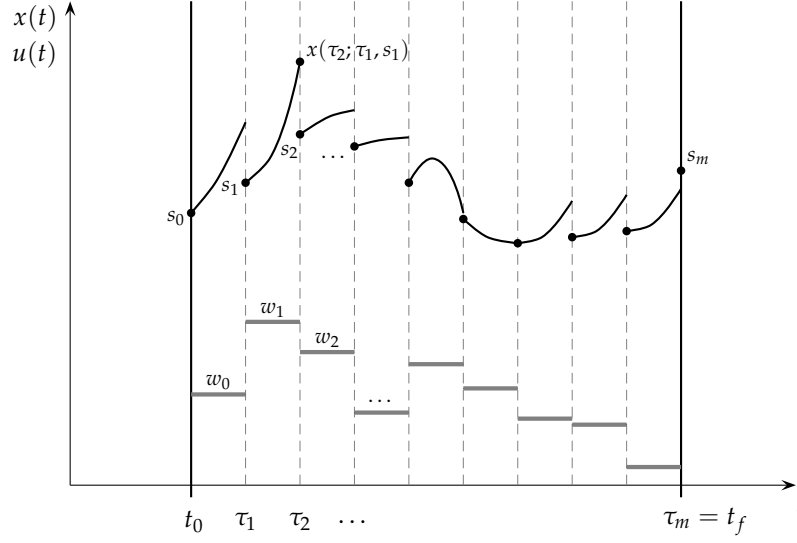
Figure 3.3: Illustration of multiple shooting with piecewise constant control

with probably nonlinear f, g, and h. Instead of considering this problem, starting with some initial value x_0, we compute the iterates x^k with a step size $t^k \in (0, 1]$,

$$x^{k+1} = x^k + t^k \Delta x^k, \tag{3.27}$$

by solving a related quadratic program (QP),

$$\min_{\Delta x} \quad \frac{1}{2} \Delta x^T H^k \Delta x + \nabla f(x^k)^T \Delta x \tag{3.28a}$$

$$\text{subject to} \quad g(x^k) + \nabla g(x^k)^T \Delta x = 0, \tag{3.28b}$$

$$h(x^k) + \nabla h(x^k)^T \Delta x \geq 0, \tag{3.28c}$$

where H^k is set e.g. to the Hessian of the Lagrangian of the problem or some kind of approximation of the Hessian. We compute the step size by a *line search*.

This is equivalent to a Newton-type method. For more information we refer to relevant literature, e.g. to *Nocedal and Wright* [33]. The Hessian resulting from the multiple shooting discretization features a special structure which can and should be exploited in the SQP algorithm.

3.4 MUSCOD-II

The methods and techniques described in the previous sections are implemented in the software package MUSCOD-II (*multiple shooting code for direct optimal control*) [30]. This package is developed in the *Simulation and Optimization* group of H.G. Bock and J.P. Schlöder and has been used to solve the optimal control problems in this thesis. Results are presented in chapter 5.

Chapter 4

A Mixed-Integer Optimal Control Approach

While the last chapter focused on methods applied for continuous optimal control, in this chapter we introduce a mixed-integer optimal control approach which has also been applied to the models presented in chapter 2. First, we explain our motivation to calculate mixed-integer respectively binary controls and give a problem formulation. Then we present an approach developed by *Sager et al.* [36, 39]. We conclude with the presentation of a new rounding heuristic, which has been implemented in MUSCOD-II for this thesis.

4.1 Motivation and Problem Formulation

The treatments included in the different models are all continuous from the model point of view. Therefore we apply continuous optimal control methods. It is possible that the optimal control of such a continuous problem is of *bang-bang* type. This means, that it piecewise takes either the maximum or the minimum feasible value. But it is still possible, see e.g. the numerical results in the next chapter, that all or part of the control consists of a *singular arc*. A *singular arc* takes values between minimum and maximum. From a mathematical respectively theoretical point of view, this is no problem. Though, even if the models are not yet good enough, calculating an optimal treatment aims to improve existing treatments in reality of course. And in reality, today it is not possible to apply a treatment which follows a singular arc [29].

Ledzewicz et al. [29] approximate the singular control by splitting the treatment interval into parts after the computation of the optimal controls. Then they approximate the optimal control by piecewise constant controls. This may lead to the same results as our direct multiple shooting approach with few nodes. As there already are efficient algorithms to compute mixed-integer or binary controls, especially if we already have continuous optimal controls, our approach differs from that one. *Sager et al.* [39] showed that every continuous control can be arbitrary closely approximated by a binary control. Hence it might be interesting to also compute binary treatment controls and to compare them to the continuous ones.

So, compared to problem (3.9), we now have additional binary control functions $w(t)$ and some binary parameters v,

$$w(t) \in \{0,1\}^{n_w}, \tag{4.1a}$$
$$v \in \{0,1\}^{n_v}. \tag{4.1b}$$

The objective function and the right hand side of the ODE may depend on both w and v, control and path constraints only on v. The resulting problem is the following *mixed-integer optimal control problem*. This is the problem class we want to solve with our mixed-integer

optimal control approach.

$$\min_{x,u,w,p,v} \quad \Phi(x,u,w,p,v) \tag{4.2a}$$

$$\text{subject to} \quad \dot{x}(t) = f(t, x(t), u(t), w(t), p, v), \tag{4.2b}$$
$$x(t_0) = \hat{x}_0, \tag{4.2c}$$
$$0 = r_e(x(t_0), x(t_f)), \tag{4.2d}$$
$$0 \leq r_i(x(t_0), x(t_f)), \tag{4.2e}$$
$$0 \leq g(t, x(t), u(t), p, v), \tag{4.2f}$$
$$w(t) \in \{0,1\}^{n_w}, \tag{4.2g}$$
$$v \in \{0,1\}^{n_v}, \tag{4.2h}$$
$$t \in [t_0, t_f]. \tag{4.2i}$$

4.2 Convexification

In this section, problem (4.2) will be convexified as in [39] with respect to the binary control w, while from other aspects the problem still may be nonconvex. This is necessary preparatory work for the theoretical results at the end of the section upon which our algorithms are based.

For simplicity, we now omit path and control constraints g and boundary conditions r_i and r_e. By doing that we derive the following binary nonlinear problem (BN) from (4.2):

$$\min_{x,u,w,p,v} \quad \Phi(x,u,w,p,v) \tag{4.3a}$$

$$\text{subject to} \quad \dot{x}(t) = f(t, x(t), u(t), w(t), p, v), \tag{4.3b}$$
$$x(t_0) = \hat{x}_0, \tag{4.3c}$$
$$w(t) \in \{0,1\}^{n_w}, \tag{4.3d}$$
$$v \in \{0,1\}^{n_v}, \tag{4.3e}$$
$$t \in [t_0, t_f]. \tag{4.3f}$$

If we replace (4.3d) by $w(t) \in [0,1]^{n_w}$, which means that w is considered to be continuous between 0 and 1 in each component, we get a new problem, which we call relaxed nonlinear (RN),

$$\min_{x,u,w,p,v} \quad \Phi(x,u,w,p,v) \tag{4.4a}$$

$$\text{subject to} \quad \dot{x}(t) = f(t, x(t), u(t), w(t), p, v), \tag{4.4b}$$
$$x(t_0) = \hat{x}_0, \tag{4.4c}$$
$$w(t) \in [0,1]^{n_w}, \tag{4.4d}$$
$$v \in \{0,1\}^{n_v}, \tag{4.4e}$$
$$t \in [t_0, t_f]. \tag{4.4f}$$

The convexification is done by a linearization of the ODE equation in w. So we replace (4.3c) by

$$\dot{x}(t) = \sum_{i=1}^{n_{\tilde{w}}} f(t, x(t), u(t), w^j, p, v)\, \tilde{w}_i(t) \tag{4.5}$$

with $\tilde{w}(t) \in \{0,1\}^{n_{\tilde{w}}}$, $\tilde{w} = (\tilde{w}_1, \ldots, \tilde{w}_{n_{\tilde{w}}})^T$. The w^j enumerate all possible binary controls, so in general $n_{\tilde{w}} = 2^{n_w}$. *Sager et al.* state that in real applications, $n_{\tilde{w}}$ is often "linear in the number of choices". To have an equivalent linearized problem, we add an *SOS1*-constraint

$$\sum_{i=1}^{n_{\tilde{w}}} \tilde{w}(t) = 1. \tag{4.6}$$

The resulting problem (binary convex—BC) is convex in $\tilde{w}$ and looks like

$$\min_{x,u,\tilde{w},p,v} \quad \Phi(x, u, \tilde{w}, p, v) \tag{4.7a}$$

$$\text{subject to} \quad \dot{x}(t) = \sum_{i=1}^{n_{\tilde{w}}} f(t, x(t), u(t), w^j, p, v)\, \tilde{w}_i(t), \tag{4.7b}$$

$$x(t_0) = \hat{x}_0, \tag{4.7c}$$

$$\tilde{w}(t) \in \{0,1\}^{n_{\tilde{w}}}, \tag{4.7d}$$

$$\sum_{i=1}^{n_{\tilde{w}}} \tilde{w}(t) = 1 \tag{4.7e}$$

$$v \in \{0,1\}^{n_v}, \tag{4.7f}$$

$$t \in [t_0, t_f]. \tag{4.7g}$$

Again, by replacing (4.7d) with $\tilde{w}(t) \in [0,1]^{n_{\tilde{w}}}$, we get the corresponding relaxed convex problem (RC), which reads

$$\min_{x,u,\tilde{w},p,v} \quad \Phi(x, u, \tilde{w}, p, v) \tag{4.8a}$$

$$\text{subject to} \quad \dot{x}(t) = \sum_{i=1}^{n_{\tilde{w}}} f(t, x(t), u(t), w^j, p, v)\, \tilde{w}_i(t), \tag{4.8b}$$

$$x(t_0) = \hat{x}_0, \tag{4.8c}$$

$$\tilde{w}(t) \in [0,1]^{n_{\tilde{w}}}, \tag{4.8d}$$

$$\sum_{i=1}^{n_{\tilde{w}}} \tilde{w}(t) = 1 \tag{4.8e}$$

$$v \in \{0,1\}^{n_v}, \tag{4.8f}$$

$$t \in [t_0, t_f]. \tag{4.8g}$$

The four different problems are used to proof theoretical results on relations between their solutions. First of all, we derive a comparison between problems BN and BC. For proofs of the theorems we refer to *Sager et al.* [39]. Note that all problems in this thesis are already in the form 4.7 respectively 4.8 as all controls enter *linearly* in the right hand side function.

Theorem 4.1 (Comparison of binary solutions [39])
If problem (BC) has an optimal solution $(x^*, \bar{w}^*, u^*, v^*, p^*)$ with objective value Φ^{BC}, then there exists an n_w–dimensional control function $w^*(\cdot)$ such that the trajectory $(x^*, w^*, u^*, v^*, p^*)$ is an optimal solution of problem (BN) with objective value Φ^{BN} and

$$\Phi^{BC} = \Phi^{BN}. \tag{4.9}$$

The converse holds as well.

The next step is a comparison between problems (BC) and (RC).

Theorem 4.2 (Comparison of solutions of the convexified problem [39])
Let problem (RC) have a feasible solution $(x^*, \bar{w}^*, u^*, v^*, p^*)$ with objective value Φ^{RC}. Let furthermore $f(x, w, u^*, v^*, p^*)$ with fixed (u^*, v^*, p^*) be globally Lipschitz continuous with respect to $x(\cdot)$ for all admissable binary controls $w(\cdot)$.

Then for any given $\epsilon > 0$ there exists a binary admissable control function $\bar{w}$ and a state trajectory $\bar{x}$ such that $(\bar{x}, \bar{w}, u^*, v^*, p^*)$ is a feasible solution of problem (BC) with objective value Φ^{BC} and

$$\Phi^{BC} \leq \Phi^{RC} + \epsilon. \tag{4.10}$$

This means that every continuous control can be arbitrarily approximated by a binary control. Though, such a solution could have to switch infinite times, which is known as *chattering* or *Zeno's phenomenon* in the literature [42, 43]. Some of the solutions in chapter 5 show such a behaviour. In [39] it has been shown that even a finite number of switches is sufficient for every $\epsilon > 0$. Finally we give a comparison of all solutions.

Theorem 4.3 (Comparison of solutions [39])
If problem (RC) has an optimal solution $(x^*, \bar{w}^*, u^*, v^*, p^*)$ with objective value Φ^{RC}, Then for any given $\epsilon > 0$ there exists a binary admissable control function $\bar{w}$ and a state trajectory $\bar{x}$ such that $(\bar{x}, \bar{w}, u^*, v^*, p^*)$ is a feasible solution of problem (BC) with objective value Φ^{BC} and a n_w–dimensional control function $w^*(\cdot)$ such that the trajectory $(\bar{x}^*, w, u^*, v^*, p^*)$ is a feasible solution of problem (BN) with objective value Φ^{BN} and it holds

$$\Phi^{RN} \leq \Phi^{RC} \leq \Phi^{BC} = \Phi^{BN} \leq \hat{\Phi}^{BN} \tag{4.11}$$

and

$$\Phi^{BN} = \Phi^{BC} \leq \Phi^{RC} + \epsilon, \tag{4.12}$$

where $\hat{\Phi}^{RN}$ is the objective function value of any feasible solution to problem (BN).

For the path and interior point constraints we omitted, one has to choose a priori tolerances $\epsilon_c, \epsilon_r > 0$. These constraints can only be fulfilled up to these tolerances and the proof of theorem 4.3 can be extended, so that the tolerances are fulfilled.

4.3 MS MINTOC–Algorithm with Sum-Up Rounding

For the solution of problem (4.2) we need to solve relaxed problems. Therefore we discretize using direct multiple shooting as described in chapter 3. In the following we refer to the time grid as $\mathcal{G} = \{\tau_0, \ldots, \tau_{m-1}\}$ and we assume piecewise constant control functions u and w. With q_i we refer to the relaxed value of w on interval I_i, $q_i \in [0, 1]^{n_w}$, and with w_i to the binary values, $w_i \in \{0, 1\}^{n_w}$. By h_i we denote the *time horizon lengths* $\tau_{i+1} - \tau_i$ for $i \in \{0, \ldots, m-1\}$.

Grid Adaptivity

By discretizing the control functions, we choose a certain subspace of the infinite-dimensional control space. So the optimal solution with discretized control functions in general will have a higher (or lower in case of max) objective value than the optimal trajectory $\mathcal{T}^*$ of the full, infinite-dimensional space.

In an optimal control, one distinguishes between bang-bang segments, where the control takes either maximum or minimum, and singular arcs, where the control lies between minimum or maximum. In case of a bang-bang control, our aim should be to select a time grid, which allows us to reproduce these bang-bang structure with our discretized control function, too. Therefore, we would need time grid points at the switching times of $\mathcal{T}^*$. As it is unlikely that our grid points meet those switching time points by chance, we want to modify our time grid correspondingly. The first method to do this is the *grid adaptivity* approach described in the following. Another possibility would be the *switching-time optimization* which we describe a little below.

We now consider a grid $\mathcal{G}^k$ with k grid points and a one-dimensional control w. Then we apply the following technique depending on the value of q_i.

$$q_i = 0 \implies \text{assume } w_i = 0 \tag{4.13a}$$

$$q_i = 1 \implies \text{assume } w_i = 1 \tag{4.13b}$$

$$q_i \notin \{0,1\} \implies \text{add additional time point } \tau^* \tag{4.13c}$$

This means that we only refine the grid where the relaxed solution is not of bang-bang type. Finally, we have to determine the exact value of $\tau^* = \tau_i + \gamma(\tau_{i+1} - \tau_i)$ and add it to our grid to get $\mathcal{G}^{k+1} := \mathcal{G} \cup \tau^*$. *Sager et al.* suggest to use

$$\gamma \approx q_i \qquad \text{if } q_{i-1} = 1 \text{ and } q_{i+1} = 0 \tag{4.14a}$$

$$\gamma \approx 1 - q_i \qquad \text{if } q_{i-1} = 0 \text{ and } q_{i+1} = 1 \tag{4.14b}$$

and a bisection

$$\gamma = \frac{1}{2} \tag{4.15}$$

if $0 < q_{i-1} < 1$ or $0 < q_{i+1} < 1$. There is an illustration in figure 4.1.

In the multi-dimensional case one can either apply the rules above to each dimension, or, since grid adaptivity is an iterative process, select the one with the highest integer gap,

$$\max_j \min(q_{j,i}, 1 - q_{j,i}). \tag{4.16}$$

Sum Up Rounding

The idea of rounding strategies is to solve the relaxed problem first and then to apply rounding heuristics on the relaxed controls. Also, after applying some grid adaptivity iterations, there may be still some q_i which are not 0 or 1, e.g. the ones corresponding to a singular arc.

In [39], three different strategies—standard rounding ("SR"), sum up rounding ("SUR") and sum up rounding with a different threshold ("SUR-0.5")—are presented. In this work, we use sum up rounding with threshold 0.5 ("SUR-0.5"):

$$w_{j,i} = \begin{cases} 1 & \text{if } \sum_{k=0}^{i} q_{j,k} - \sum_{k=0}^{i-1} w_{j,k} \geq 0.5 \\ 0 & \text{else} \end{cases} \tag{4.17}$$
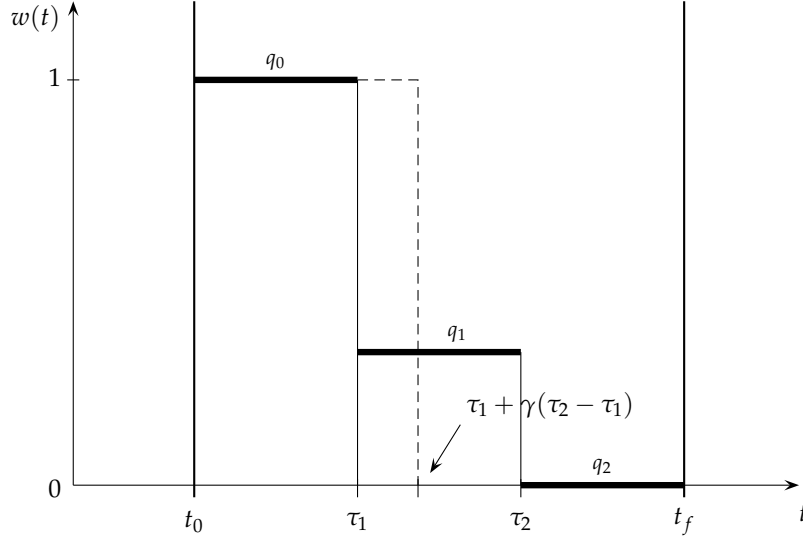
Figure 4.1: Illustration of grid adaptivity in MS MINTOC

SOS1-variables need special care, as the SOS1 constraint could be violated by the rules above. For such variables, with $\hat{q}_{j,k} := \sum_{k=0}^{i} q_{j,k} - \sum_{k=0}^{i-1} w_{j,k}$ a modified rule is used:

$$w_{j,i} = \begin{cases} 1 & \text{if } \hat{q}_{j,i} \geq \hat{q}_{k,i} \forall k \neq j \quad \text{and} \quad j < k \ \forall k \text{ with } \hat{q}_{j,i} = \hat{q}_{k,i} \\ 0 & \text{else} \end{cases} \tag{4.18}$$

With such rounding strategies, of course, the solution is binary. But on the other hand, in general it is suboptimal and may not even be feasible.

Switching Time Optimization

In switching time optimization, one considers a fixed control function (first for the one-dimensional case $n_w = 1$)

$$w(t) = \begin{cases} 1 & \text{if } t \in I_i \text{ with } i \text{ even} \\ 0 & \text{if } t \in I_i \text{ with } i \text{ odd} \end{cases} \tag{4.19}$$

and instead of free control values, the switching times τ_i respectively the time horizons h_i and the number of grid points are considered free. See figure 4.2 for an illustration. We need to add the constraint

$$\sum_{k=0}^{m-1} h_k = t_f - t_0. \tag{4.20}$$

For multi-dimensional controls we use

$$w(t) = w^i \quad \text{if } t \in I_k \text{ with } k = j2^{n_w} + i - 1 \tag{4.21}$$

for some $j \in \mathbb{N}_0$ and some $i \in \{1, \ldots, 2^{n_w}\}$, while the w^i enumerate all possible values for $w(t)$. These problems can be considered as *multi-stage mixed-integer optimal control problems*
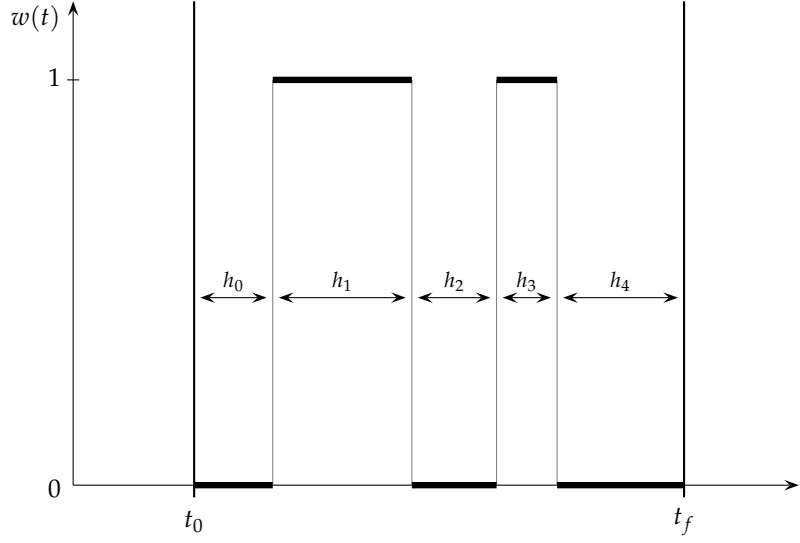
Figure 4.2: Illustration of switching time optimization in MS MINTOC

with h_i and m as free parameters. For details we refer to *Sager et al.* [39]. Note that for our applications we are interested in a fixed time grid due to practical restrictions (hospital, pharmacy) so we do not apply any grid refinement technique.

MS MINTOC

Now we bring all the techniques described above together in the following MS MINTOC-algorithm as proposed by *Sager et al.* The proof of the well-posedness of this algorithm is given in [37, 36]. For applications, e.g. to automobile test drives, see [38] and [26]. A *benchmark library* of *mixed-integer optimal control problems* is available at [35].

Algorithm 4.4 (MS MINTOC [39])
Let $\mathcal{G}_0$ be an initial discretization grid for which a feasible trajectory of the relaxed problem exists. Let furthermore be $\epsilon > 0$ which determines how large the gap between relaxed and binary solution may be.

1. *Convexify problem (4.2) with respect to $w(\cdot)$ as described in section 4.2.*

2. *Relax this problem to $\tilde{w}(\cdot) \in [0,1]^{n_{\tilde{w}}}$.*

3. *Solve this problem for control discretization $\mathcal{G}^0$, obtain grid-dependent optimal value $\Phi_{\mathcal{G}^0}^{RC}$ of the trajectory $\mathcal{T}_0$*

4. *Refine control discretization grid n_{ext} times as described above and obtain $\Phi_{\mathcal{G}^{n_{ext}}}^{RC}$ as the objective function value on the finest grid $\mathcal{G}^{n_{ext}}$. Set $\Phi^{RC} = \Phi_{\mathcal{G}^{n_{ext}}}^{RC}$ to this upper bound on Φ^* and $\mathcal{T} = \mathcal{T}^{n_{ext}}$.*

5. *If the optimal control on $\mathcal{G}^{n_{ext}}$ is binary admissable then* stop, *else $k = n_{ext}$.*

6. *Fix the variables $u^*(\cdot), p^*, v^*$ and the initial values x_0^*.*

7. Repeat

   a) *Apply a rounding heuristic to $\mathcal{T}$*

   b) *Use switching time optimization, see above, initialized with the rounded solution of the previous step. If the obtained trajectory is feasible, obtain upper bound Φ^S. If $\Phi^S < \Phi^{RC} + \epsilon$ then* stop.

   c) *Refine the control grid $\mathcal{G}^k$ as described above, based on the control values of trajectory $\mathcal{T}$*

   d) *Solve relaxed problem, $\mathcal{T} = \mathcal{T}^k$, $k = k + 1$.*

4.4 Decomposed MILP/Integral Approximation–Algorithm

Binary optimal controls computed with the MS MINTOC-algorithm with sum-up rounding may show a *chattering* behaviour. In the introduction, we explained that we are interested in mixed-integer respectively binary solutions because of the medical feasibility. A solution with *chattering* of course will not be more applicable than a singular arc. To avoid chattering in a solution, one could wish to limit the number of switches in the optimal solution. In this thesis, we investigate the heuristics described in the following for this purpose.

Instead of applying sum-up rounding—step 7. a) in MS MINTOC—, we solve a *mixed-integer linear program* (*MILP*) for each control w_i—decomposed from our optimization framework as described in chapter 3. For simplicity, we consider only the case of binary controls. The values of the binary control w are identified as w_i and for the relaxed control values we write q_i with $i \in \{0, \ldots, m-1\}$ and m the number of time grid points τ_i. Again, we assume piecewise constant controls, compare section 3.2.

Powerful commercial *MILP* solvers and advances in *MINLP* (*mixed-integer nonlinear program*) solvers, [4, 7], make the usage of general purpose MILP/MINLP solvers more and more attractive. The *mixed-integer optimal control problem* (*MIOCP*) may be discretized by a direct method and results in MILP, e.g. [32], or a MINLP, e.g. [23], with a finite number of mixed-integer variables. However, due to the high complexity of MINLPs and the increase in the number of integer variables, whenever the discretization grid is refined, this only works for small problems with limited time horizons, see [40] for a discussion.

Our aim is to minimize the difference between binary and continuous control on the one hand and to keep the number of switches in the binary control below some N on the other hand. The first point is realized by

$$\min_{\eta, w, s} \quad \eta \tag{4.22a}$$

$$\text{subject to} \quad \left| \sum_{j=0}^{i} w_j - q_j \right| \leq \eta \qquad \forall i \in \{0, \ldots, m-1\}. \tag{4.22b}$$

We need the constraint (4.22b) $\forall i \in \{0, \ldots, m-1\}$ because we want to minimize the difference between the w_i and the q_i for *each* time $t \in [t_0, t_f]$ respectively, as an approximation, on the corresponding time grid $\{\tau_0, \ldots, \tau_m\}$. For the restriction of the number of switches, we introduce *slack variables* s_j with $j \in \{0, \ldots, m-2\}$ and add the restrictions

$$\left| w_j - w_{j+1} \right| \leq s_j \qquad \forall j \in \{0, \ldots, m-2\}, \tag{4.23a}$$

$$\sum_{j=0}^{m-2} s_j \leq N. \tag{4.23b}$$

Hence, we get the following *mixed-integer nonlinear program* (*MINLP*):

$$\min_{\eta,w,s} \quad \eta \tag{4.24a}$$

$$\text{subject to} \quad \left| \sum_{j=0}^{i} w_j - q_j \right| \le \eta \qquad \forall i \in \{0, \dots, m-1\}, \tag{4.24b}$$

$$\left| w_j - w_{j+1} \right| \le s_j \qquad \forall j \in \{0, \dots, m-2\}, \tag{4.24c}$$

$$\sum_{j=0}^{m-2} s_j \le N. \tag{4.24d}$$

This problem can be easily tranformed into a *mixed-integer linear program* by replacing the norms in (4.24b) and (4.24c) by

$$\sum_{j=0}^{i} w_j - q_j \le \eta \qquad \forall i \in \{0, \dots, m-1\}, \tag{4.25a}$$

$$-\sum_{j=0}^{i} w_j - q_j \le \eta \qquad \forall i \in \{0, \dots, m-1\}, \tag{4.25b}$$

and

$$w_j - w_{j+1} \le s_j \qquad \forall j \in \{0, \dots, m-2\}, \tag{4.26a}$$

$$-w_j + w_{j+1} \le s_j \qquad \forall j \in \{0, \dots, m-2\}. \tag{4.26b}$$

The derived MILP reads as follows. For this problem class, there are lots well-known standard techniques and lots of solvers. In this work, we use `Cbc` [2], an open-source branch-and-cut-solver from the COIN-OR project [1]. The problem is formulated in `AMPL` [21], so we use the solver via the `AMPL` solver interface.

$$\min_{\eta,w,s} \quad \eta \tag{4.27a}$$

$$\text{subject to} \quad \sum_{j=0}^{i} w_j - q_j \le \eta \qquad\qquad \forall i \in \{0, \dots, m-1\}, \tag{4.27b}$$

$$-\sum_{j=0}^{i} w_j - q_j \le \eta \qquad\qquad \forall i \in \{0, \dots, m-1\}, \tag{4.27c}$$

$$w_j - w_{j+1} \le s_j \qquad\qquad \forall j \in \{0, \dots, m-2\}, \tag{4.27d}$$

$$-w_j + w_{j+1} \le s_j \qquad\qquad \forall j \in \{0, \dots, m-2\}, \tag{4.27e}$$

$$\sum_{j=0}^{m-2} s_j \le N. \tag{4.27f}$$

The *Integral Approximation* solutions converge against the relaxed solution when N and the number of grid points go to infinity, but not necessarily in a monotone way in N on a fixed grid. An implementation of this algorithm in the `MUSCOD-II` framework is part of this work. Results of the application on some of the models from chapter 2 are given in the next chapter. Additional analytical insight is subject of current research in the workgroup of *Sebastian Sager*.

Chapter 5

Numerical Results: Optimal Control of Cancer Chemotherapy Models

In this chapter, we present the numerical results derived from the models presented in chapter 2 by applying the methods from chapter 3 and 4. Where no optimal control problems were posed, we formulate one. The chapter is split into a section for each parameter set we investigated. As already mentioned before, the *Hahnfeldt*-model has only been used to verify our simulation results. For all other models respectively parameter sets, optimal control results are given.

5.1 Hahnfeldt Simulation

First of all, we recall the model equations (2.9):

$$\dot{x}_0(t) = -\zeta\, x_0(t) \log\left(\frac{x_0(t)}{x_1(t)}\right), \tag{5.1a}$$

$$\dot{x}_1(t) = b\, x_0(t) - \mu\, x_1(t) + d\, x_0(t)^{\frac{2}{3}} x_1(t) - G\, g(t)\, x_1(t), \tag{5.1b}$$

$$g(t) = \int_0^t u_0(t') \exp\left(-\gamma\,(t - t')\right) dt', \tag{5.1c}$$

$$0 \leq u_0(t), x_0(t), x_1(t), \tag{5.1d}$$

$$t \in [t_0, t_f]. \tag{5.1e}$$

There are three different drugs (*Angiostatin*, *Endostatin*, and *TNP-470*) that have been applied to mice in different doses and different treatment lengths. The dosage $u_0(t')$ was taken to be

$$c(t') = D \cdot \left(\delta(t' - t_1) + \cdots + \delta(t' - t_{n_d})\right) \tag{5.2}$$

where D is the actual dosage, t_i the drug admission times, n_d the number of drug admissions, and δ the delta distribution. The delta distribution is used to simulate injections. This cannot be realized in our discretized framework, so we approximated the dosage function by using 24 grid points for each day (one for each hour) and setting the dosage function to

$$c(t') = \frac{D}{1/24} \tag{5.3}$$

on the first interval of each treatment day.

From the different combinations of initial values, treatment lengths, and drugs, we picked at least one per drug to verify our results. Exact values from *Hahnfeldt et al.* are not known, hence we use the plots from the paper for verification. A part of the plots shows measurement points

$x_0(t_0)$	$x_1(t_0)$	treatment	length	grid points	
200	625	none (control group)	20 days	100	figure 5.1
200	625	none (control group)	50 days	100	figure 5.1
177	625	Endostatin, 20 mg/kg/day	10 days	240	figure 5.2
170	625	Angiostatin, 20 mg/kg/day	14 days	336	figure 5.3
170	625	TNP-470, 30 mg/kg, every second day	14 days	336	figure 5.4

Table 5.1: Combinations of initial values, treatment lengths, and drugs which have been used for verification of the results from *Hahnfeldt et al.*

and deviations onto which the parameters have been fitted. In table 5.1, the combinations we used are listed.

The results from the article could all be reproduced correctly, as far as one can tell from the plots. See figures 5.1, 5.2, 5.3, and 5.4 for the comparisons. Note that these results are not *optimal control* results but *simulation* results.

5.2 d'Onofrio Optimal Control

The model is described by the equations (2.18), which read

$$\dot{x}_0(t) = -\zeta\, x_0(t) \ln\left(\frac{x_0(t)}{x_1(t)}\right) - F\, x_0(t)\, u_1(t), \tag{5.4a}$$

$$\dot{x}_1(t) = b\, x_0(t) - \mu\, x_1(t) + d\, x_0(t)^{\frac{2}{3}} x_1(t) \\ - G\, u_0(t)\, x_1(t) - \eta\, x_1(t)\, u_1(t), \tag{5.4b}$$

$$\dot{x}_2(t) = u_0(t), \tag{5.4c}$$

$$\dot{x}_3(t) = u_1(t), \tag{5.4d}$$

$$0 \le a - u_0(t), \tag{5.4e}$$

$$0 \le c - u_1(t), \tag{5.4f}$$

$$0 \le A - x_2(t_f), \tag{5.4g}$$

$$0 \le C - x_3(t_f), \tag{5.4h}$$

$$0 \le u_0(t), u_1(t), x_0(t), x_1(t), \tag{5.4i}$$

$$t \in [t_0, t_f]. \tag{5.4j}$$

Different optimal control problems, called *scenarios*, are solved in the article. They all share the same objective,

$$\min \quad x_0\left(t_f\right) + 0.005 \int_{t_0}^{t_f} u_0(t)^2 \quad dt, \tag{5.5}$$

while the end time t_f is free. The differences between them lie in the different bounds c and C and in the initial values. Table 5.2 gives an overview.

The different techniques from chapter 3 and 4 have been applied to this model. We tried to reproduce the results from the paper first. Comparisons for each scenario are given in
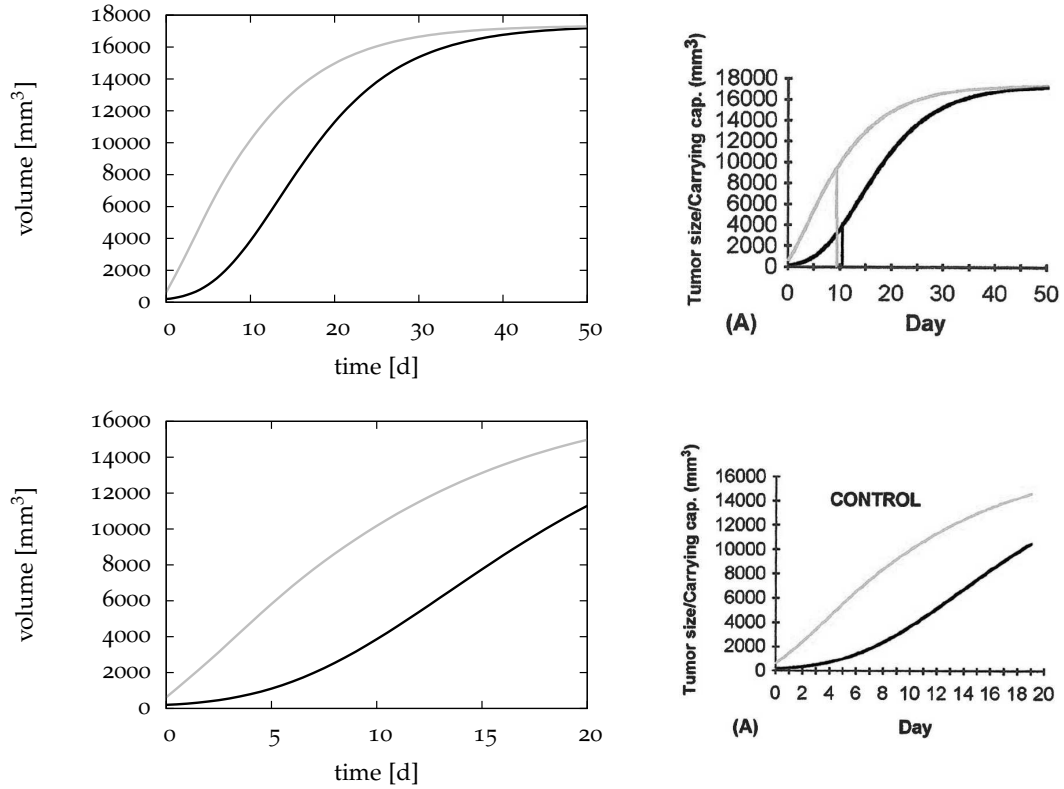
Figure 5.1: Comparison between MUSCOD-II simulation results (left) and *Hahnfeldt et al.* (right), control group. Top: 50 days, bottom: 20 days. Vasculature volume is bright, tumor volume dark.
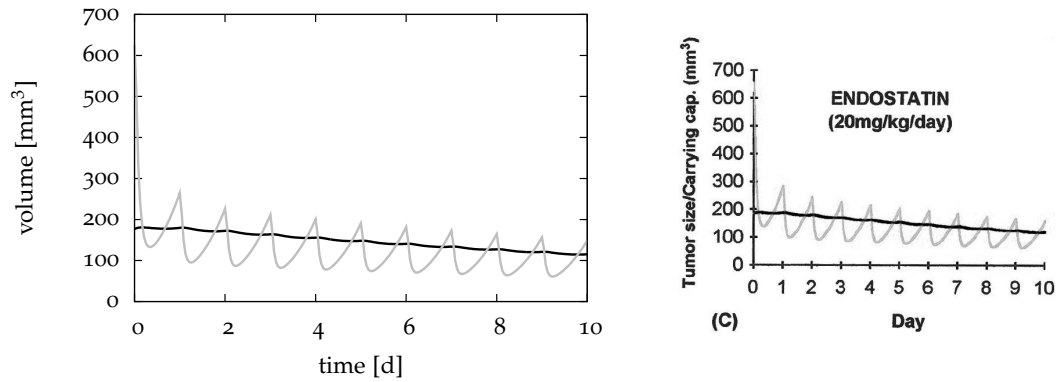
Figure 5.2: Comparison between MUSCOD-II simulation results (left) and *Hahnfeldt et al.* (right), endostatin therapy, 10 days. Vasculature volume is bright, tumor volume dark. Dose was 20mg/kg/day.
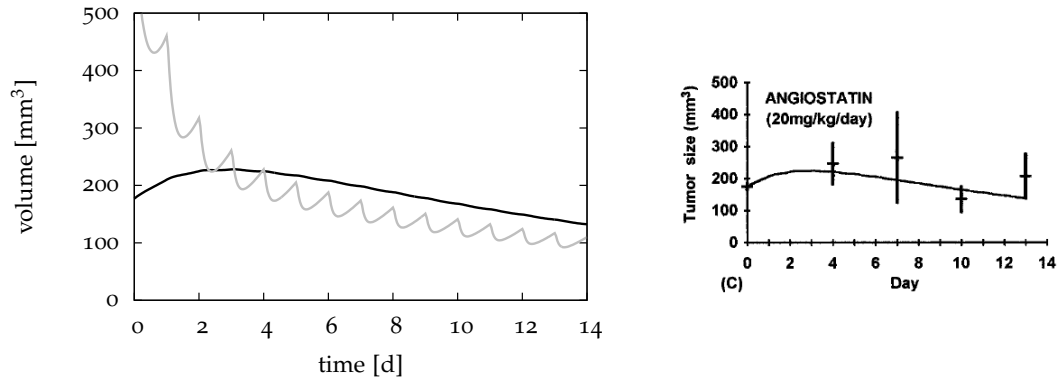
Figure 5.3: Comparison between MUSCOD-II simulation results (left) and *Hahnfeldt et al.* (right), angiostatin therapy, 14 days. Vasculature volume is bright, tumor volume dark. Dose was 20mg/kg/day.
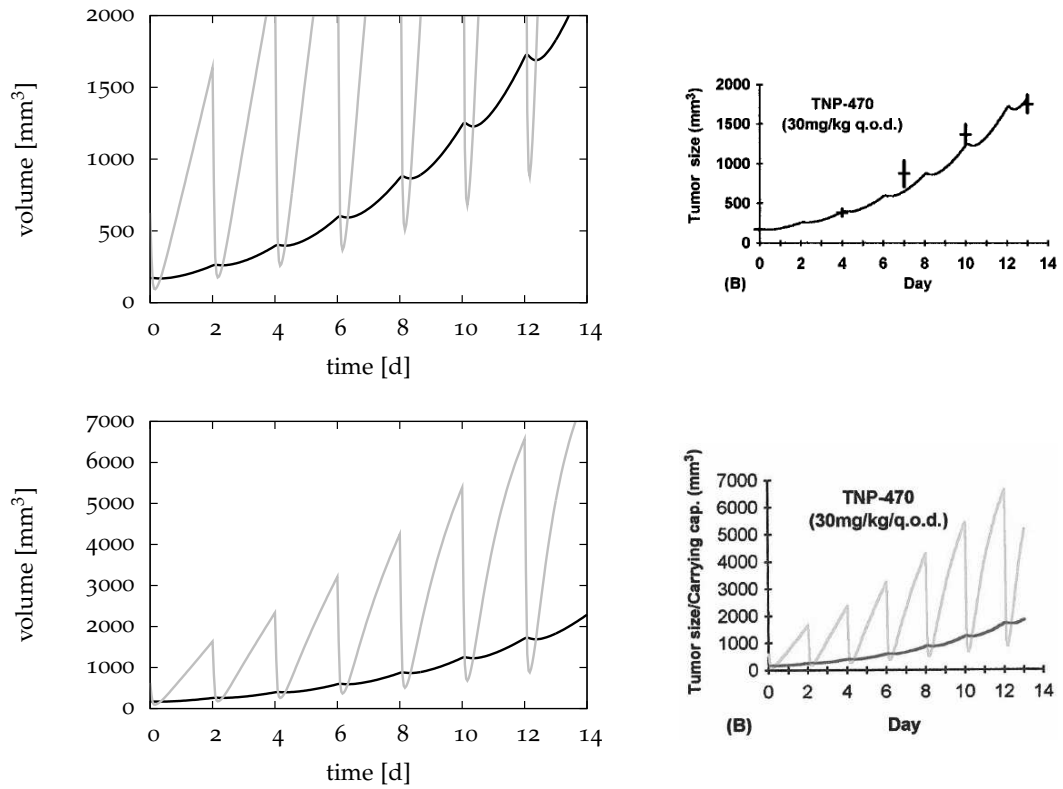
Figure 5.4: Comparison between MUSCOD-II simulation results (left) and *Hahnfeldt et al.* (right), TNP-470 therapy, 14 days. Vasculature volume is bright, tumor volume dark. Dose was 30mg/kg every second day.

Scenario	$x_0(t_0)$	$x_1(t_0)$	Parameters
1	12,000	15,000	$c = 1.0, C = 2.0$
2	12,000	15,000	$c = 2.0, C = 10.0$
3	14,000	5,000	$c = 1.0, C = 2.0$
4	14,000	5,000	$c = 2.0, C = 10.0$

Table 5.2: Different scenarios in *d'Onofrio et al.*

figures 5.5, 5.6, 5.7, and 5.8. The different scenarios feature different solution structures, but this is just how they were chosen. One can determine from the plots that the results could be reproduced on the whole, especially the control structure is the same. However, the end times in the MUSCOD-II results are between 3.5% (scenario 3) and 10.8% (scenario 2) above the ones in *d'Onofrio et al.*—e.g. 6.958 (MUSCOD-II) vs. 6.647 (4.7%) in scenario 1. The differences between the populations though are much smaller: 7020.83 vs. 7019.09 for tumors and 7328.09 vs. 7365.27 in scenario 1 for example, which corresponds to 0.02% respectively 0.5%. The differences in the other scenarios are pretty much the same. All solutions have been computed with 100 nodes.

Another question one may ask is how much we gain by optimal control. For this purpose, we changed the objective function to

$$\min \quad -x_0\left(t_f\right) + 0.005 \int_0^{t_f} u_0(t)^2 \quad dt, \tag{5.6}$$

and computed an optimal control for scenario 1 with end time fixed to $t_f = 7.0$ and the amount of drugs given over the total time fixed to the bounds 300 respectively 2. This corresponds to a maximization of the tumor size at the end time. The result is shown in figure 5.9 together with a simulation without any therapy. Tumor volume under maximization is at 8045.02, which is about 40.3% lower than the volume without any treatment (13484.83) on the one hand, but on the other hand also 14.6% higher than the volume under the optimal control (7020.83).

One observes a different structure of the optimal control, which (almost) is of bang-bang type. Obviously, under a maximization of the tumor volume it is optimal (in this model) to administer a big part of the drugs at the start of the treatment, because the fraction of cells killed is lower when the volumes are relatively low. As angiogenic treatment has a delayed influence on the tumor volume, the full-dose part at the end of the time scale plays no role for the tumor volume.

The next point is the comparison of the continuous result with binary controls derived by sum-up rounding and the decomposed MILP-algorithm. Figure 5.10 shows all three types. With sum up rounding, we get a tumor volume at the end time of 7027.67, which is only 0.1% higher than the continuous value 7020.83. This solution shows a *chattering* tendency, though, which reduces its benefit for possible practical purposes. The decomposed MILP-result with a maximum of 6 switches is signifcantly higher at 7745.93—about 10% more. This is only 3.7% less than the maximized tumor volume with continuous control.

Finally, we compared decomposed MILP-solutions with different numbers of switches. In three runs we allowed a maximum of 4, 6 and 8 switches in scenario 1. See figure 5.11 for a
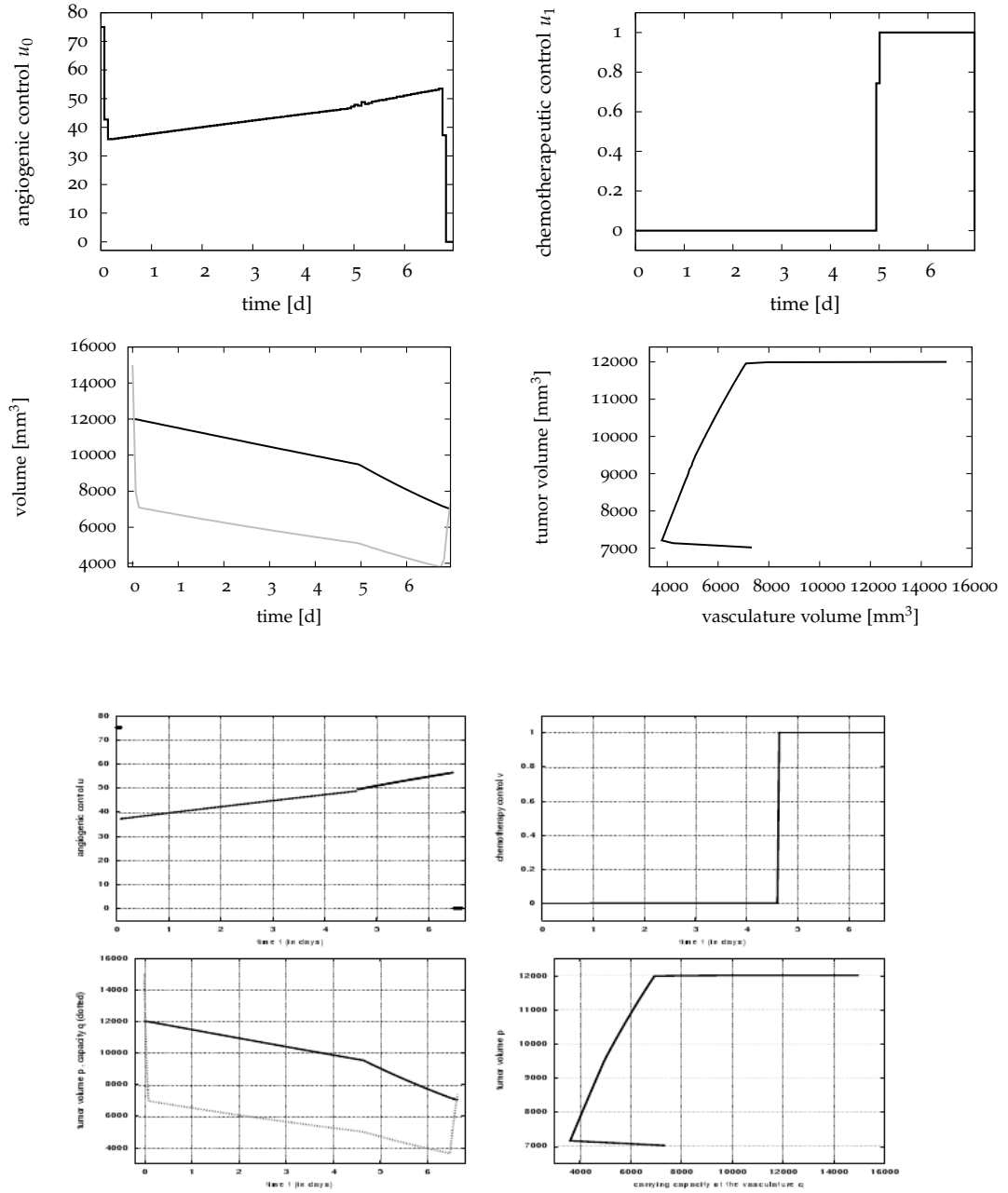
Figure 5.5: Optimization results compared to results of *d'Onofrio et al.*, scenario 1. Upper part: `MUSCOD-II` results, lower part: *d'Onofrio et al.* In each part: upper left: angiogenic control u_0, upper right: chemotherapeutic control u_1, lower left: tumor and vasculature volume (tumor dark, vasculature bright), lower right: tumor vs. vasculature volume
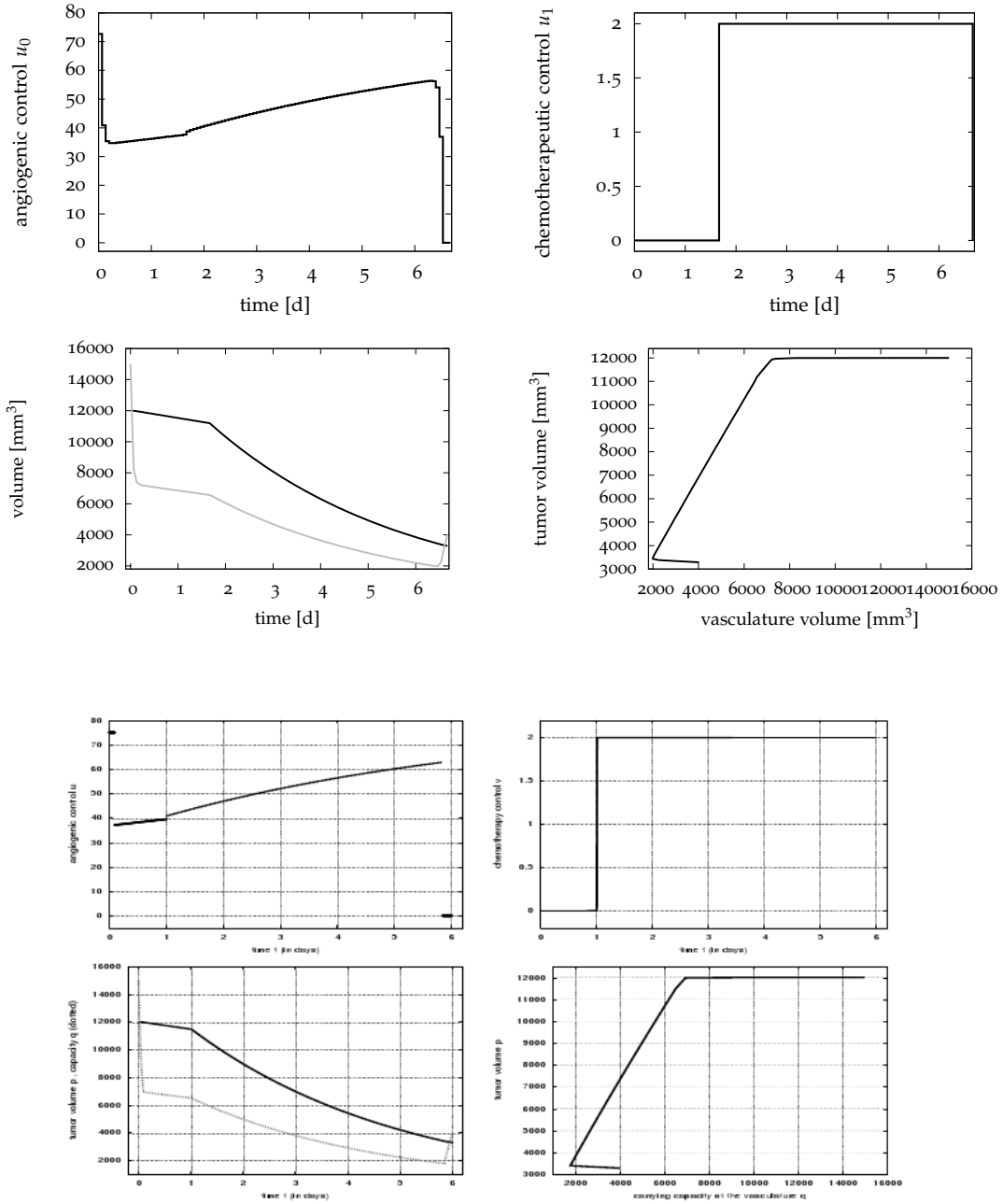
Figure 5.6: Optimization results compared to results of *d'Onofrio et al.*, scenario 2. Upper part: MUSCOD-II results, lower part: *d'Onofrio et al.* In each part: upper left: angiogenic control u_0, upper right: chemotherapeutic control u_1, lower left: tumor and vasculature volume (tumor dark, vasculature bright), lower right: tumor vs. vasculature volume
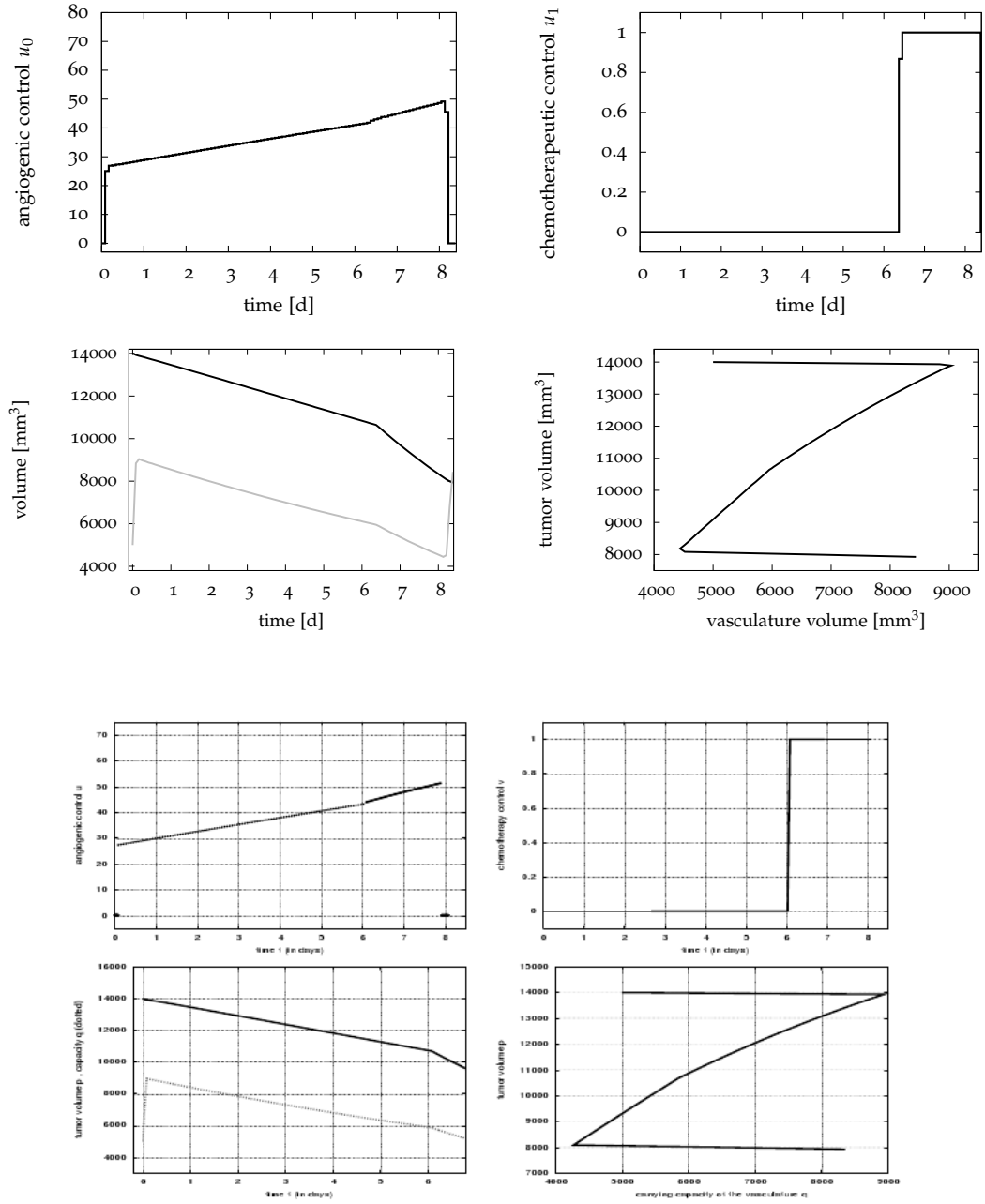
Figure 5.7: Optimization results compared to results of *d'Onofrio et al.*, scenario 3. Upper part: `MUSCOD-II` results, lower part: *d'Onofrio et al.* In each part: upper left: angiogenic control u_0, upper right: chemotherapeutic control u_1, lower left: tumor and vasculature volume (tumor dark, vasculature bright), lower right: tumor vs. vasculature volume
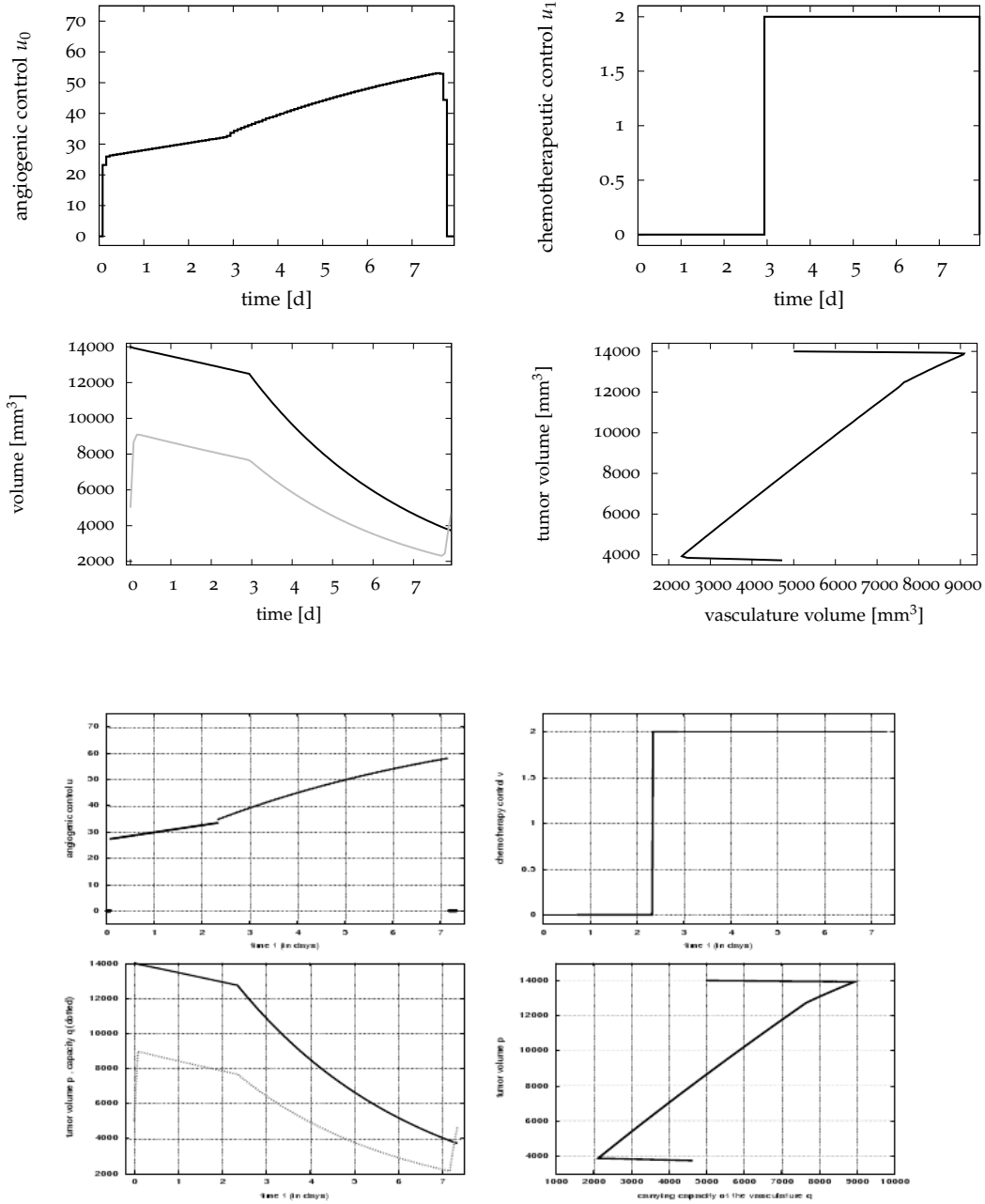
Figure 5.8: Optimization results compared to results of *d'Onofrio et al.*, scenario 4. Upper part: `MUSCOD-II` results, lower part: *d'Onofrio et al.* In each part: upper left: angiogenic control u_0, upper right: chemotherapeutic control u_1, lower left: tumor and vasculature volume (tumor dark, vasculature bright), lower right: tumor vs. vasculature volume
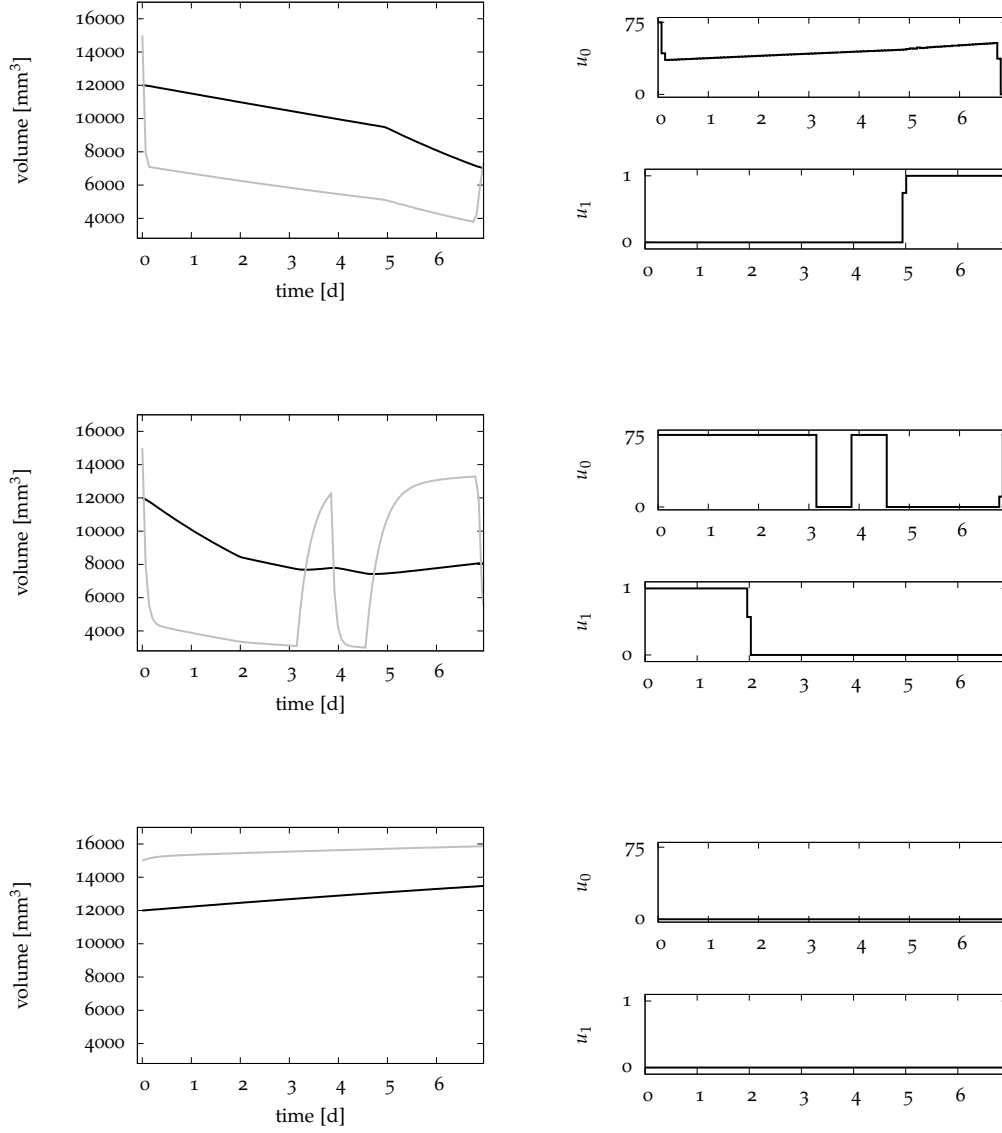
Figure 5.9: Comparison between min, max and no therapy, scenario 1. Left column contains tumor (dark) and vasculature (bright) volume, right column immunotherapy (upper) and chemotherapy (lower) controls. Top: minimiztion of tumor volume at end time, middle: maximization of tumor volume at end time with fixed drug amount, bottom: no therapy. The end value of the tumor population under maximization is about 10% higher than the minimized value, which is the maximal difference lost by bad timing of drug admission.
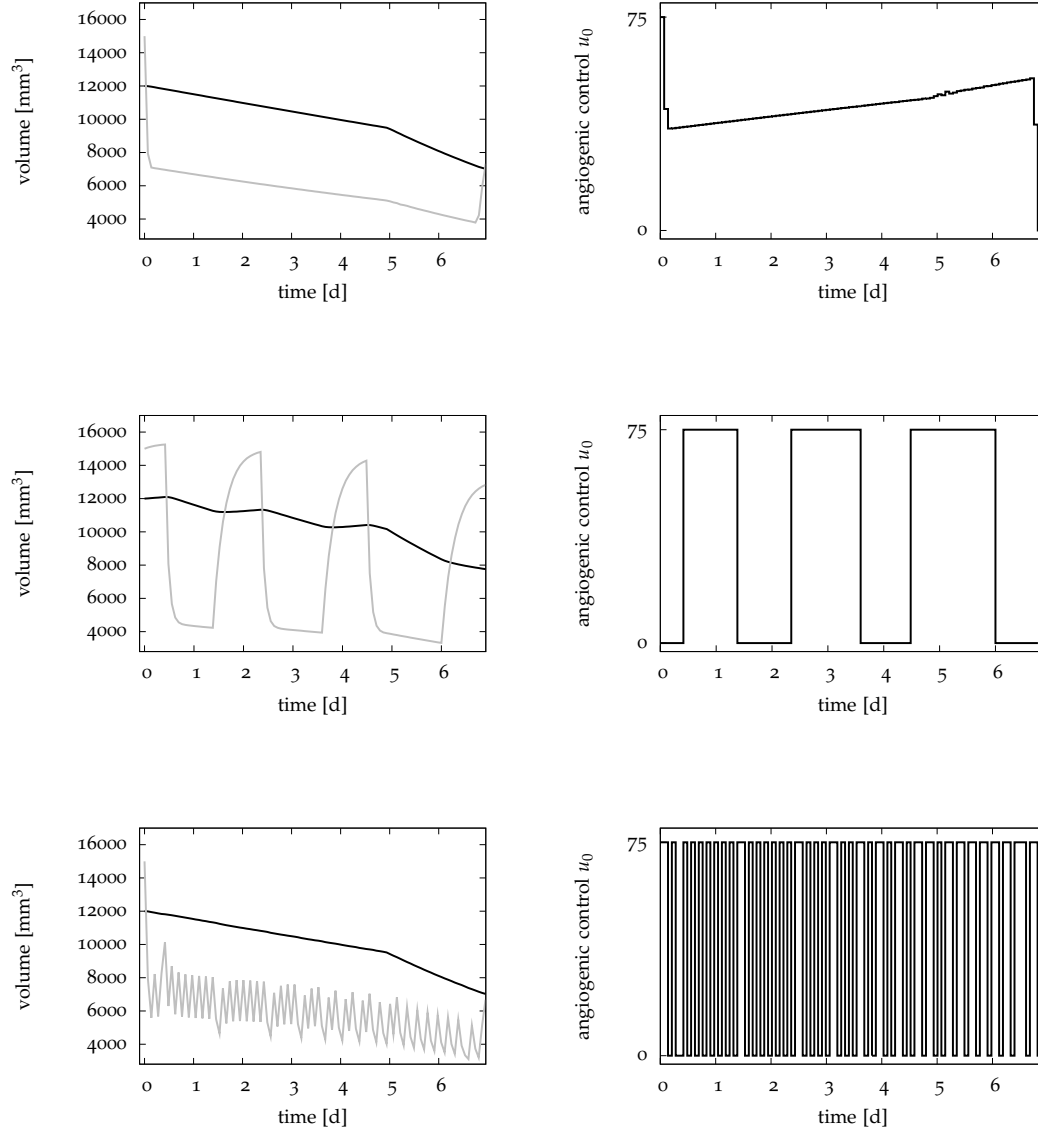
Figure 5.10: Comparison between continuous control, sum-up rounding and decomposed MILP in *d'Onofrio* model. Top: continuous, middle: decomposed MILP with a maximum of 6 switches, bottom: sum-up rounding. Tumor volume is dark, vasculature volume bright.

comparison. One would suppose that the tumor volume decreases with increasing maximal number of switches. With 4 switches we get 7627.75, 7758.12 with 6, and 7536.35 with 8. Surprisingly, the value with 6 switches is higher than the one with 4 switches. This may be due to the fact that in the *MILP* we optimize the deviation from the continuous control while the objective function of the original problem is ignored. So it is possible that the approximation of the control is better with the 6 switches solution while the tumor volume is higher.

All the values are closer to the "max-volume" than to the min one. The results are 8.6%, 10.5%, and 7.3% higher than the optimal value but only 6.3%, 3.6%, and 5.2% lower than the maximized tumor volume.

5.3 Mouse Optimal Control (de Pillis 2006)

In this section, we present the optimal control results from the *mouse* parameter set, which is one of three parameter sets in *de Pillis et al. 2006* [10]. Again, we recall the model equations (2.31):

$$\dot{x}_0 = a\,x_0\,(1 - b\,x_0) - c\,x_1\,x_0 - D\,x_0 - K_T\left(1 - \mathrm{e}^{-x_4}\right)x_0, \tag{5.7a}$$

$$\dot{x}_1 = e\,x_3 - f\,x_1 + g\,\frac{x_0{}^2}{h + x_0{}^2}x_1 - p\,x_1\,x_0 - K_N\left(1 - \mathrm{e}^{-x_4}\right)x_1, \tag{5.7b}$$

$$\begin{aligned}
\dot{x}_2 = {}&-m\,x_2 + j\,\frac{D^2\,x_0{}^2}{k + D^2\,x_0{}^2}x_2 - q\,x_2\,x_0 + (r_1\,x_1 + r_2\,x_3)\,x_0 \\
&- v\,x_1\,x_2{}^2 - K_L\left(1 - \mathrm{e}^{-x_4}\right)x_2 + \frac{p_I\,x_2\,x_5}{g_I + x_5} + u_2,
\end{aligned} \tag{5.7c}$$

$$\dot{x}_3 = \alpha - \beta\,x_3 - K_C\left(1 - \mathrm{e}^{-x_4}\right)x_3, \tag{5.7d}$$

$$\dot{x}_4 = -\gamma\,x_4 + u_0, \tag{5.7e}$$

$$\dot{x}_5 = -\mu_I\,x_5 + u_1, \tag{5.7f}$$

$$D = d\,\frac{(x_2/x_0)^l}{s + (x_2/x_0)^l}, \tag{5.7g}$$

$$0 \le x_0, x_1, x_2, x_3, x_4, x_5, \tag{5.7h}$$

$$0 \le u_0, u_1, u_2, \tag{5.7i}$$

$$t \in [t_0, t_f] \tag{5.7j}$$

In the numerical simulations in *de Pillis et al. 2006* [10], they mostly use a time horizon of 120 days, but there are some treatments with a duration of 40 respectively 80 days. We decided to investigate three different time scales: a short one with $t_f = 40$, the one from [10] with $t_f = 120$ and a free end time t_f. To these times we refer in the following as $t = 1$, $t = 2$, and $t = 3$, see table 5.3. For the *tumor infiltrating lymphocytes*, it is not clear how much TIL can be injected and how often. For the drugs the maximum amount which can be given is also not certain, but as *TIL* models an injection of lymphocytes which have been highly stimulated outside the body, the question how much of these cells are available in what time is a lot more important. Because of these uncertainities, we did not consider *TIL* at all. For the mouse model which contains no *IL-2* therapy, this means we consider a classical chemo-monotherapy. *De Pillis et al.* set the dosage in their numerical experiments to 1.0, which is the value we used in our experiments, too.
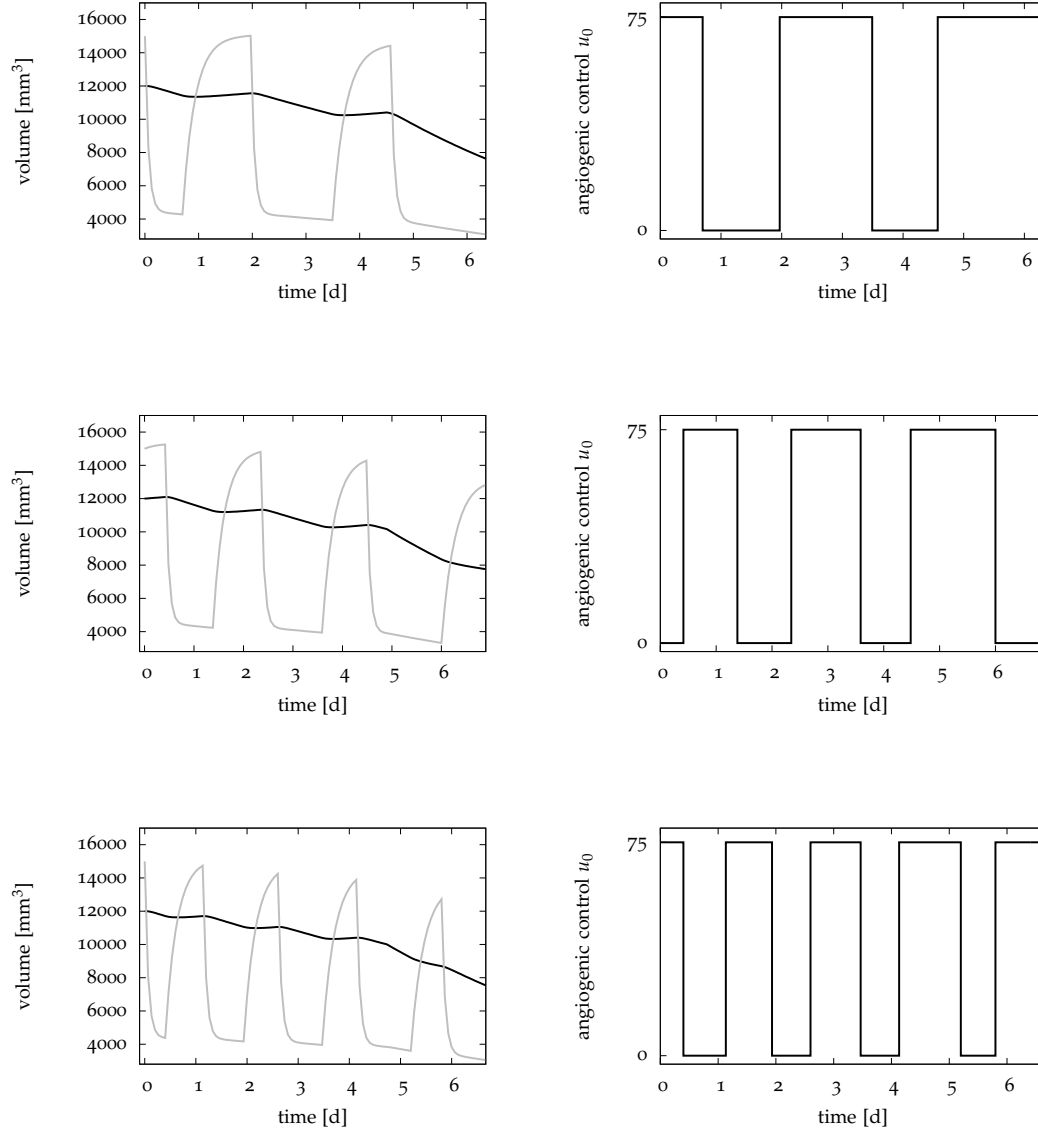
Figure 5.11: Decomposed MILP results for *d'Onofrio* model with a maximum of 4, 6, and 8 switches in scenario 1. Top: 4 switches, middle: 6 switches, bottom: 8 switches. Tumor volume is dark, vasculature volume bright.

$t = 1$	$t_f = 40$	40 grid points
$t = 2$	$t_f = 120$	120 grid points
$t = 3$	t_f free	40 grid points

Table 5.3: Time horizons used for *de Pillis et al. 2006*

No optimal control was done in the paper, so we had to choose objective functions. Of course, the overall aim is to minimize the tumor population. So a first objective ($p = 2$) is to minimize x_0 at the end time t_f,

$$\min x_0(t_f). \tag{5.8}$$

As in [17], we also considered this objective together with a penalty P on the chemotherapeutic control u_0 ($p = 3$):

$$\min x_0(t_f) + p_2 \cdot \int_{t_0}^{t_f} u_0(t)\, dt. \tag{5.9}$$

However, some results with this objective functions do not look "nice", as during a major part of the treatment, controls are zero while the tumor population is on a very high level, see e.g. figure 5.15. This is not a desired therapy, so we chose a *weighted sum* as a third objective ($p = 1$):

$$\min p_0 \cdot x_0(t_f) + \cdot \int_{t_0}^{t_f} p_1 \cdot x_0(t)^2 + p_2 \cdot u_0(t) + p_3 \cdot u_1(t)\, dt. \tag{5.10}$$

Under that objective, the tumor population is minimized over the whole time, see the Lagrangian part, in addition. We have again penalties on the controls. The other two objectives can be written in this form, too. Table 5.4 shows the values of the p_i which were used. In the following, we refer to the different objectives with $p = 1$, $p = 2$, and $p = 3$. The seven different initial value sets form *de Pillis et al. 2006* are called $s = 1$ to $s = 7$, see table 5.5.

	p_0	p_1	p_2	p_3
$p = 1$	$5.0 \cdot 10^{-3}$	$1.0 \cdot 10^{-11}$	$1.0 \cdot 10^4$	0.0
$p = 2$	1.0	0.0	0.0	0.0
$p = 3$	1.0	0.0	1.0	0.0

Table 5.4: Objective function parameters used for *de Pillis et al. 2006*

For the verifcation of the models' implementations in `MUSCOD-II` we ran some simulations. The results of [10] for the *mouse* set could be reproduced, for chemotherapy as well as without any therapy, see figure 5.12. Exact values are not given, so we have to rely on the plots.

Optimal control results of the *mouse* model for continuous controls are shown in figures 5.13, 5.14, and 5.15. In general, not all combinations of t, p, and s could be solved because of different problems, e.g. with the generation of derivatives or with the QP solution. We give an overview of the calculation results for the *mouse* set as well as for the *human* sets in table 5.6.

One observes that under $p = 1$, chemotherapy is applied later but the peak is earlier and tumor cells are on a lower level in general whereas the end level is some orders of magnitude

	$x_0(t_0)$	$x_1(t_0)$	$x_2(t_0)$	$x_3(t_0)$	$x_4(t_0)$	$x_5(t_0)$	Parameter set
$s = 1$	$1 \cdot 10^6$	$5 \cdot 10^4$	$1 \cdot 10^2$	$1.1 \cdot 10^7$	0	0	Mouse
$s = 2$	$1 \cdot 10^6$	$1 \cdot 10^5$	$1 \cdot 10^2$	$6 \cdot 10^{10}$	0	0	Human 9/10
$s = 3$	$1 \cdot 10^6$	$1 \cdot 10^3$	1	$6 \cdot 10^8$	0	0	Human 9
$s = 4$	$2 \cdot 10^7$	$1 \cdot 10^3$	1	$6 \cdot 10^8$	0	0	Human 9
$s = 5$	$1 \cdot 10^8$	$1 \cdot 10^3$	1	$6 \cdot 10^8$	0	0	Human 9/10
$s = 6$	$1 \cdot 10^7$	$1 \cdot 10^3$	1	$6 \cdot 10^8$	0	0	Human 9
$s = 7$	$1 \cdot 10^5$	$1 \cdot 10^5$	$1 \cdot 10^2$	$6 \cdot 10^{10}$	0	0	Human 10

Table 5.5: Initial values used for *de Pillis et al. 2006*
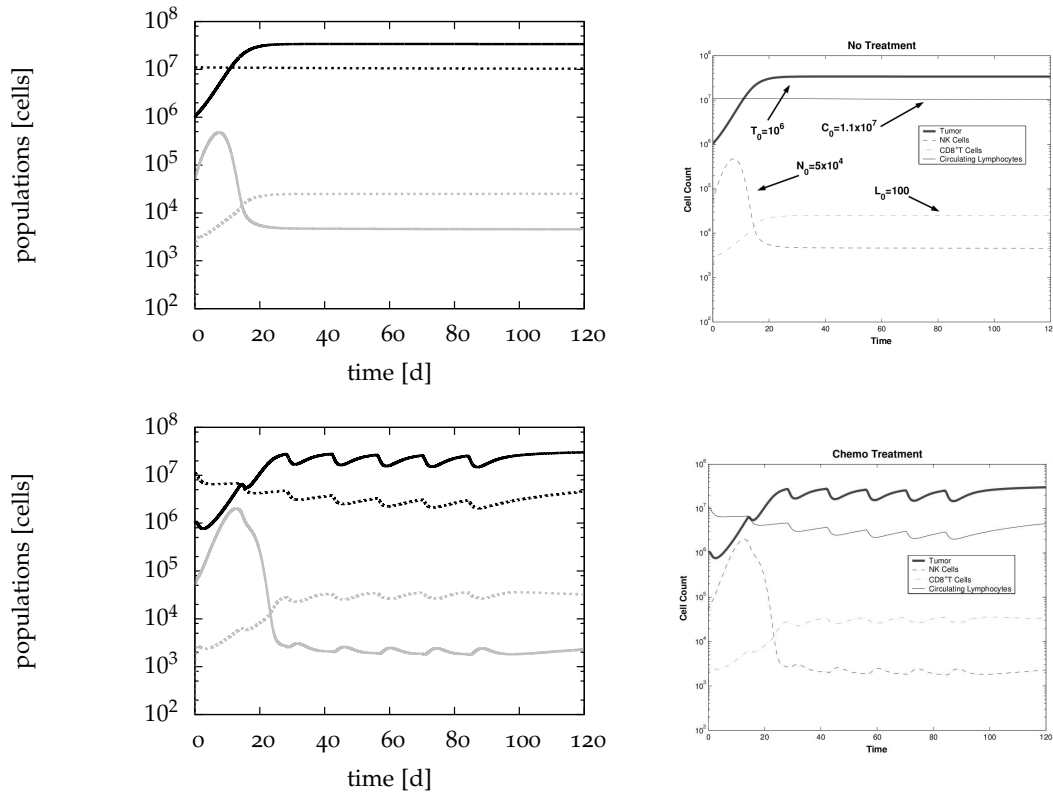
Figure 5.12: Comparison between `MUSCOD-II` simulation results (left) and *de Pillis et al. 2006* (right), Mouse. Top: $s = 1$ without treatment, bottom: $s = 1$ with chemotherapy (7 doses, 1 day each, strength 1, every 14 days). Tumor population is black solid, NK cells are black dashed, CD8+ T cells gray solid and circulating lymphocytes gray dashed.
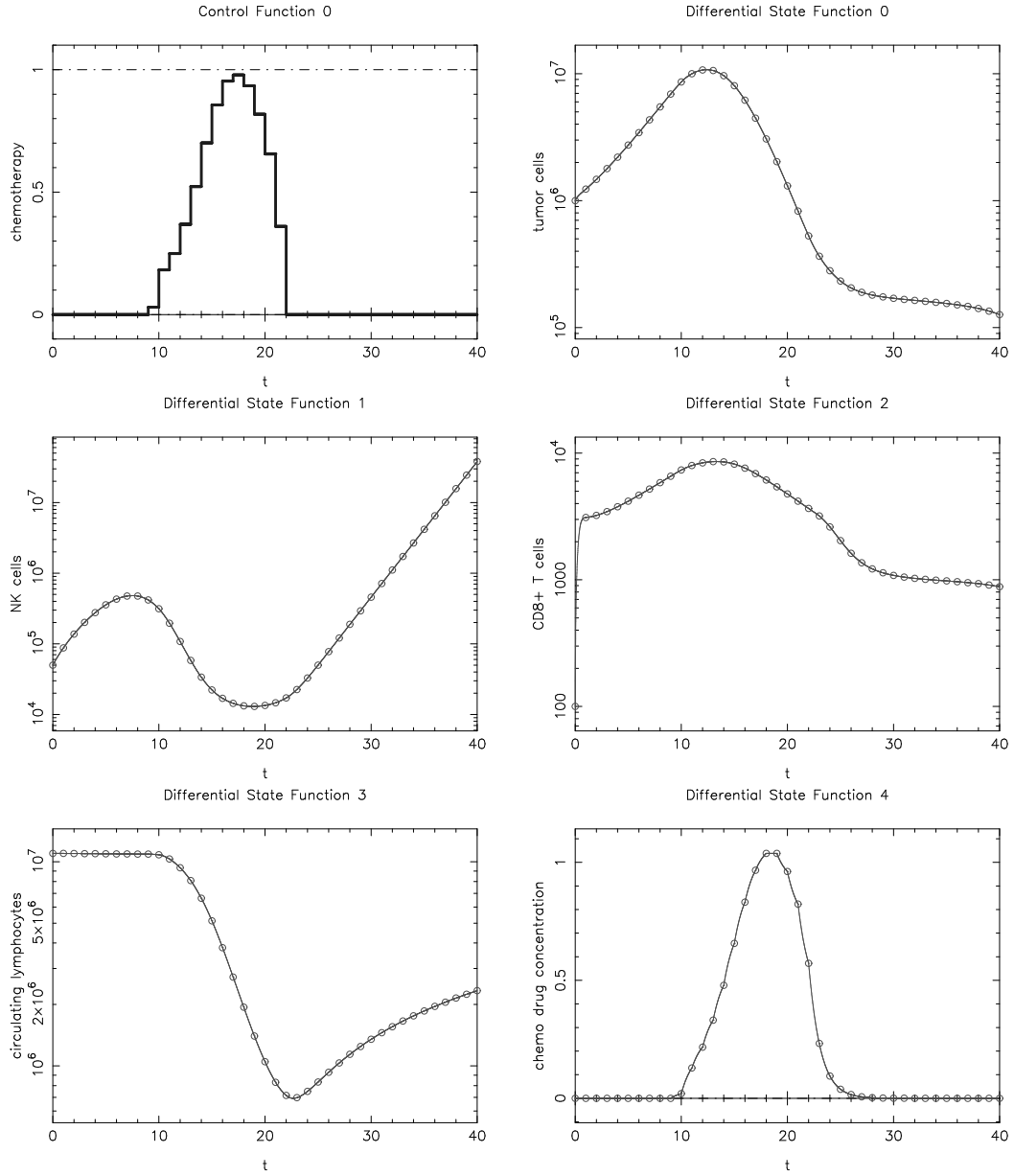
Figure 5.13: Optimal control result of *de Pillis et al. 2006, mouse. t = 1, p = 1, s = 1.*
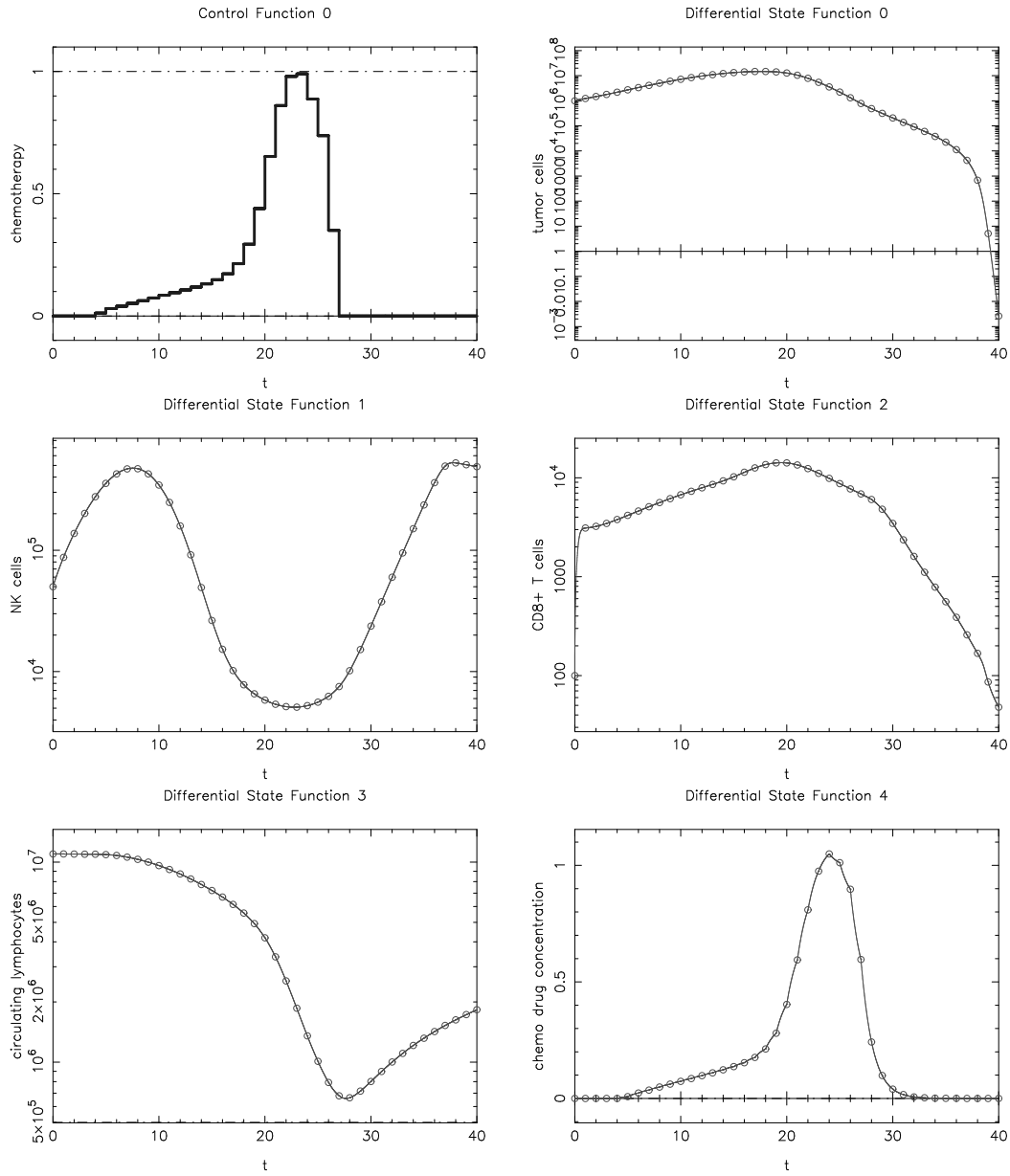
Figure 5.14: Optimal control result of *de Pillis et al. 2006, mouse. t = 1, p = 3, s = 1*.
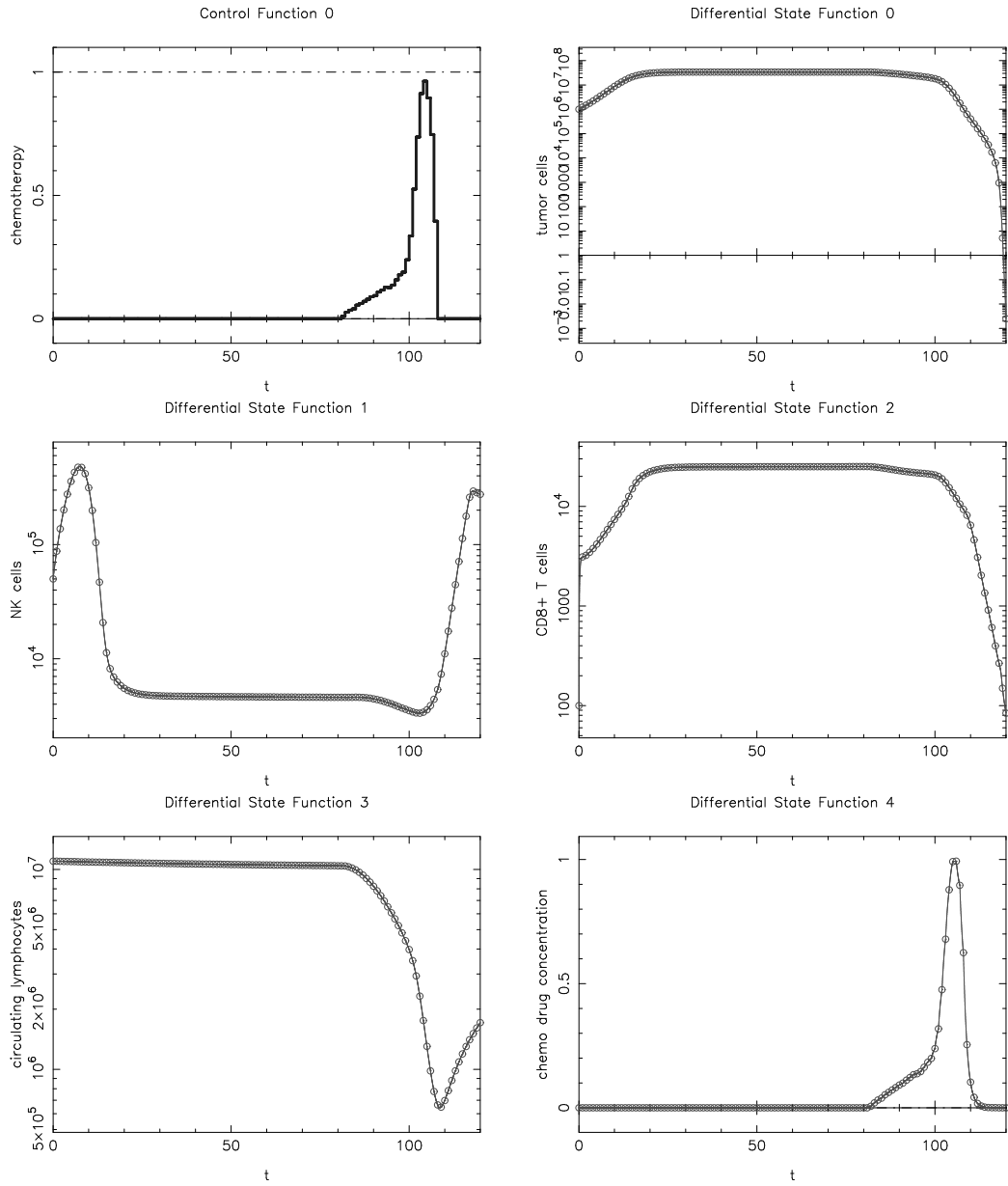
Figure 5.15: Optimal control result of *de Pillis et al. 2006, mouse. t = 2, p = 3, s = 1.*

lower with $p = 3$. The 120 day treatment with $p = 3$ shows the problem of a high level tumor without chemotherapy applied.

For $t = 1$, $p = 1$, $s = 1$, we fixed the amount of drugs given to the values of the optimal solution, changed the sign of p_0 and p_1 and started the optimization again. This corresponds to a maximization of tumor cells over the whole time and at the end time. We give a comparison to the minimization result and to a standard treatment as applied by *de Pillis et al.* in figure 5.17. The benefit from optimal control looks a lot better in this scenario compared to the results in section 5.2. While the maximized tumor at the end time is at about $2 \cdot 10^7$ cells, the minimal value is only about 10^5 cells. This corresponds to 0.5% of the maximal value. The standard treatment is even a little higher than the maximized one, but the amount of drugs given is notably lower, too.
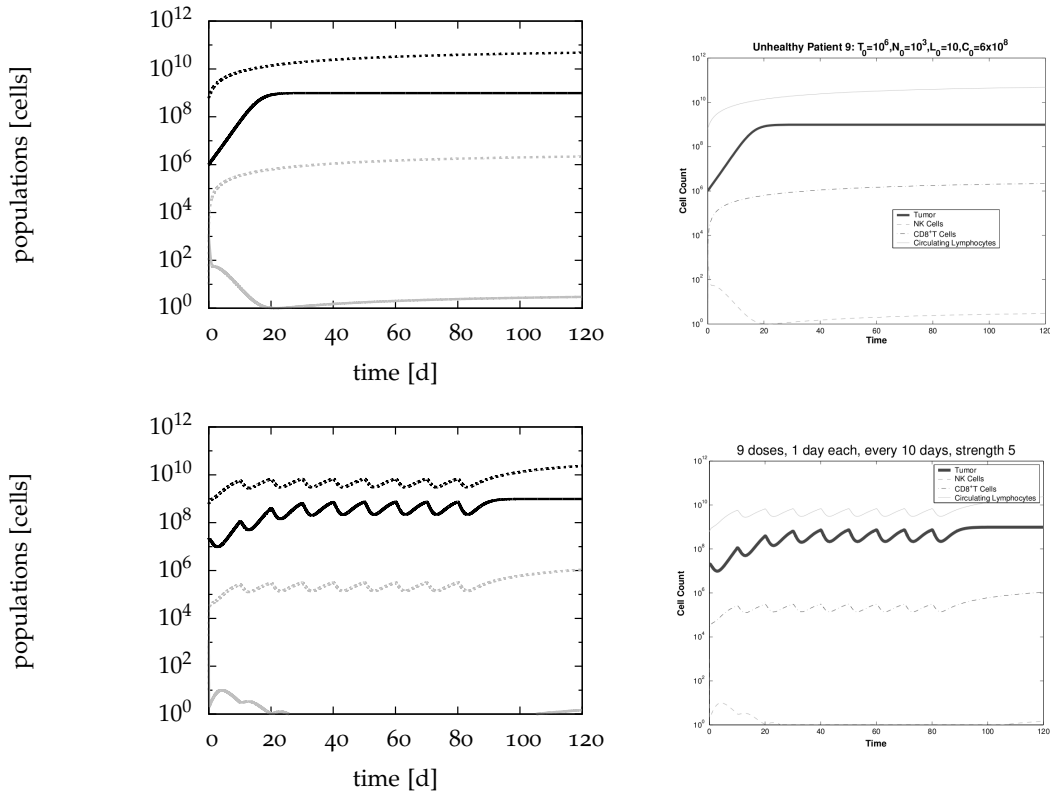
Figure 5.16: Comparison between MUSCOD-II simulation results (left) and *de Pillis et al. 2006* (right), Human 9. Top: $s = 3$ without treatment, bottom: $s = 4$ with chemotherapy (9 doses, 1 day each, strength 5, every 10 days). Tumor population is black solid, NK cells are black dashed, CD8+ T cells gray solid and circulating lymphocytes gray dashed.
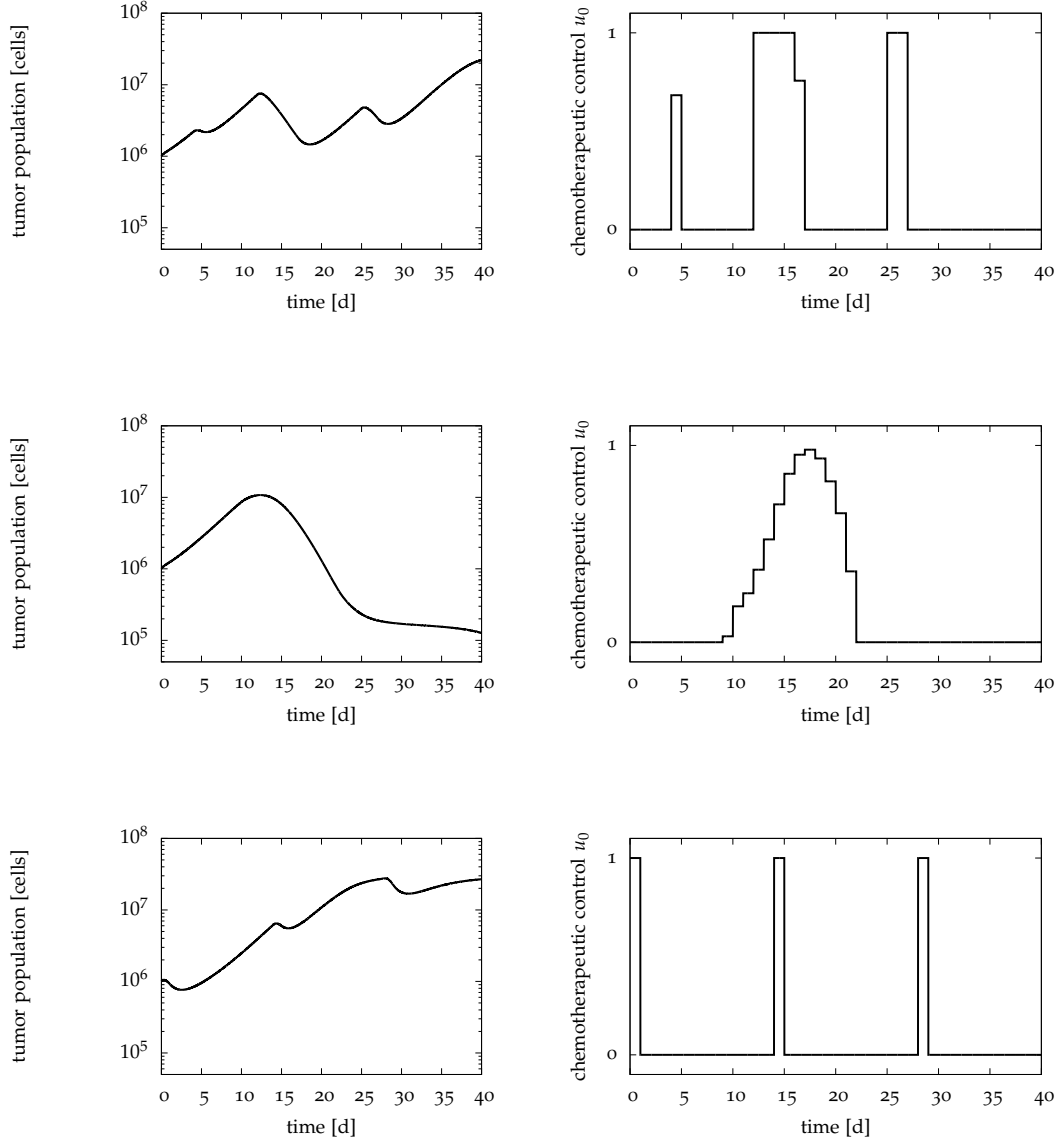
Figure 5.17: Comparison between maximization, minimization and standard treatment of *de Pillis et al. 2006, mouse.* $t = 1$, $p = 1$, $s = 1$. Top: maximization (with fixed drug amount), middle: minimization, bottom: standard therapy (example). Tumor volume is shown on the left side, chemotherapy control on the right side. Note that the given drug amount in the standard treatment is significantly lower, so that the result is even worse than the maximized one.

5.4 Human 9 Optimal Control (de Pillis 2006)

The *human 9* model is the second parameter set from *de Pillis et al. 2006*. Thus it uses the same equations as the *mouse* model. We picked out two scenarios to verify our implementation successfully, the results are shown in figure 5.16. The dose of chemotherapy has been changed to 5.0 (the authors give no reason for the higher dose) and the immunotherapeutic pulses are said to be at $5.0 \cdot 10^6$ in one experiment and at $5.0 \cdot 10^5$ in another one. Perhaps the latter is a typing error, as the upper bound of both *IL-2* concentration plots is $5.0 \cdot 10^5$, which makes sense for a dosage of $5.0 \cdot 10^6$ with the equation

$$\dot{x}_5 = -10 \cdot x_5 + u_1. \tag{5.11}$$

Eventually we decided to take 1.0 respectively $5.0 \cdot 10^6$ as upper bounds for the chemotherapeutic respectively immunotherapeutic control. For chemotherapy, the drug amount applied in our solutions is notably higher than in the *standard* treatments tried in [10], so it might be reasonable to take a smaller upper bound. Additionally, we remind that the *human* parameter sets are based on mostly *murine* data and that there is no reason given for a higher chemotherapy level in the article. For some remarks on the immunotherapy level, see below.

Figures 5.18, 5.19, 5.20, 5.21, 5.22, 5.23, and 5.24 contain our optimization results. As it is shown in table 5.6, only about the half of the problems could be solved. In the free time scenarios, t_f often converged to zero. Obviously, these results are not very interesting so there are no plots of them. Among the *good* results we made a selection and omitted similar solutions.

For $s = 2$ in this parameter set, the tumor vanishes without any therapy. So the optimal control is at the minimum, zero, in general (figure 5.18). While figure 5.20 features a full dose chemotherapy, in figures 5.19 and 5.21 there is a full dose part at the beginning followed by a short singular arc leading into a zero part. A solution like this occurs in some more scenarios of *human 9*. The free end time scenario in 5.23 (end time about 26) looks very similar, too. Figures 5.22 and 5.24 show again the problem of a delayed therapy. The free end time of the latter is at 315 days.

Except in 5.20, immunotherapy does not play a role in the treatment. Often it is at such low levels (e.g. 10^{-7} with an upper bound of $5 \cdot 10^6$) that it cannot be considered a therapy at all. Note also that none of the objective functions contained a penalty on the immunotherapeutic control u_1, so perhaps immunotherapy would diminish totally with a penalty. There are mathematical reasons for this low influence of immunotherapy. The control u_1 enters only in equation (5.7f), which reads

$$\dot{x}_5 = -\mu_I x_5 + u_1. \tag{5.12}$$

With a full dose of $u_1(t) = 5.0 \cdot 10^6$ and $\mu_I = 10$, $x_5(t)$ should be about $5.0 \cdot 10^5$. The state x_5 itself only plays a role in equation (5.7c), where the corresponding terms are

$$\dot{x}_2 = \cdots + \frac{p_I x_2 x_5}{g_I + x_5} + \ldots \tag{5.13}$$

with $p_I = 1.25 \cdot 10^{-1}$ and $g_I = 2.00 \cdot 10^7$. For a x_2 which is most of the time at a level of at least 10^5, we have

$$\frac{p_I x_2 x_5}{g_I + x_5} \approx \frac{10^{-1} 10^5 10^5}{10^7 + 10^5} \approx \frac{10^9}{10^7} \approx 10^2 \tag{5.14}$$
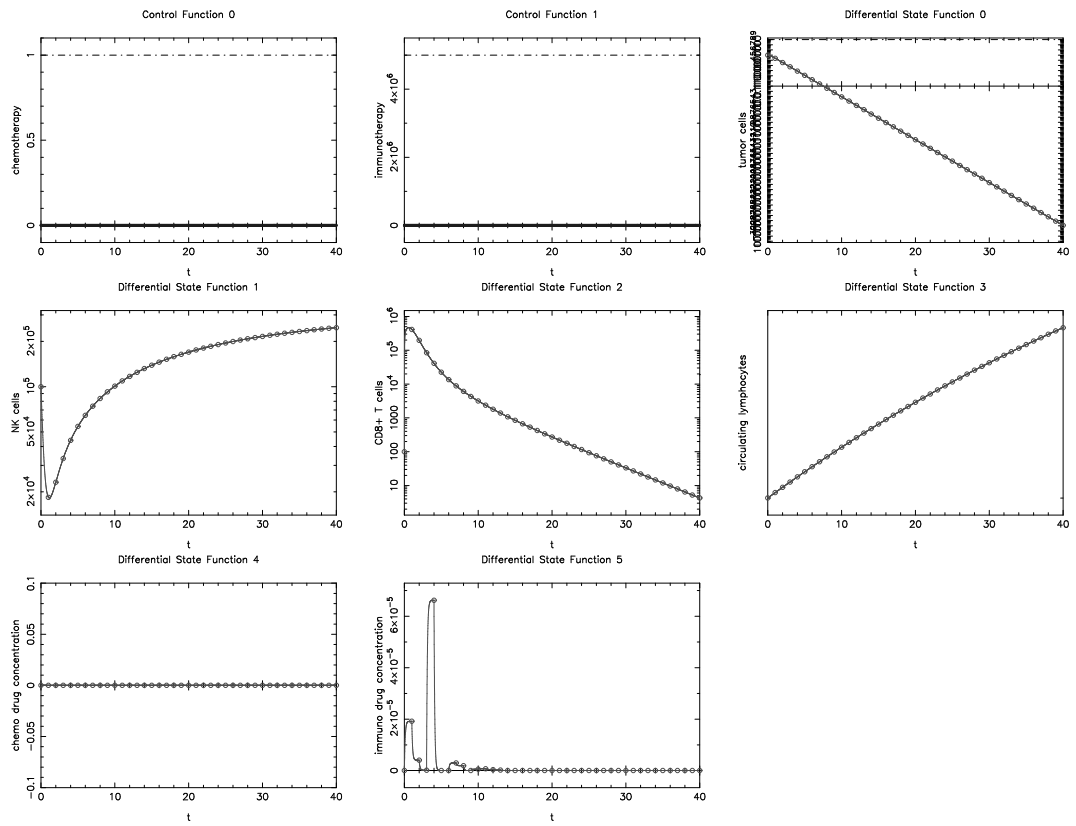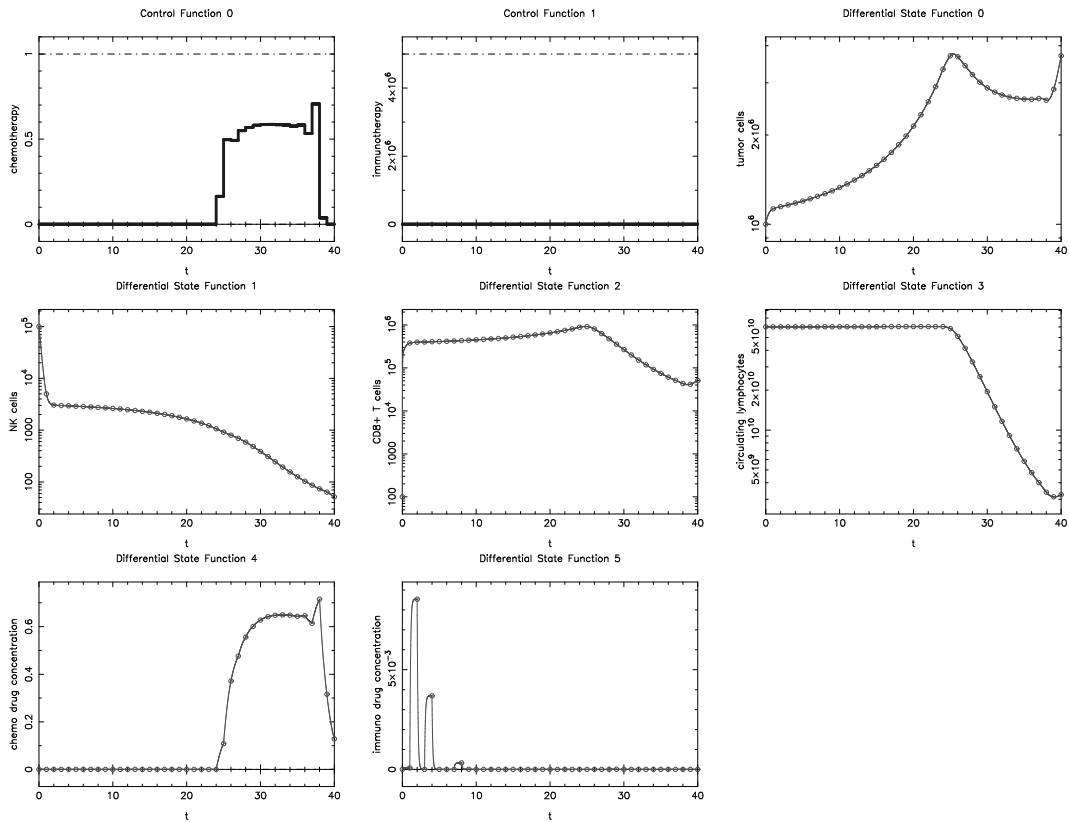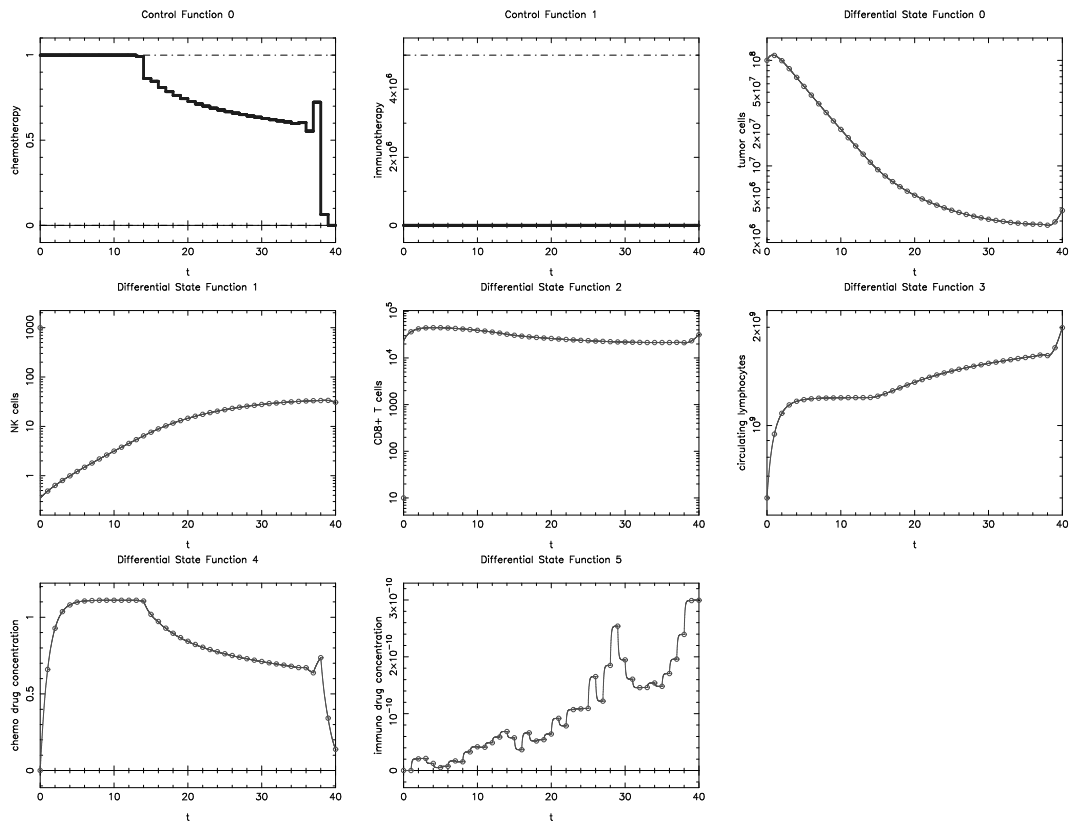
Figure 5.18: Optimal control result of *de Pillis et al. 2006, human 9.* $t = 1$, $p = 1$, $s = 2$.
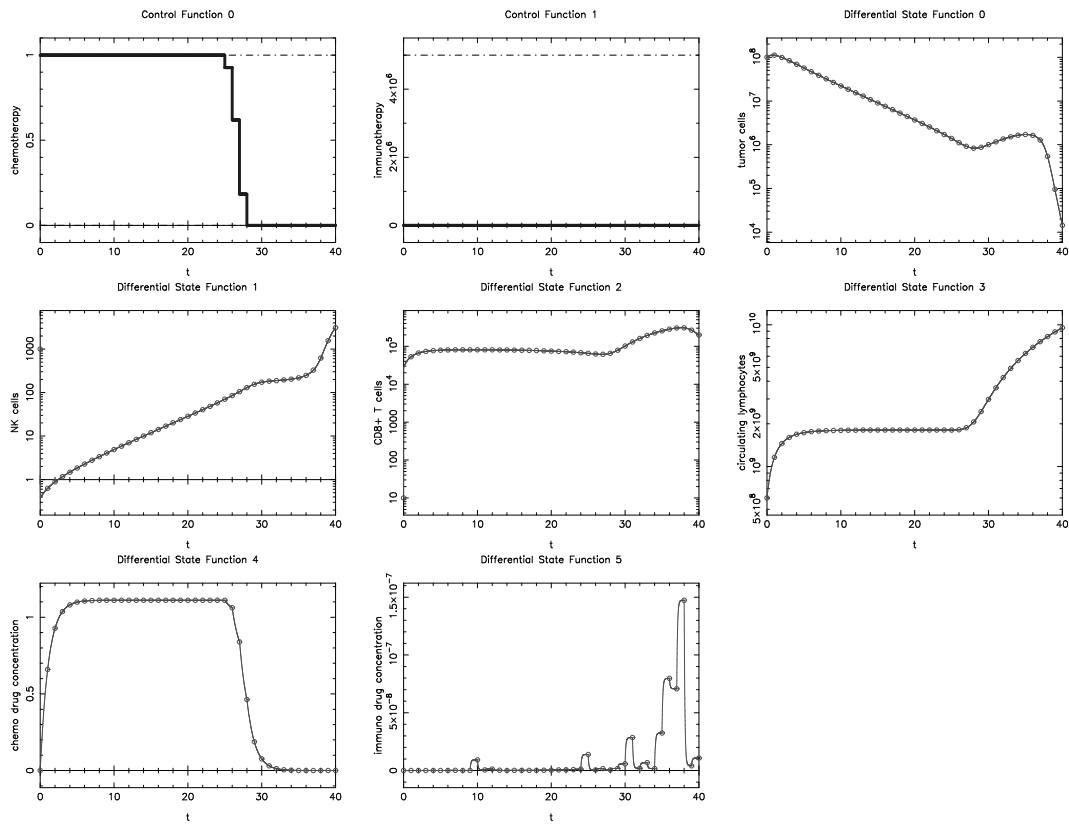
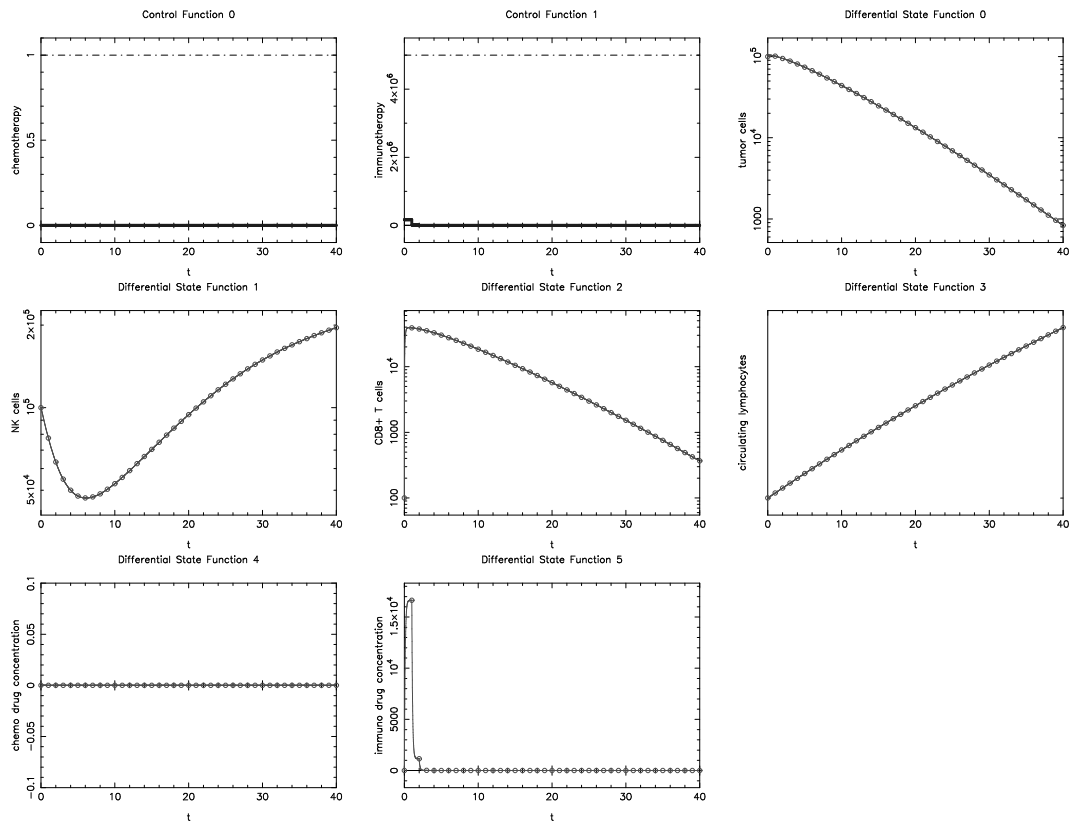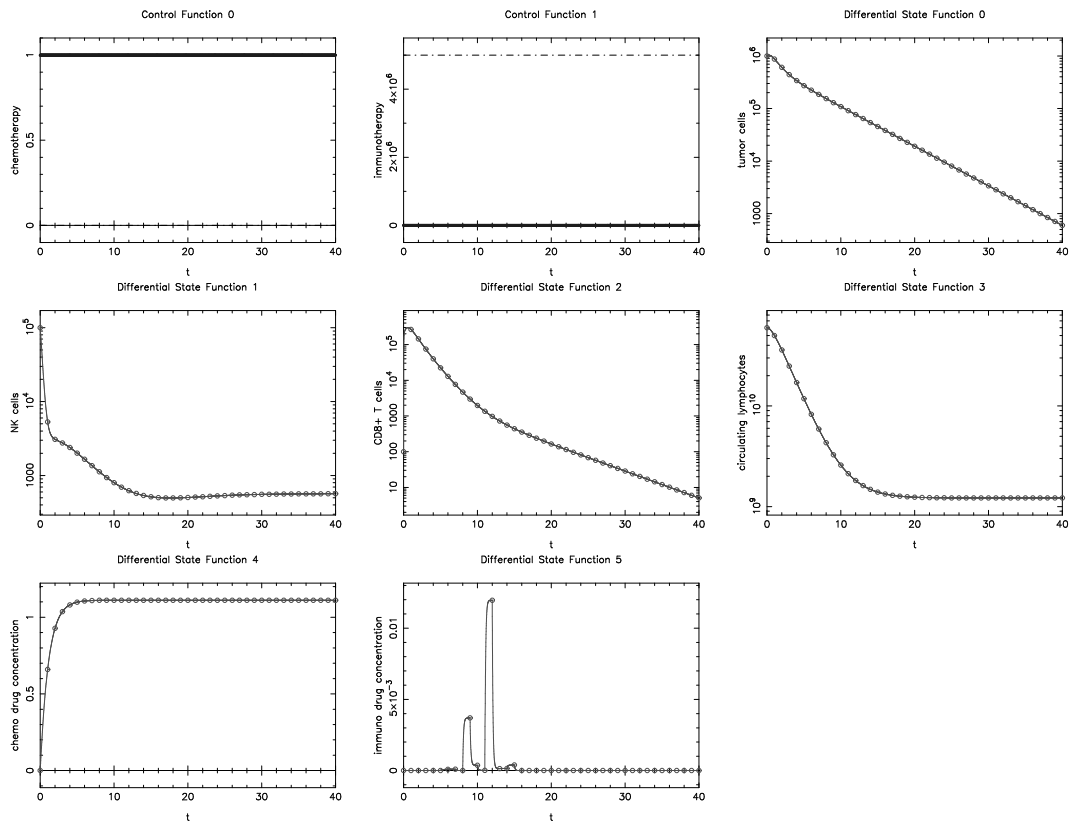**Figure 5.19:** Optimal control result of *de Pillis et al. 2006, human 9*. $t = 1$, $p = 1$, $s = 5$.
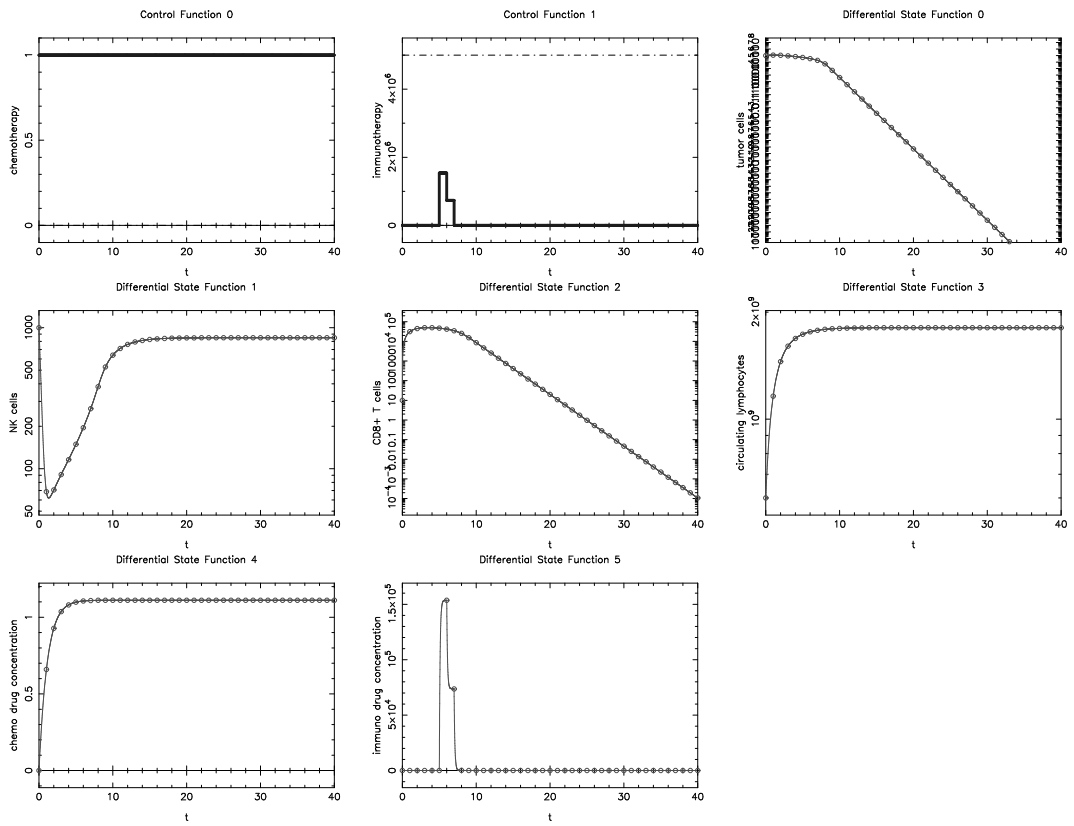
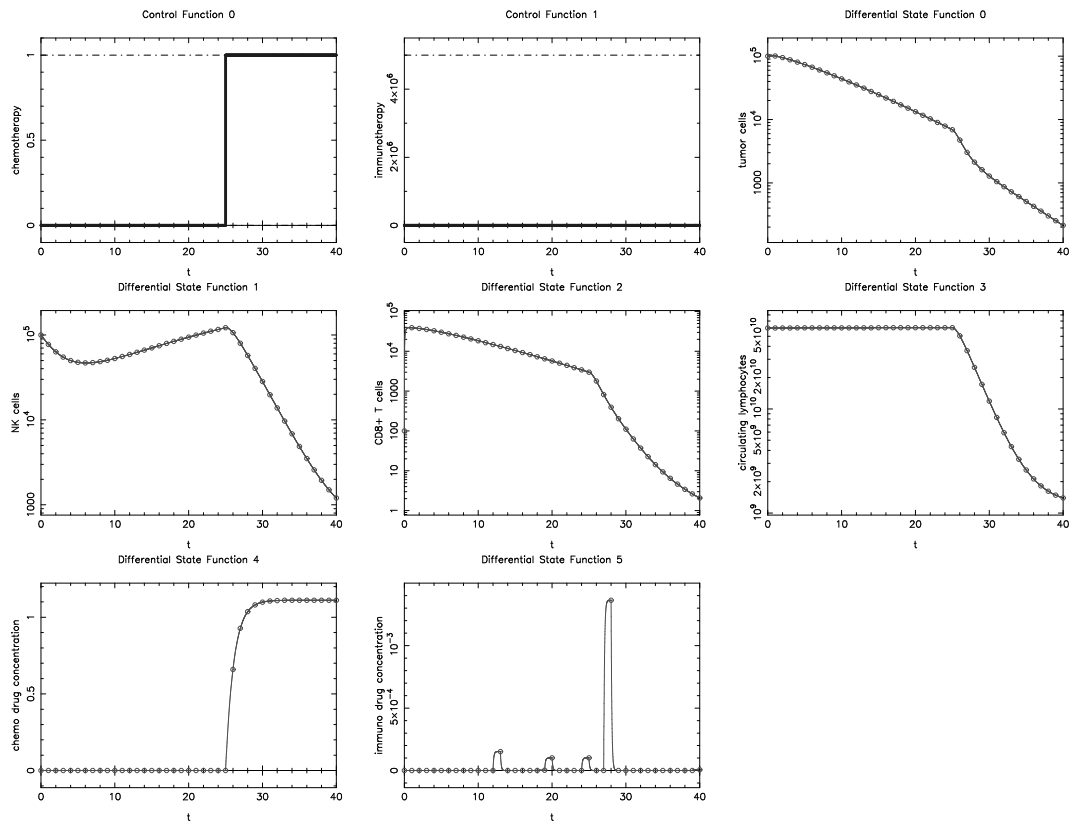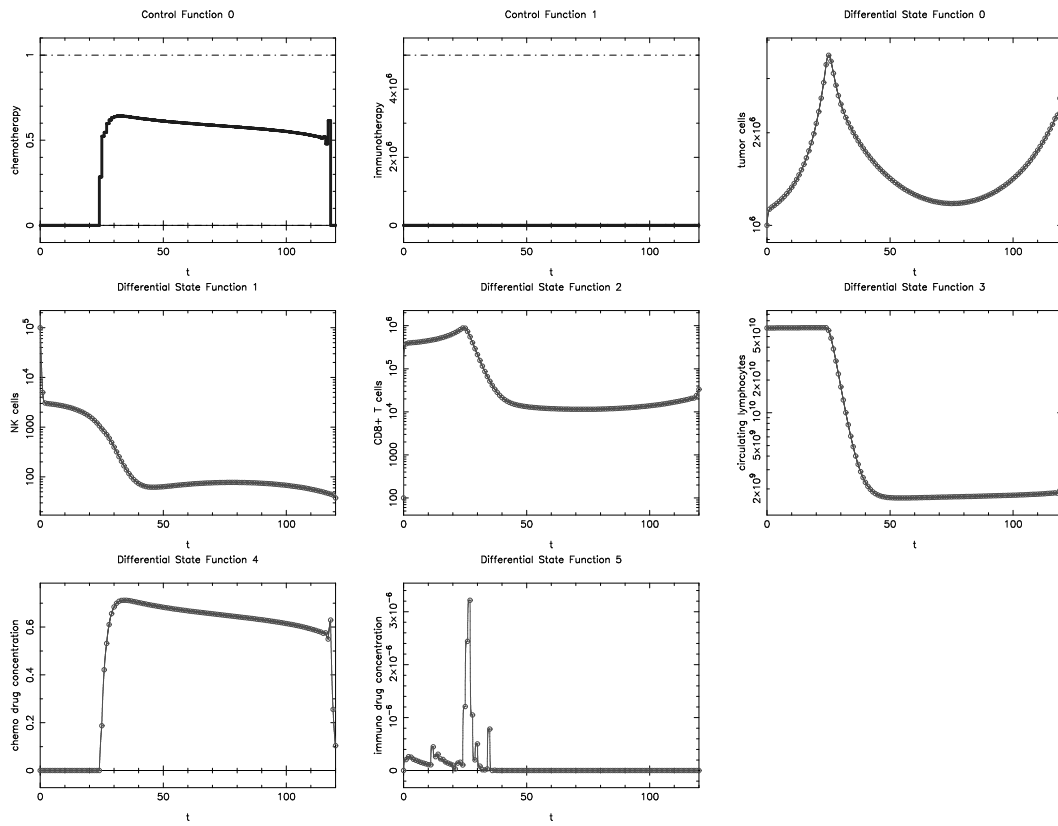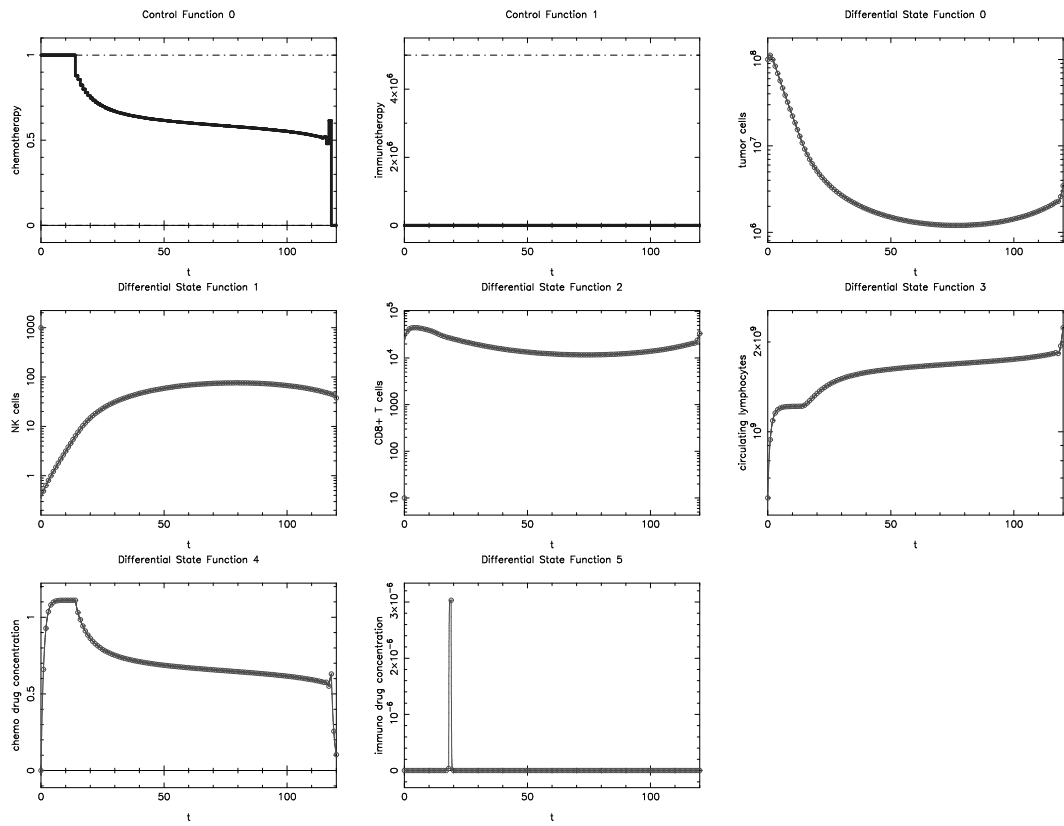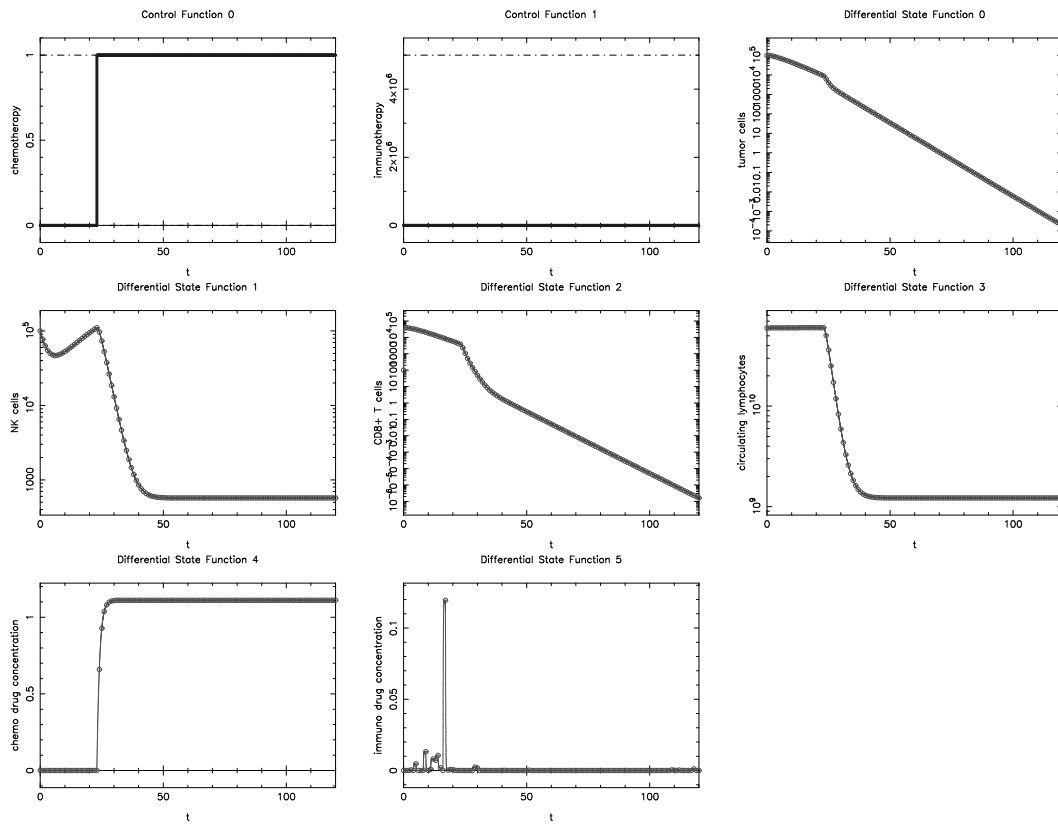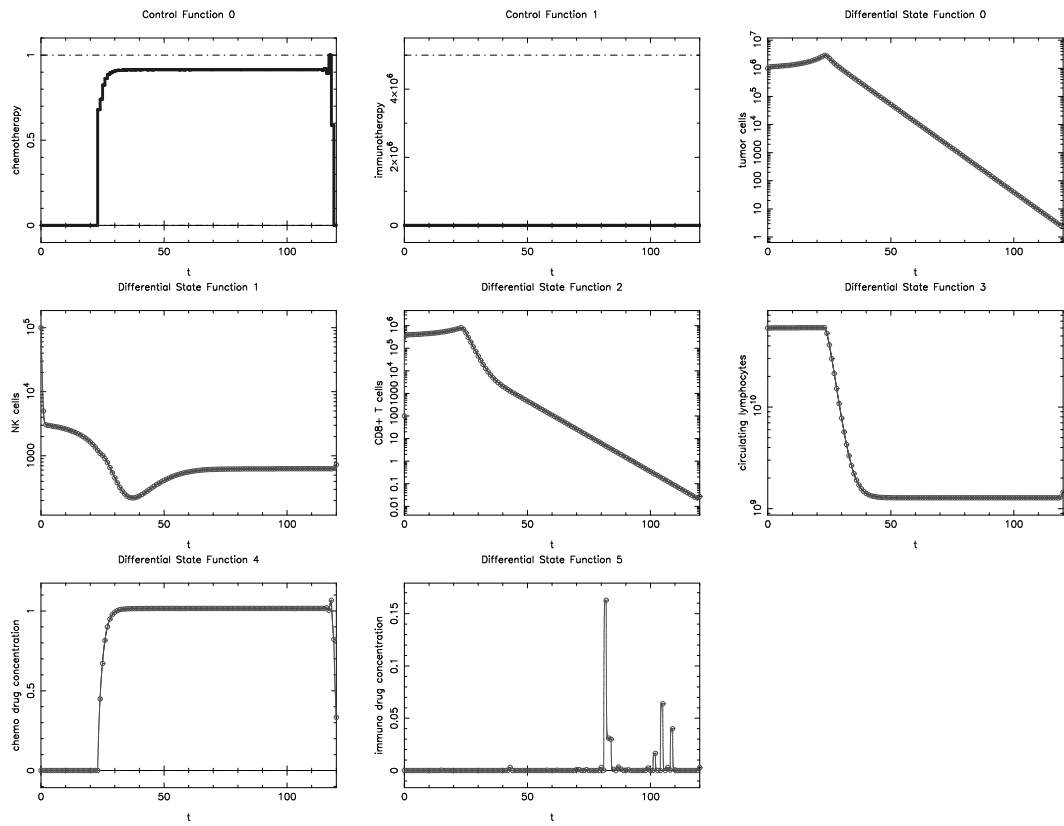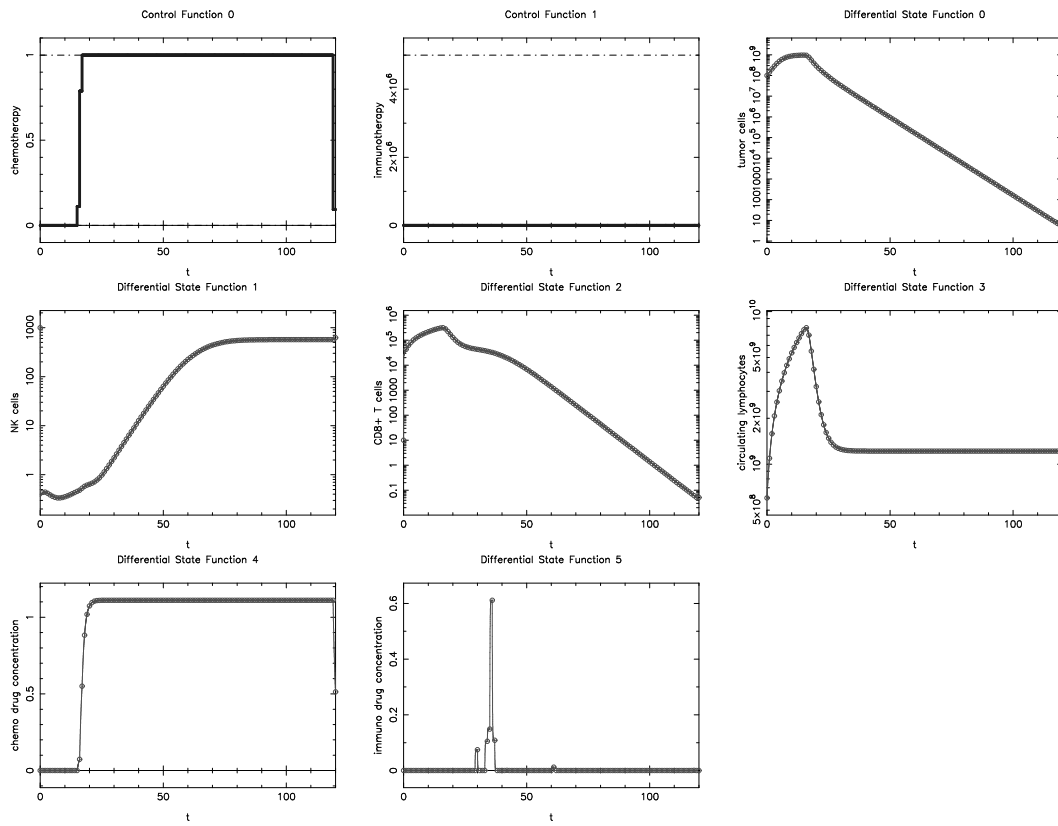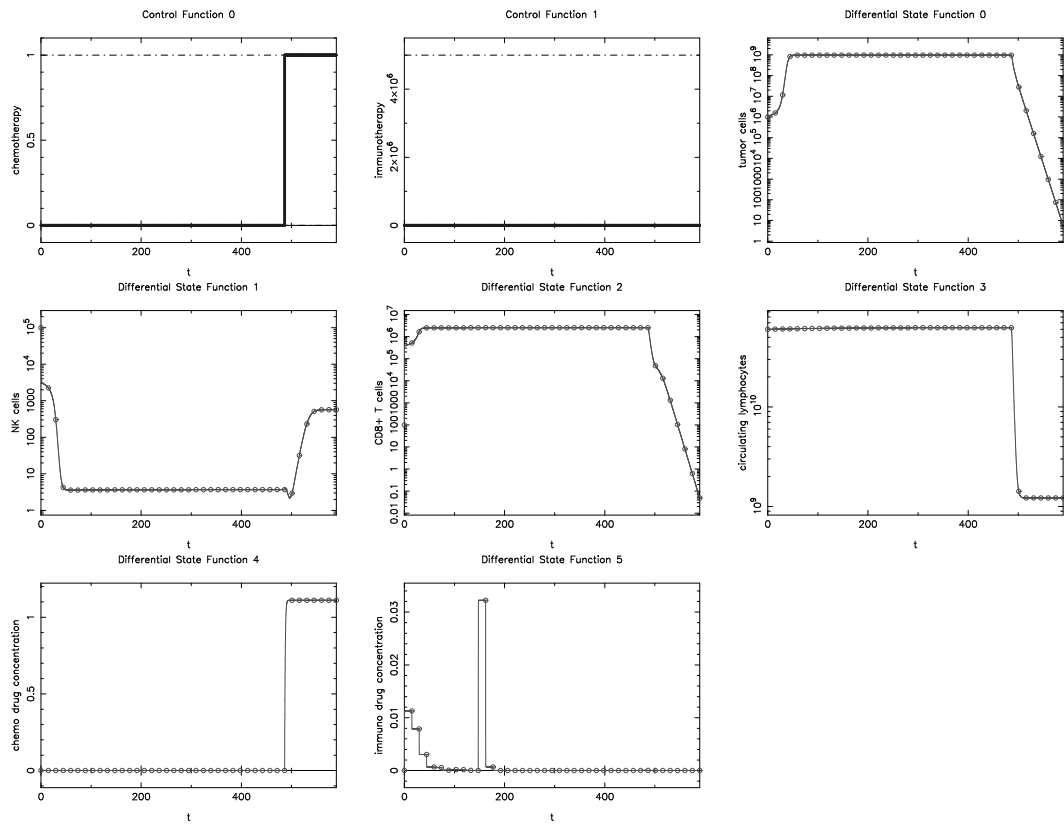**Figure 5.20:** Optimal control result of *de Pillis et al. 2006, human 9*. $t = 1$, $p = 2$, $s = 3$.
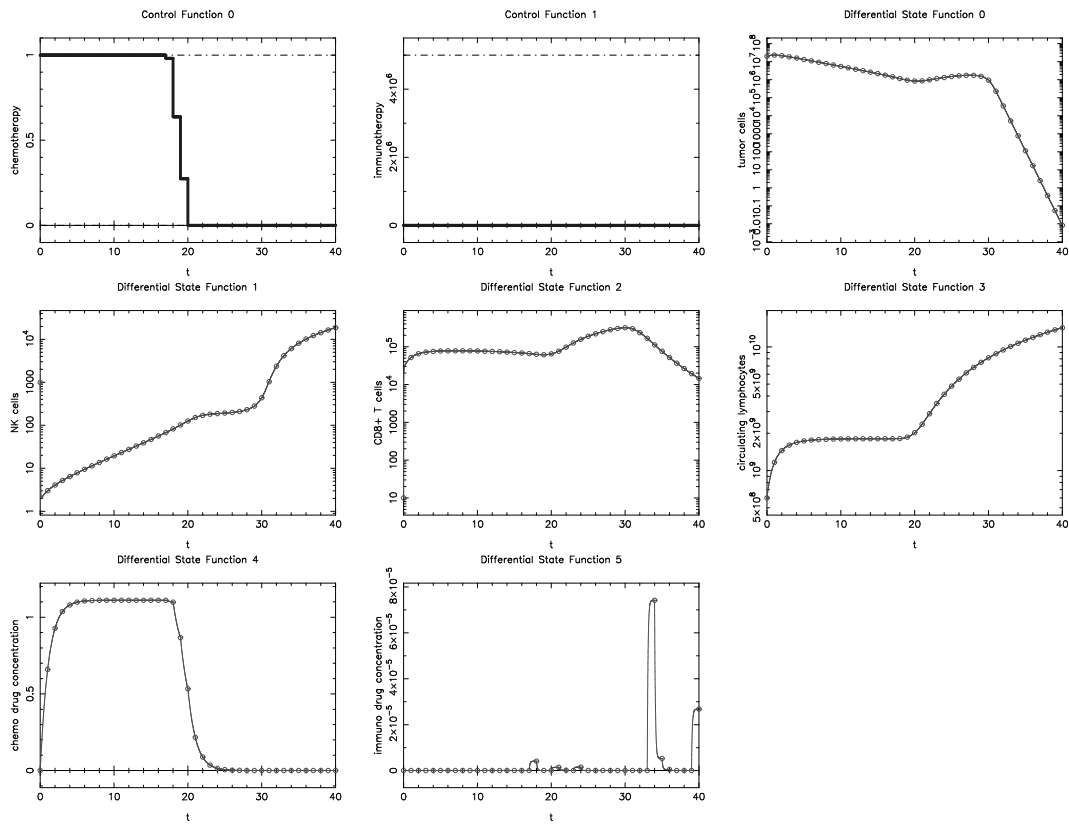
**Figure 5.21:** Optimal control result of *de Pillis et al. 2006, human 9.* $t = 1$, $p = 3$, $s = 4$.
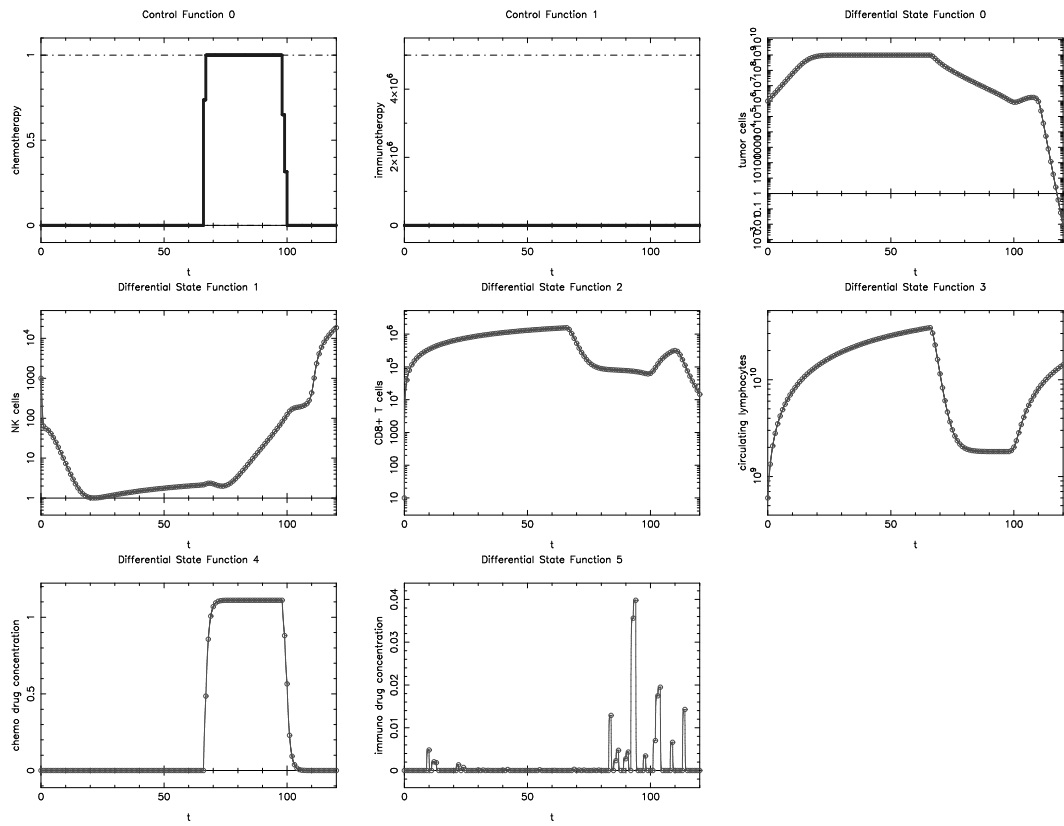
Figure 5.22: Optimal control result of *de Pillis et al. 2006, human 9. $t = 2$, $p = 3$, $s = 3$.*
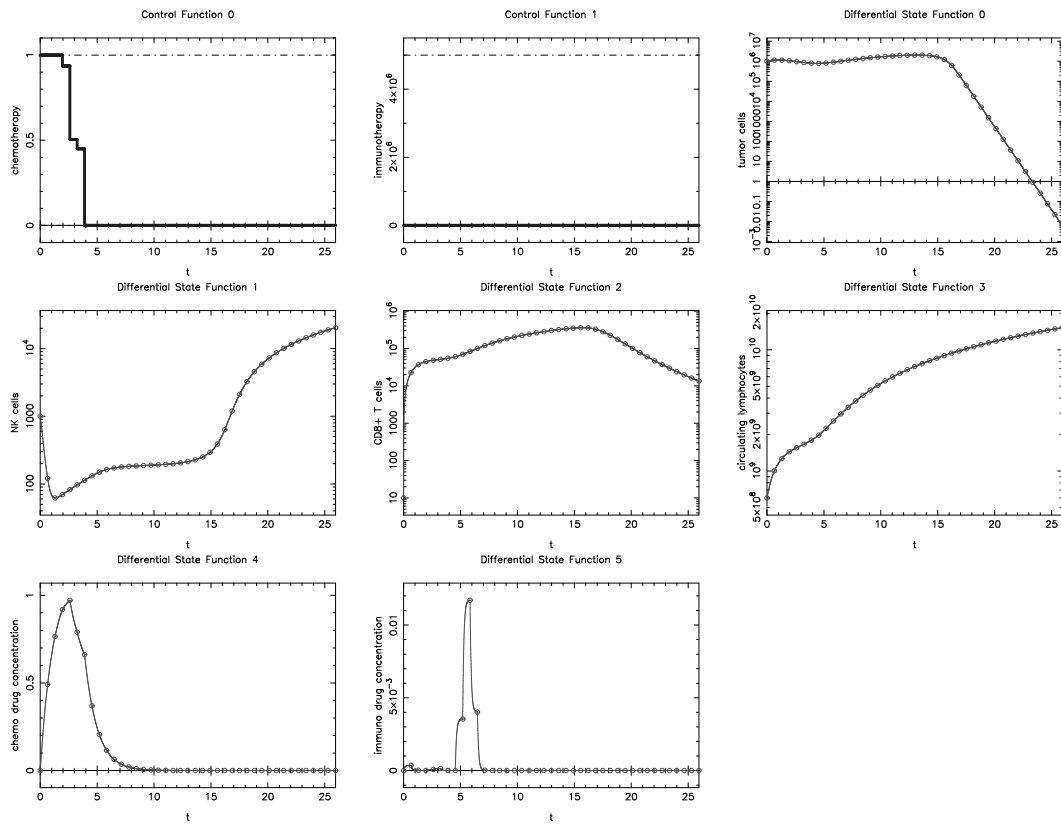
Figure 5.23: Optimal control result of *de Pillis et al. 2006, human 9. t = 3, p = 1, s = 3.*
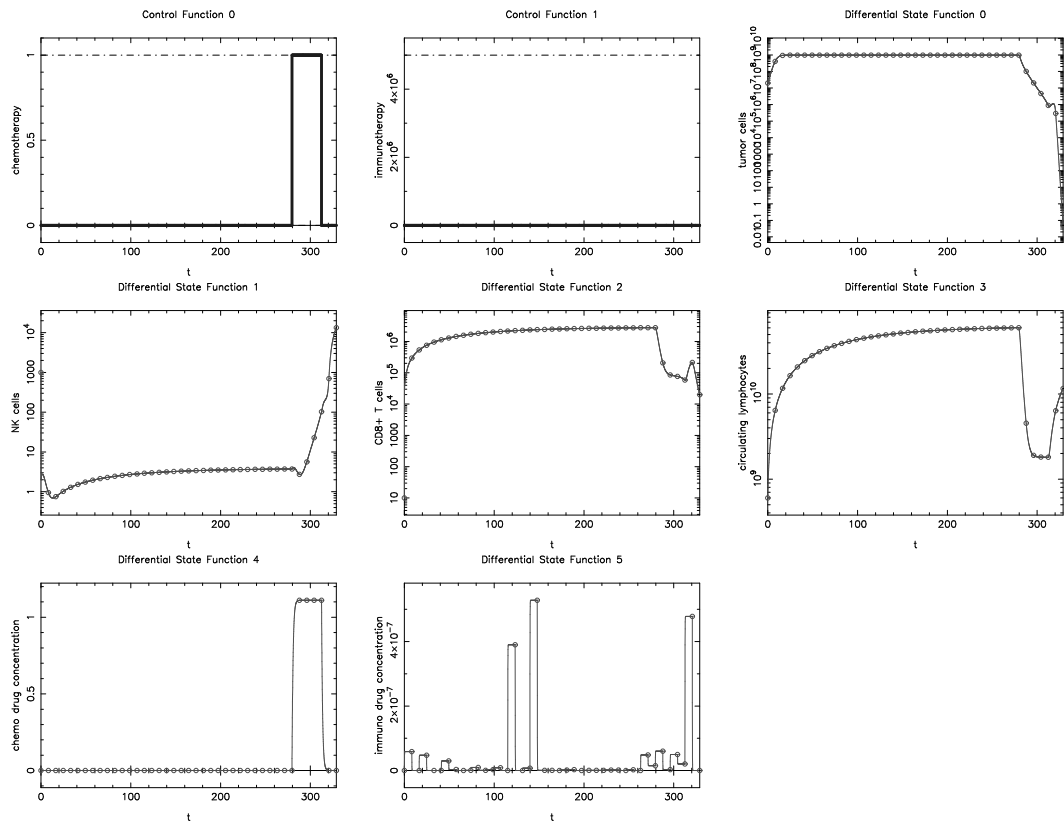
Figure 5.24: Optimal control result of *de Pillis et al. 2006, human 9. t = 3, p = 3, s = 4.*

and the influence of a 10^2 term on a 10^5 state indeed might be low.

Finally, we have a look at the comparison between maximized and minimized tumor populations. The procedure was the same as in the *mouse* section. We fixed the drug amount to the minimization value, changed the sign of the corresponding objective parameters, i.e. $p_0 = -1.0$ for $p = 3$, and started the optimization again. The difference is even higher with a maximal tumor of almost 10^9 and a minimum one with less than 1, which corresponds to less than 0.000001‰. Again the standard treatment is even a little worse than the maximization, but the drug amount for the maximization also was about 150% more. See also the plots in figure 5.25.

5.5 Human 10 Optimal Control (de Pillis 2006)

Like *human 9*, the *human 10* parameter set shares the equations with the *mouse* model. We start with the reproduction of the results in the article, see figure 5.26. The first two scenarios without any treatment could be verified by the plots. In the third, we observed some differences, and the last one could not be reproduced at all. The differences seem to arise from the influence of *IL-2*. The third plot shows a treatment with 10^9 *TIL* from day 8 to day 9 and *IL-2* from day 8 to day 11. The next one features additional *IL-2* from days 11 through 13, 20 through 25, and 80 through 90. Unlike we showed in the section above, in the plots of [10] *IL-2* treatment has a big impact on CD8+ T cells. The differences in the third plot may result from this, too. Note that *IL-2* therapy here causes an increase of CD8+ T cells of about 10^7. According to (5.14), with $x_2 \approx 1$,

$$\frac{p_I \, x_2 \, x_5}{g_I + x_5} \approx \frac{10^{-1} \cdot 1 \cdot 10^5}{10^7 + 10^5} \approx \frac{10^4}{10^7} \approx 10^{-3}, \tag{5.15}$$

this seems even more unlikely to be caused by immunotherapy.

In the optimal control computations, we used $s = 5$ instead of $s = 6$ due to more interesting results. A selection of the optimal solutions is presented in figures 5.27 to 5.37. Immunotherapy is again on very low levels as expected. Many solutions for chemotherapy show a singular arc (figures 5.27, 5.28, 5.32, 5.33, 5.35). Note however, that these are solutions under objective $p = 1$. Only 5.35 contains a singular solution with objective $p = 3$. With $s = 7$ the tumor diminishes by itself, so depending on the objective, there is no treatment at all (figure 5.29) or only treatment at the end (figures 5.31, 5.34). The free time scenario, figure 5.37, has an end time of about 600 days, with the therapy only in the last sixth.

The different singular results look interesting for applying the rounding heuristics from chapter 4, *sum up rounding* and *decomposed MILP*. About half of the sum up rounding results (figures 5.38, 5.39, 5.40, and 5.41) show a *chattering* tendency, which is not surprising since the controls are at about the middle of the interval $[0, 1]$. Of course, sum up rounding applied to controls that are already or almost of *bang-bang* type results in a control which is (very) similar to the original continuous one. Such cases have been omitted as well as similar results. Whereas the overall performance with respect to the tumor population is as good as expected, the controls with *chattering* may not be applicable in medical practice. So we also computed solutions with only 4, 6, and 8 switches with our *decomposed MILP* algorithm, see figures 5.42, 5.43, 5.45, 5.44, and 5.46. For $t = 1$, $p = 1$, $s = 2$, the end value is about twice as high as with the sum up results and about three times as high as with continuous controls. The performance gets better almost linearly with a growing number of switches. Especially for
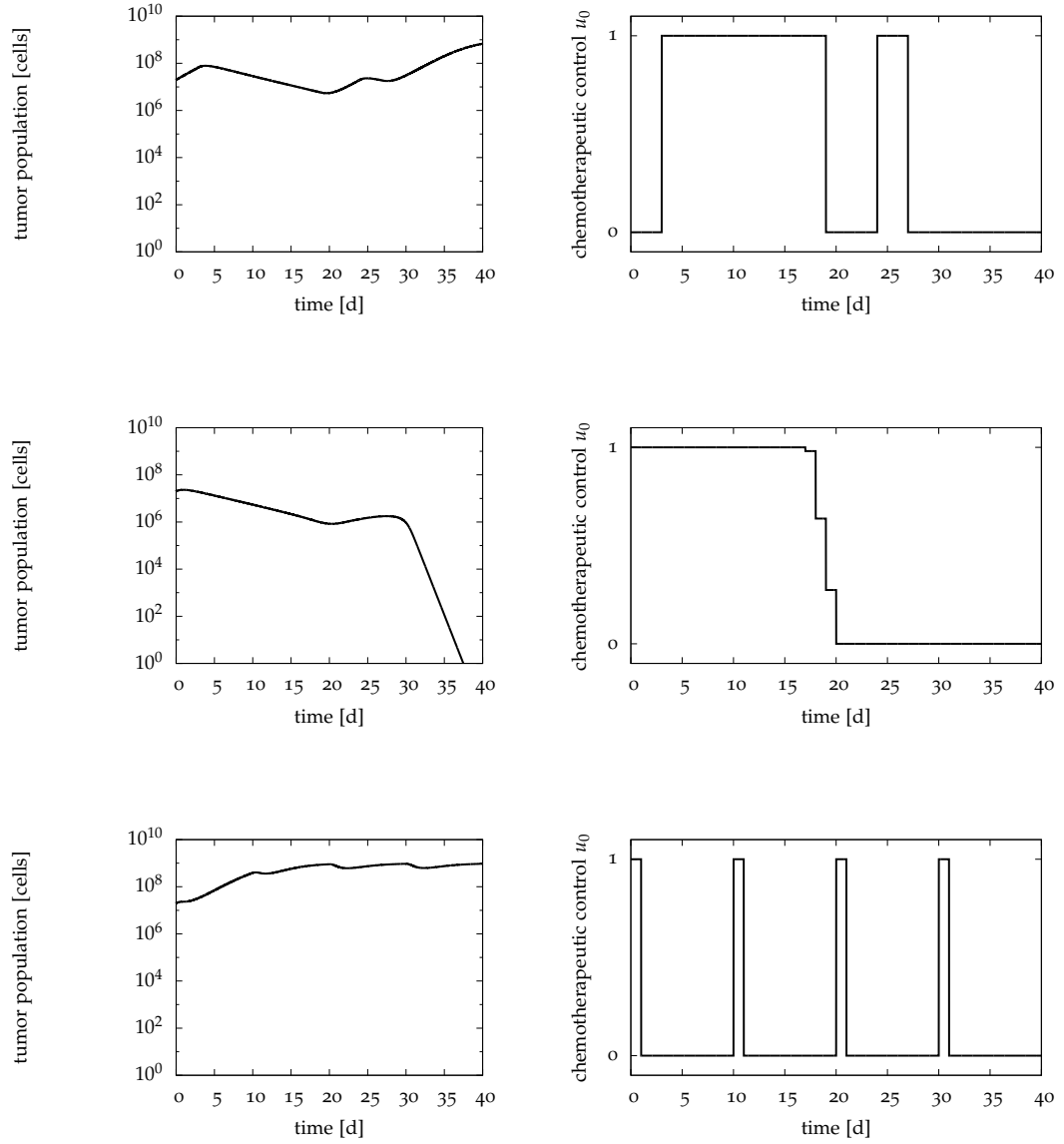
Figure 5.25: Comparison between maximization, minimization and standard treatment of *de Pillis et al. 2006, human 9*. $t = 1$, $p = 3$, $s = 4$. Top: maximization, middle: minimization, bottom: standard therapy (example). Tumor volume is shown on the left side, chemotherapy control on the right side. Compare figure 5.21 for the total optimal control result.
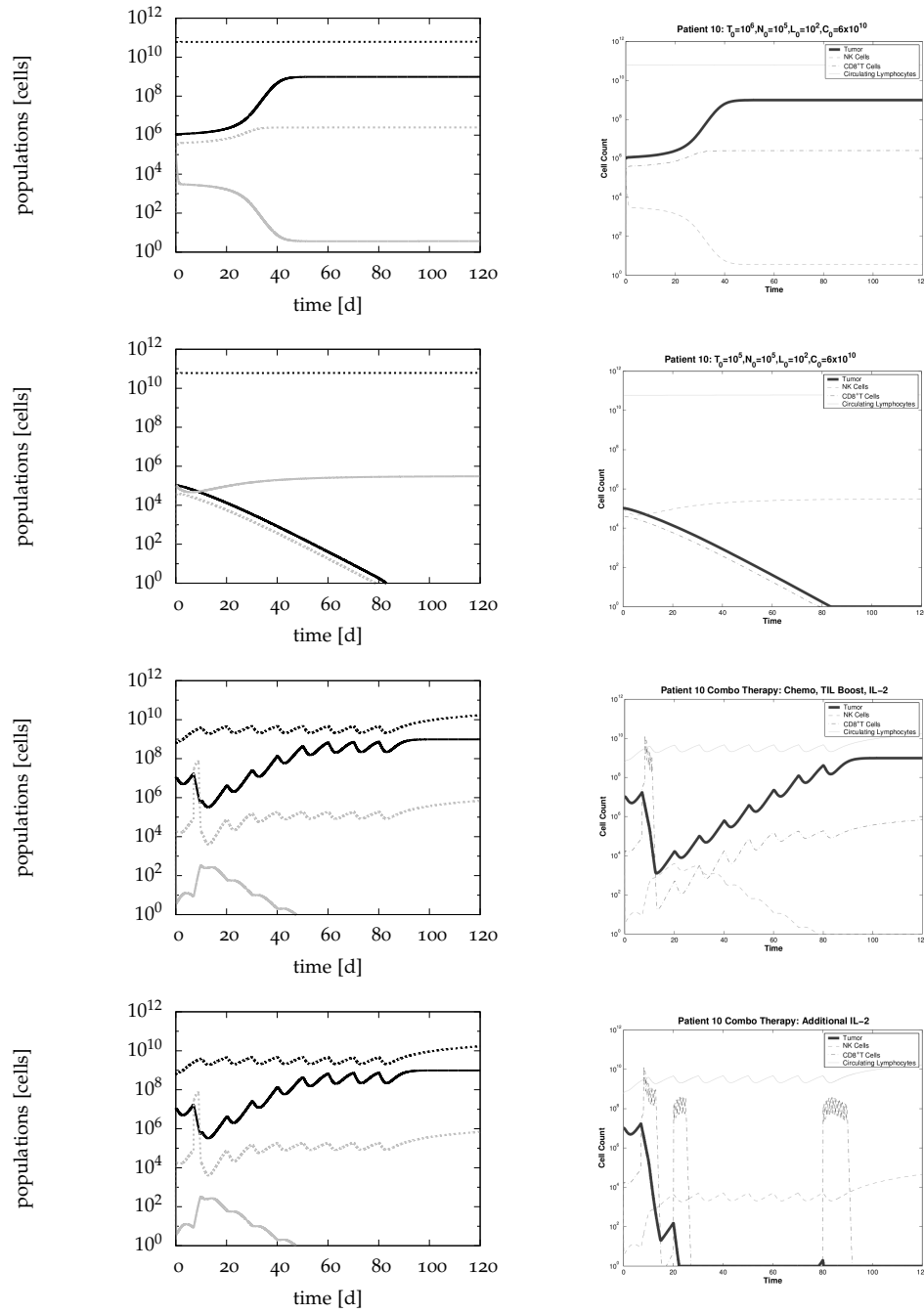
Figure 5.26: Comparison between MUSCOD-II simulation results (left) and *de Pillis et al. 2006* (right), Human 10. From top to bottom: $s = 2$ without treatment, $s = 7$ without treatment, $s = 6$ with combination therapy, $s = 6$ with additional IL-2. Tumor population is black solid, NK cells are black dashed, CD8+ T cells gray solid and circulating lymphocytes gray dashed.

the short time scenarios, the *decomposed MILP* results look promising for a transfer to medical practice. For the higher times, see figures 5.45 and 5.44, the number of switches seems to be too low. With a rising number of nodes and switches, the calculation times for the solution of the *MILP* grow exponentially, though. For example, when the time for the four switches control lies at a few minutes, the computation of the six switches takes about 20 minutes.

Finally, we again have a look at a maximization compared to a minimization and a *standard* treatment in figure 5.47. Again our approach was to fix the amount of drug, change the sign of the corresponding parameters (p_0 and p_1) and restart the optimization. Here the maximization is a bit lower as the minimization at the end time (a little bit more than 10^6), but as the objective function was $p = 1$, the aim was to maximize/minimize the tumor population over the whole time. Under this aspect, the maximization is significantly higher, especially in the first third of the treatment. The standard treatment is at about 10^9, but the drug amounts of the two other experiments were about 500% higher.

Figure 5.27: Optimal control result of *de Pillis et al. 2006, human 10. $t = 1$, $p = 1$, $s = 2$.*

Figure 5.28: Optimal control result of *de Pillis et al. 2006, human 10.* $t = 1$, $p = 1$, $s = 5$.

Figure 5.29: Optimal control result of *de Pillis et al. 2006, human 10. t = 1, p = 1, s = 7.*

Figure 5.30: Optimal control result of *de Pillis et al. 2006, human 10.* $t = 1$, $p = 2$, $s = 2$.

Figure 5.31: Optimal control result of *de Pillis et al. 2006, human 10.* $t = 1$, $p = 2$, $s = 7$.

Figure 5.32: Optimal control result of *de Pillis et al. 2006, human 10.* $t = 2$, $p = 1$, $s = 2$.

Figure 5.33: Optimal control result of *de Pillis et al. 2006, human 10*. $t = 2$, $p = 1$, $s = 5$.

Figure 5.34: Optimal control result of *de Pillis et al. 2006, human 10*. $t = 2, p = 2, s = 7$.

Figure 5.35: Optimal control result of *de Pillis et al. 2006, human 10.* $t = 2$, $p = 3$, $s = 2$.

Figure 5.36: Optimal control result of *de Pillis et al. 2006, human 10.* $t = 2$, $p = 3$, $s = 5$.

Figure 5.37: Optimal control result of *de Pillis et al. 2006, human 10.* $t = 3$, $p = 3$, $s = 2$.
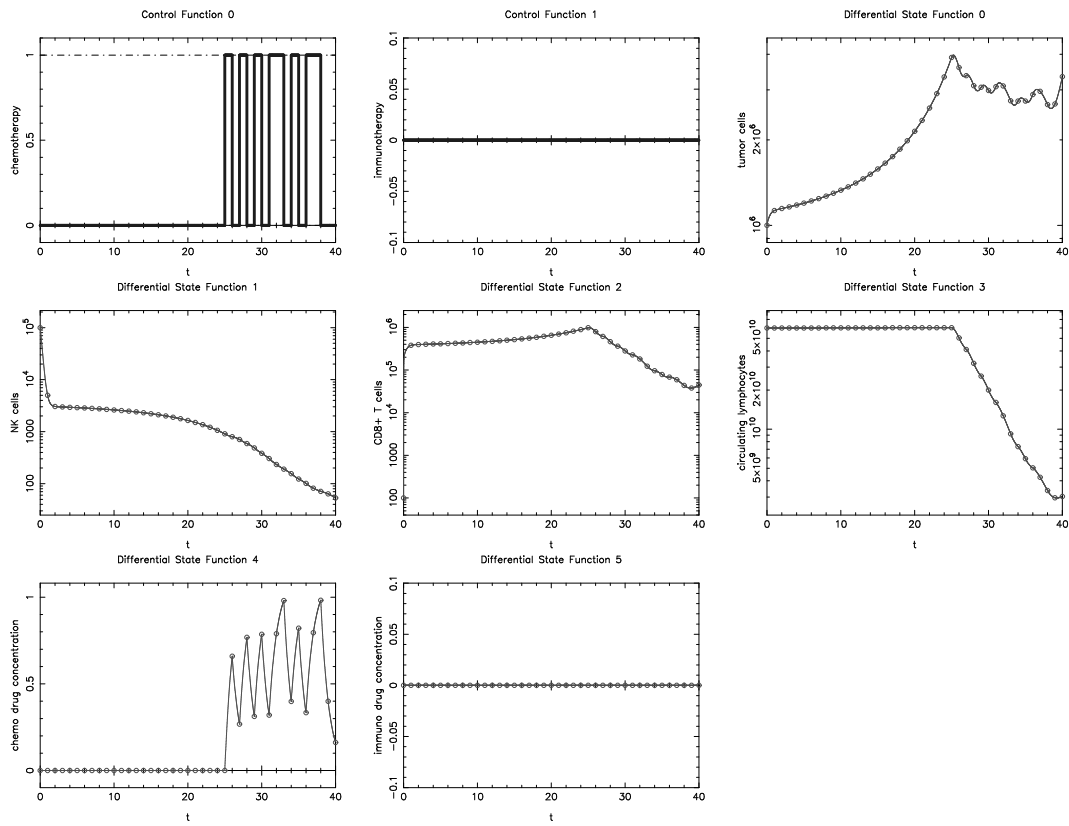
Figure 5.38: Sum up rounding result of *de Pillis et al. 2006, human 10*. $t = 1$, $p = 1$, $s = 2$.
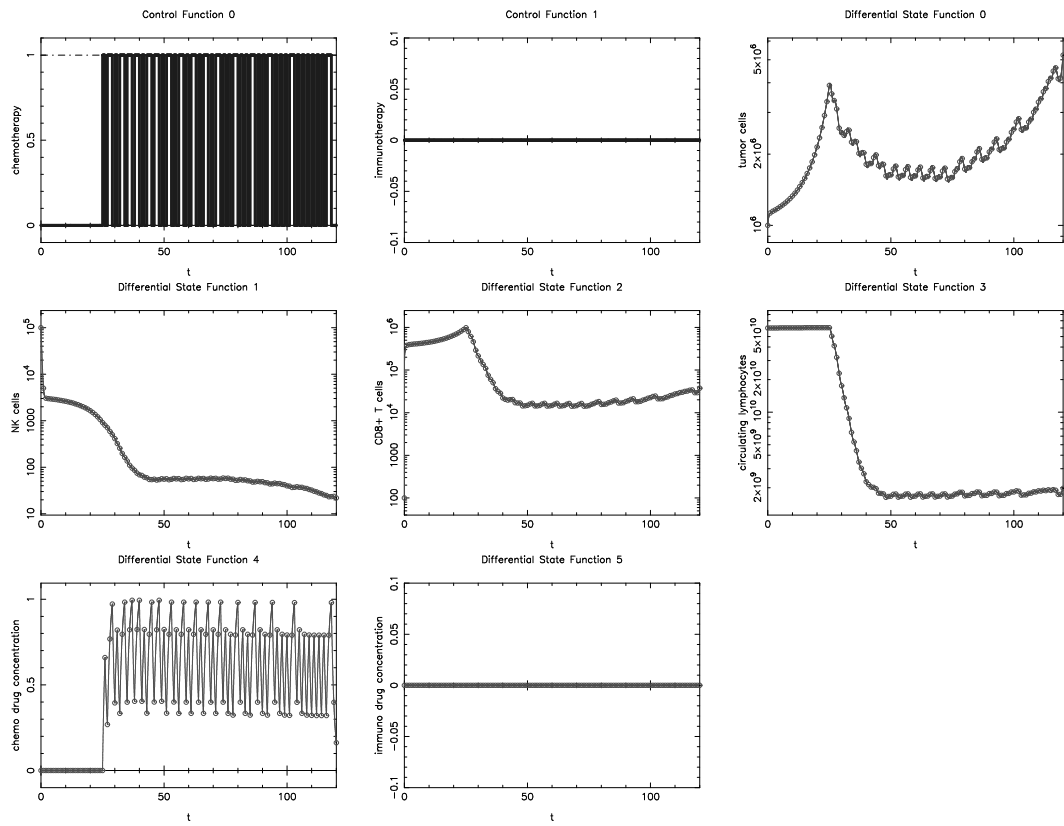
Figure 5.39: Sum up rounding result of *de Pillis et al. 2006, human 10. t = 2, p = 1, s = 2.*
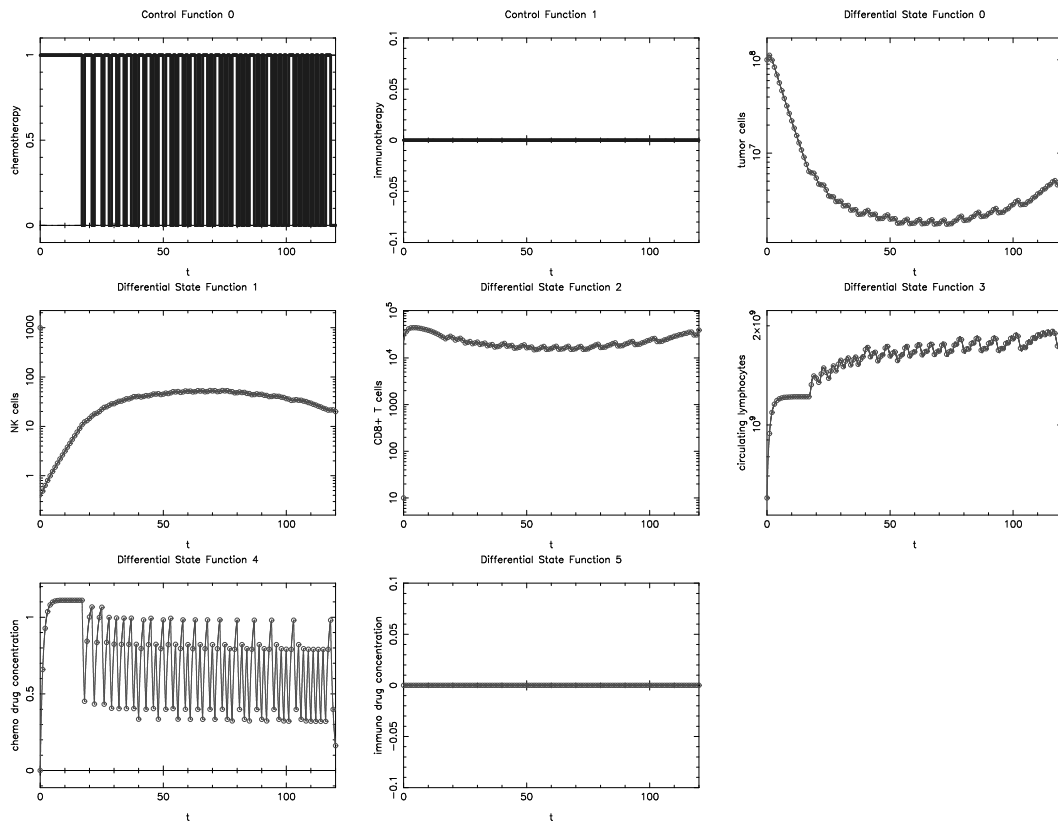
Figure 5.40: Sum up rounding result of *de Pillis et al. 2006, human 10.* $t = 2$, $p = 1$, $s = 5$.
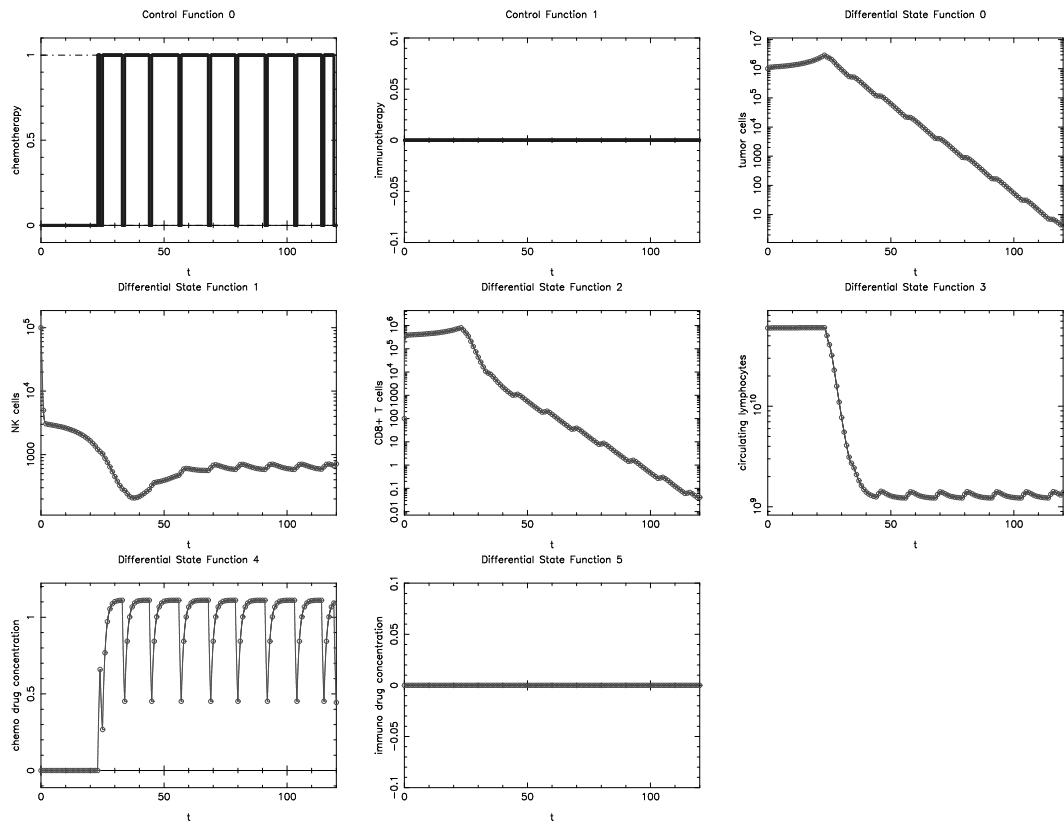
Figure 5.41: Sum up rounding result of *de Pillis et al. 2006, human 10.* $t = 2$, $p = 3$, $s = 2$.

		Mouse	Human 9					Human 10		
		$s=1$	$s=2$	$s=3$	$s=4$	$s=5$	$s=6$	$s=2$	$s=5$	$s=7$
	$p=1$	★	■	◊	★	★	■	★	★	■
$t=1$	$p=2$	◊	■	■	◊	◊	◊	■	■	■
	$p=3$	★	◊	★	★	■	■	■	■	■
	$p=1$	◊	■	◊	◊	◊	◊	★	★	■
$t=2$	$p=2$	◊	◊	◊	◊	◊	◊	◊	■	■
	$p=3$	■	◊	■	■	■	■	★	■	■
	$p=1$	♦	■	■	♦	♦	♦	♦	♦	■
$t=3$	$p=2$	◊	◊	◊	◊	◊	◊	◊	♦	◊
	$p=3$	◊	◊	◊	■	■	◊	■	■	◊

Table 5.6: Overview of results from *de Pillis et al. 2006*. s refers to the different initial value sets, p to the different objective functions, and t to the different time horizons (see also tables 5.5, 5.4, and 5.3).
■= Bang-bang result, ★= Singular result, ♦= $t_f \to 0$, ◊= Calculation failed, e.g. because of problems with the generation of derivatives or the QP solution.

5.6 De Pillis 2008 Optimal Control

We recall the model equations given in (2.35), which are derived by the ones for the models in the three sections above:

$$\dot{x}_0 = a\,x_0\,(1 - b\,x_0) - c\,x_1\,x_0 - D\,x_0 - K_T\,x_4\,x_0, \tag{5.16a}$$

$$\dot{x}_1 = \alpha_1 - f\,x_1 + g\,\frac{x_0}{h + x_0}x_1 - p\,x_1\,x_0 - K_N\,x_4\,x_1, \tag{5.16b}$$

$$\begin{aligned}\dot{x}_2 = &-m\,x_2 - q\,x_2\,x_0 + r_2\,x_3\,x_0 \\ &- v\,x_2{}^2 - K_L\,x_4\,x_2 + \frac{p_I\,x_2\,x_5}{g_I + x_5} + u_2,\end{aligned} \tag{5.16c}$$

$$\dot{x}_3 = \alpha - \beta\,x_3 - K_C\,x_4\,x_3, \tag{5.16d}$$

$$\dot{x}_4 = -\gamma\,x_4 + u_0, \tag{5.16e}$$

$$\dot{x}_5 = \frac{p_T\,x_2\,x_0}{g_T + x_0} - w\,x_2\,x_5 - \mu_I\,x_5 + u_1, \tag{5.16f}$$

$$D = d\,\frac{(x_2/x_0)^l}{s + (x_2/x_0)^l}, \tag{5.16g}$$

$$0 \le x_0, x_1, x_2, x_3, x_4, x_5, \tag{5.16h}$$

$$0 \le u_0, u_1, u_2, \tag{5.16i}$$

$$t \in [t_0, t_f] \tag{5.16j}$$
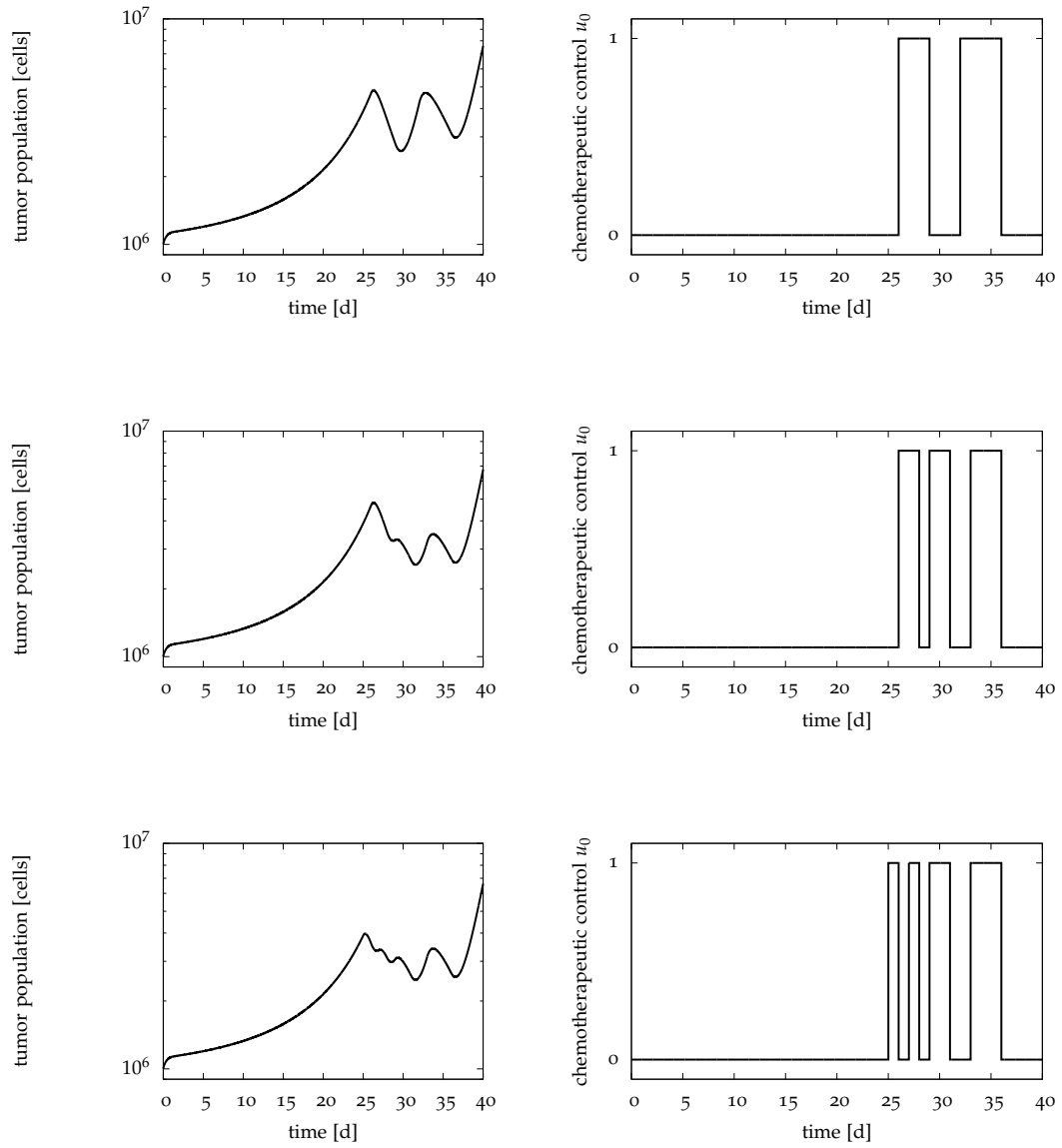
Figure 5.42: Comparison of different decomposed MILP results of *de Pillis et al. 2006*, *human 10*. $t = 1$, $p = 1$, $s = 2$. Top: 4 switches, middle: 6 switches, bottom: 8 switches. Tumor volume is shown on the left side, chemotherapy control on the right side.
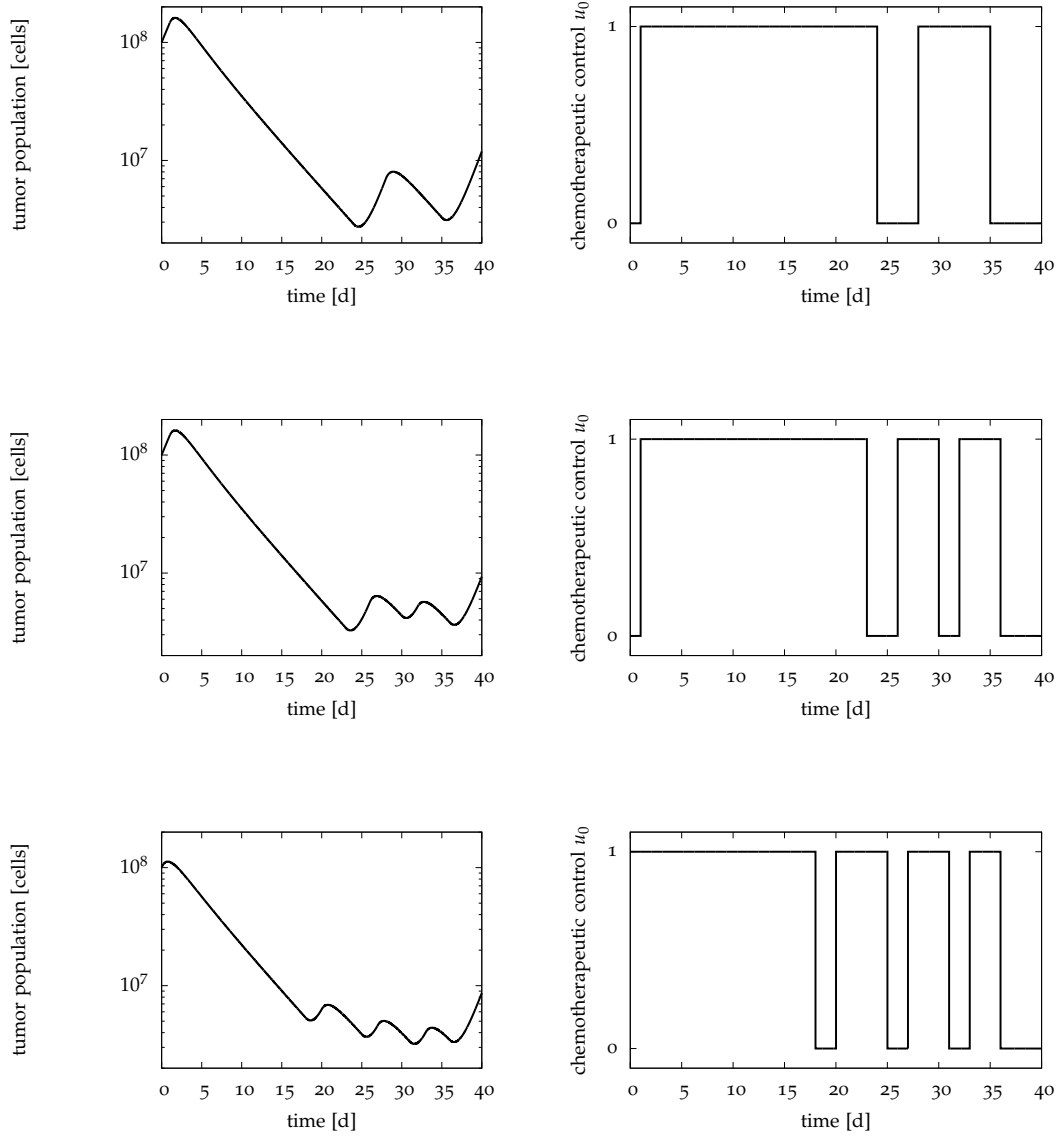
Figure 5.43: Comparison of different decomposed MILP results of *de Pillis et al. 2006*, *human 10*. $t = 1$, $p = 1$, $s = 5$. Top: 4 switches, middle: 6 switches, bottom: 8 switches. Tumor volume is shown on the left side, chemotherapy control on the right side.
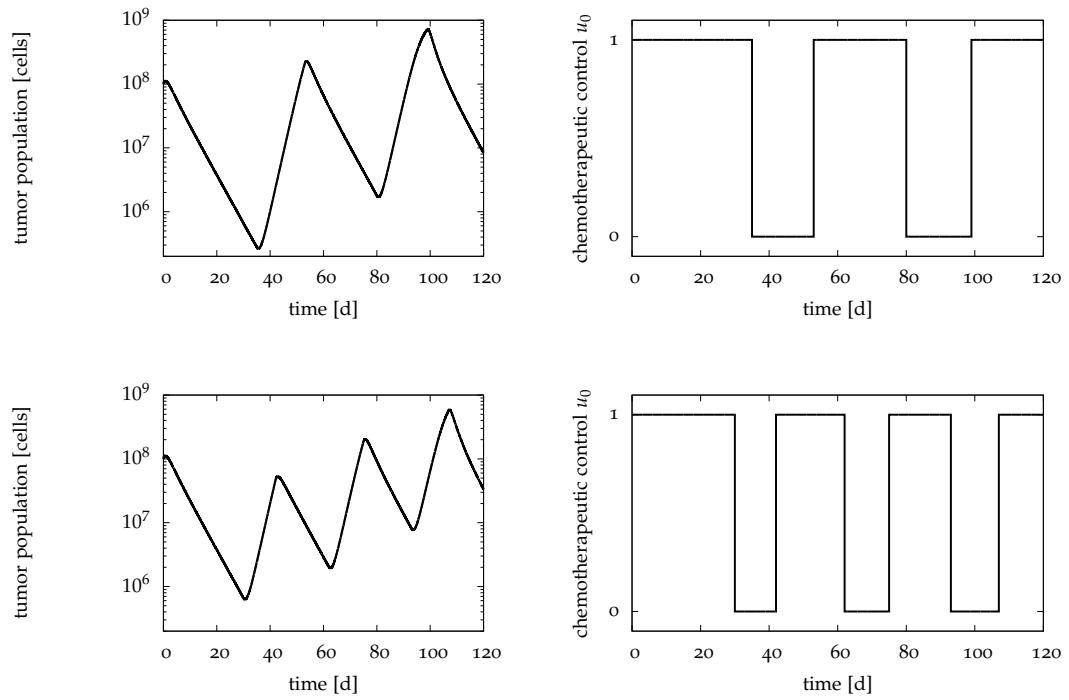
Figure 5.44: Comparison of different decomposed MILP results of *de Pillis et al. 2006*, *human 10*. $t = 2$, $p = 1$, $s = 5$. Top: 4 switches, bottom: 6 switches. Tumor volume is shown on the left side, chemotherapy control on the right side.
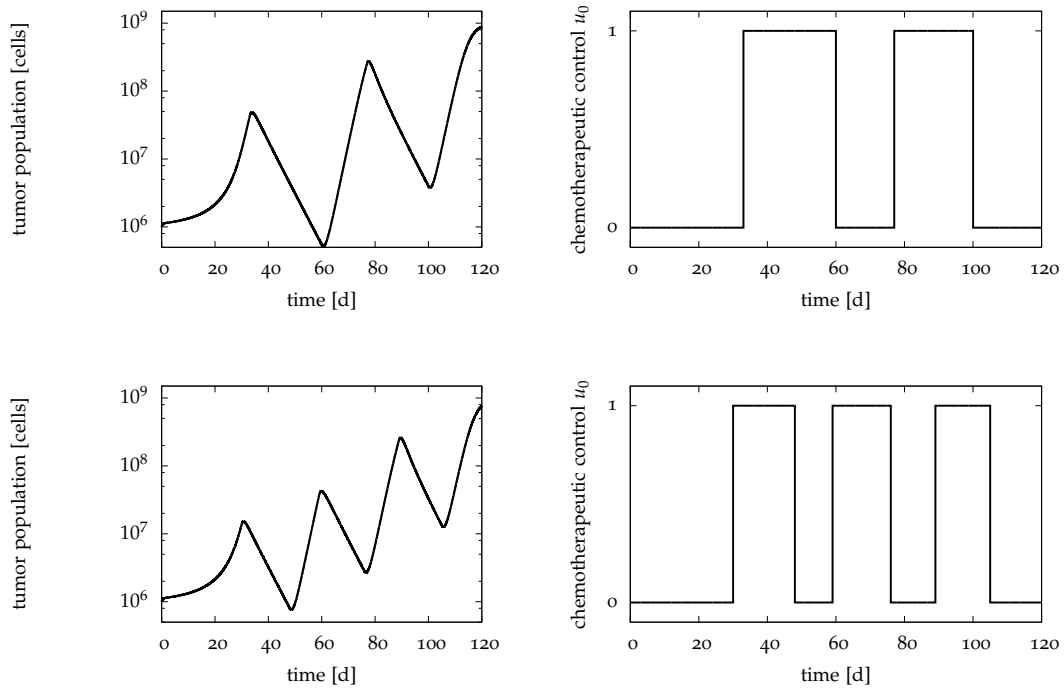
Figure 5.45: Comparison of different decomposed MILP results of *de Pillis et al. 2006*, *human 10*. $t = 2$, $p = 1$, $s = 2$. Top: 4 switches, bottom: 6 switches. Tumor volume is shown on the left side, chemotherapy control on the right side.
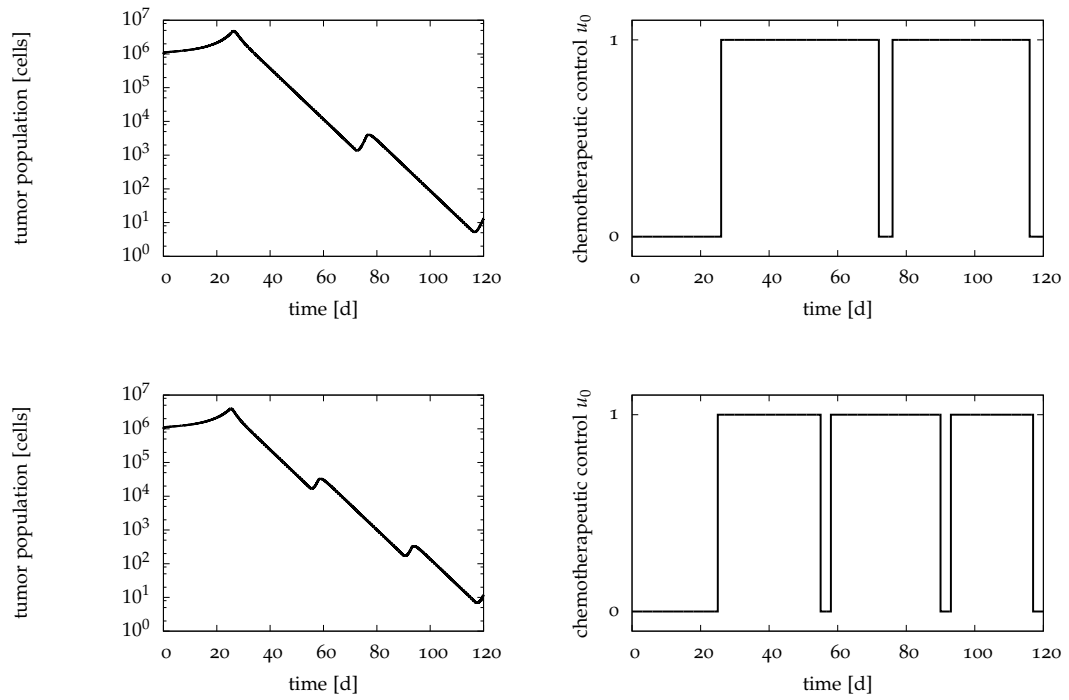
Figure 5.46: Comparison of different decomposed MILP results of *de Pillis et al. 2006*, *human 10*. $t = 2$, $p = 3$, $s = 2$. Top: 4 switches, bottom: 6 switches. Tumor volume is shown on the left side, chemotherapy control on the right side. Continuous solution is shown in figure 5.27
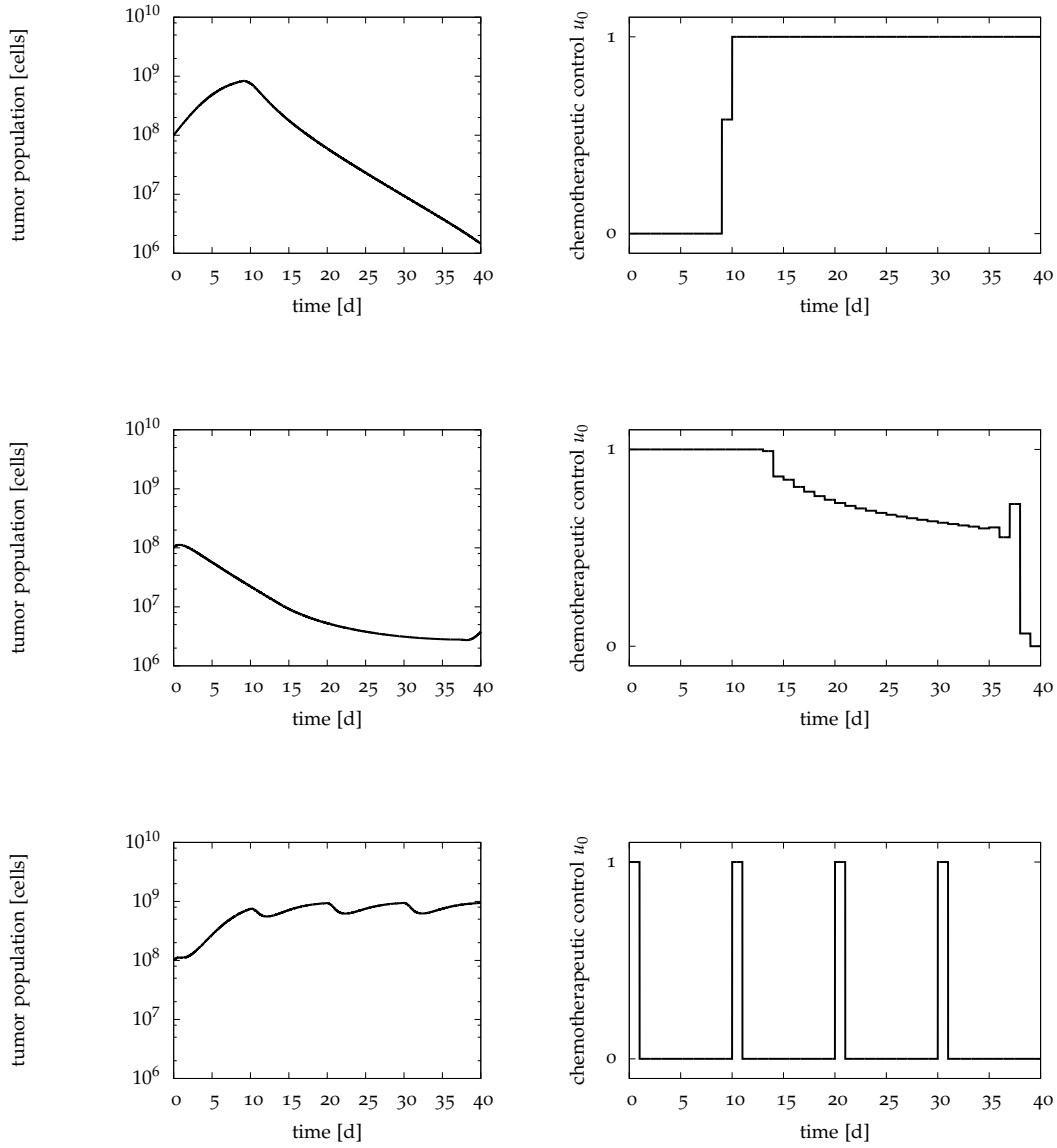
Figure 5.47: Comparison between maximization, minimization and standard treatment of *de Pillis et al. 2006*, *human 10*. $t = 1$, $p = 1$, $s = 5$. Top: maximization, middle: minimization, bottom: standard therapy (example). Tumor volume is shown on the left side, chemotherapy control on the right side. Note that the objective function is a weighted sum, so that minimization and maximization refers to a sum of the integral *and* the end value of the tumor population. This explains that the minimized end value of the tumor population is higher than the maximized one.

Different scenarios are subject of the optimal control computations in the article. There are three objective functions, which all have the form

$$\min_{x,u} \int_{t_0}^{t_f} x_0(t) + \frac{p_0}{2} u_0(t)^2 + \frac{p_1}{2} u_1(t)^2 + \frac{p_2}{2} u_2(t)^2 \quad dt. \tag{5.17}$$

These objectives will be denoted by $p = 1$, $p = 2$, and $p = 3$ in the following, see table 5.7 for the different parameter values. Additionally, there are two initial value sets, shown in table 5.8, to which we refer to as $s = 1$ and $s = 2$. All combinations have been investigated by the authors. The time horizon was 5 days for all scenarios except $p = 3$, $s = 2$ with 10 days.

p_0	p_1	p_2	
$1 \cdot 10^7$	$1 \cdot 10^7$	0	$p = 1$
$1 \cdot 10^7$	0	$1 \cdot 10^7$	$p = 2$
$1 \cdot 10^7$	$1 \cdot 10^5$	$1 \cdot 10^5$	$p = 3$

Table 5.7: Different objective function parameters for *de Pillis et al. 2008*

$x_0(t_0)$	$x_1(t_0)$	$x_2(t_0)$	$x_3(t_0)$	$x_4(t_0)$	$x_5(t_0)$	
$1 \cdot 10^2$	$3 \cdot 10^4$	$3 \cdot 10$	$5 \cdot 10^6$	0	0	$s = 1$
$1 \cdot 10^7$	$5 \cdot 10^5$	$2 \cdot 10^3$	$4.17 \cdot 10^{10}$	0	0	$s = 2$

Table 5.8: Initial value sets in *de Pillis et al. 2008*

We started with an attempt to reproduce the optimization results from [9]. There are no exact values given, so we have to stick to the plots for verification. First we had a look at the scenario $s = 2$, $p = 1$. Our results can be found in figure 5.48. With the parameters given by *de Pillis et al. 2008*, our result differs by up to 12 orders of magnitude from theirs. So we checked our implementation and especially the parameter values again, and with a trial and error approach changed some parameters to values similar to the ones in [10]. Eventually, we found that we could more or less exactly reproduce the result of *de Pillis 2008 et al.* with a tumor growth parameter $a = 4.0$ instead of $a = 2.0 \cdot 10^{-3}$.

The next scenario, which has been investigated, is $s = 1$, $p = 1$. We first tried to reproduce the result with $a = 2.0 \cdot 10^{-3}$ but again the differences were high (up to 6 orders of magnitude). Furthermore, with $a = 4.0$ (no plot available) we could not reproduce their results either. With some trial and error experiments however, we observed that $a = 2.0$ does quite a good job. The states could be almost perfectly verified. In the controls though there are some differences, especially in the structure of chemotherapy u_0. Anyhow, the level of the controls is that low that the influence of the two therapies is barely measurable, compare figure 5.49. In contrast, an effect can be observed in figure 5.48 in which at least the chemotherapy is 6 orders of magnitude higher.

Because of these deviations, we tried to contact the authors several times. Finally, L.G. de Pillis stated that it could be possible that there is a typo in the paper but that she had not enough time to have a look at the code. She referred us to her co-authors, but we did not get

any further response. Note, however, that in our calculations, it seemed that a typing error of the parameter value of *a* only would not be sufficient, since we could not reproduce the results in different scenarios with the *same* value for *a*.

Concerning the optimal therapies for another $s = 1$ scenario, the treatments are again on very low levels (10^{-5}), where they might have almost no effect. Note also that in all experiments by *de Pillis et al. 2008*, immunotherapy is so low that even with a 10^{-6} scale it cannot be told apart from zero. This, however, conforms to our results for the models from *de Pillis et al. 2006* [10], where the influence of immunotherapy was negligibly small.

As it is not clear where the differences originate from, especially as they do not seem to come from a single wrong parameter value, we eventually decided not to further investigate this model and its remaining scenarios.

5.7 AG Lebiedz Test Optimal Control

The model is represented by the set of ODEs shown in (2.43):

$$\dot{x}_0(t) = \nu\, x_0(t) \left(1 - \frac{x_0(t)}{K} \right) - \mu_M\, x_6(t)\, x_0(t), \tag{5.18a}$$

$$\dot{x}_1(t) = k_t\, x_1(t) \left[\left(\frac{B}{x_5(t)} \right)^{\gamma} - \alpha \left(1 - \frac{x_7(t)^N}{k^N + x_7(t)^N} \right) x_6(t) - 1 \right], \tag{5.18b}$$

$$\dot{x}_2(t) = k_t\, x_1(t) - k_t\, x_2(t), \tag{5.18c}$$

$$\dot{x}_3(t) = k_t\, x_2(t) - k_t\, x_3(t), \tag{5.18d}$$

$$\dot{x}_4(t) = k_t\, x_3(t) - k_t\, x_4(t), \tag{5.18e}$$

$$\dot{x}_5(t) = k_t\, x_4(t) - k_t\, x_5(t), \tag{5.18f}$$

$$\dot{x}_6(t) = -\alpha_M\, x_6(t) + \beta_M\, u_0(t), \tag{5.18g}$$

$$\dot{x}_7(t) = -\alpha_L\, x_7(t) + \beta_L\, u_1(t), \tag{5.18h}$$

$$0 \le x_0(t), x_1(t), x_2(t), x_3(t), x_4(t), x_5(t), x_6(t), x_7(t), \tag{5.18i}$$

$$0 \le u_0(t), u_1(t), \tag{5.18j}$$

$$t \in [t_0, t_f]. \tag{5.18k}$$

We started with a simulation of a standard treatment as it was implemented in the *MATLAB* version of the model to successfully verify the `MUSCOD-II` implementation in figure 5.50. Time scale for testing purposes was 2000 hours (time scale in the plots, though, is hours, not days as in the other sections), which has been used for the optimal control calculations, too. Initial values were

$$x_0(t_0) = 3.0 \cdot 10^2, \qquad x_1(t_0) = 7.0, \qquad x_2(t_0) = 7.0, \tag{5.19a}$$

$$x_3(t_0) = 7.0, \qquad x_4(t_0) = 7.0, \qquad x_5(t_0) = 7.0, \tag{5.19b}$$

$$x_6(t_0) = 0.0, \qquad x_7(t_0) = 0.0 \tag{5.19c}$$

in all scenarios. The level of the leucocyte stem cells x_1 can be considered a measure of the patient's health. Anyhow, a reasonable lower bound on x_1 was not known to us until the completion of this work. For our computations though we chose different exemplary values, 2.0 and 4.0, corresponding to the test initial value of 7.0.
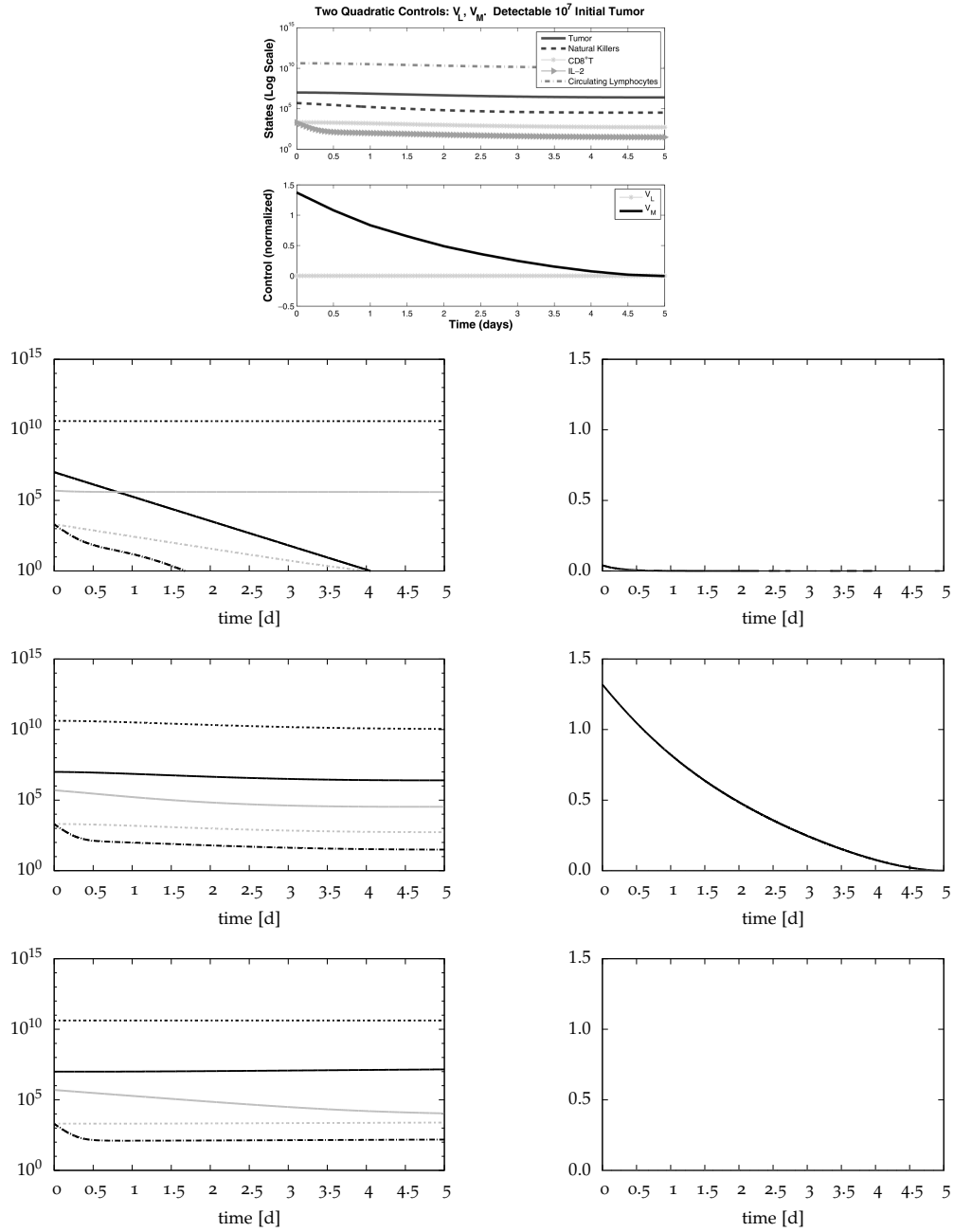
Figure 5.48: Optimal control results of *de Pillis et al. 2008*, $p = 1$, $s = 2$. From top to bottom: result from *de Pillis et al. 2008*, `MUSCOD-II` optimal control result with $a = 2.0 \cdot 10^{-3}$, `MUSCOD-II` optimal control result with $a = 4.0$, `MUSCOD-II` simulation (no therapy) with $a = 4.0$. Left part shows the states, while tumor cells are dark solid, NK cells gray solid, CD8+ T cells gray dashed, circulating lymphocytes dark dot-dashed and IL-2 gray dashed. Right part shows the controls while chemotherapy is dark, immunotherapy is bright, but almost always zero or very close to zero.
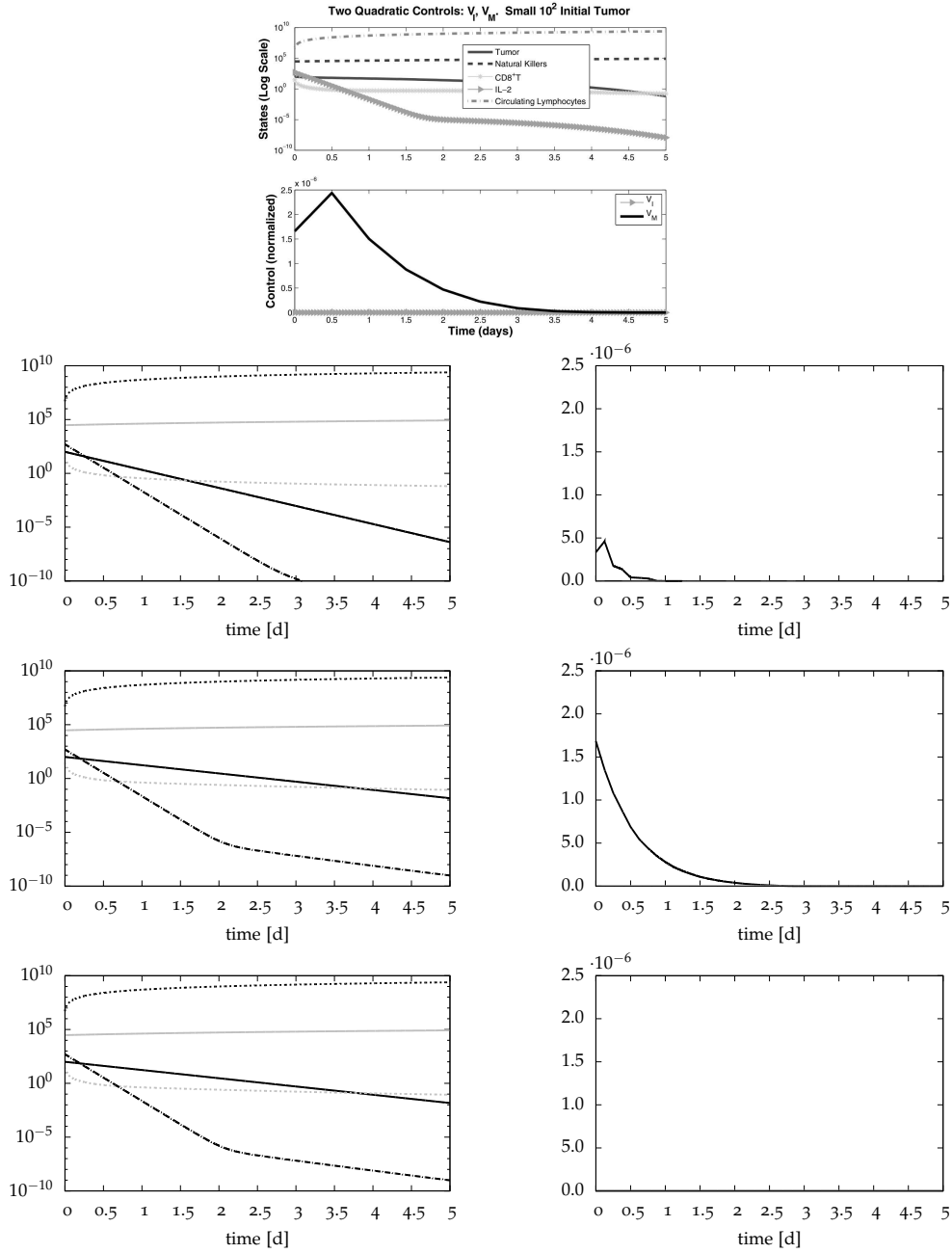
Figure 5.49: Optimal control results of *de Pillis et al. 2008*, $p = 1$, $s = 1$. From top to bottom: result from *de Pillis et al. 2008*, `MUSCOD-II` optimal control result with $a = 2.0 \cdot 10^{-3}$, `MUSCOD-II` optimal control result with $a = 2.0$, `MUSCOD-II` simulation (no therapy) with $a = 2.0$. Left part shows the states, while tumor cells are dark solid, NK cells gray solid, CD8+ T cells gray dashed, circulating lymphocytes dark dot-dashed and IL-2 gray dashed. Right part shows the controls while chemotherapy is dark, immunotherapy is bright, but almost always zero or very close to zero.

As the optimal control results generally are on a lower level than the doses of the standard treatment, in the following we lower the upper bound on the MTX control (chemotherapy) u_0. This makes the control curve better visible and is only a small restriction to the constraint at the beginning of the time horizon, if any. The objective function has been chosen as the tumor value at the end time ($p_0 = 1$), with a small penalty $p_1 = p_2 = 10^{-5}$ on the controls,

$$\min_{x,u} p_0 \cdot x_0(t_f) + \int_{t_0}^{t_f} p_1 \cdot u_0(t)^2 + p_2 \cdot u_1(t)^2 \quad dt. \tag{5.20}$$

The result without a lower bound > 0 on the leucocyte stem cells, figure 5.52, shows an almost constant chemotherapy and no use of the rescue package. This may seem the same as in the *de Pillis et al. 2006* models with immunotherapy, but the situation here is different. We ran the standard treatment simulation again without rescue package, see figure 5.51 and the immune cell populations are significantly lower than with it, especially when a chemotherapy is followed by another one in a relatively short time, e.g. at $t = 400$ and $t = 1400$. This means, that the rescue package has a significant influence in this model but with this objective it does not pay off, maybe because the tumor can be kept on a very low level with chemotherapy only while the immune cells are above the bounds.

The results with lower bounds 2.0 (figures 5.53 and 5.54) respectively 4.0 (figure 5.55) show a very similar control scheme. Again the rescue package plays no role—perhaps one should try different objectives, compare e.g. the one in [8], in future investigations. At the beginning there is a high dose first, which pushes the tumor down and the leucocyte stem cells to the bound. This high dosage is followed by an almost constant low level dosage, which follows the bound on the leucocytes and pushes the tumor further down, but less strong.

Sum up rounding has been applied to the different scenarios. Regarding the tumor, the performance is good and despite the low dosage more or less significantly better than the standard treatments. For example, the $u_0 \leq 3.0$, $x_0 \geq 4.0$ scenario uses 480 of the chemotherapeutic drug vs. 420 in the standard scheme, but pushes the tumor down to 15.66 instead of 26.75. This means a 41% smaller tumor with only 14% more drugs. The number of switches is a bit high, e.g. in the scenario with $u_0 \leq 2.0$ and $x_0 \geq 2.0$, but with a time scale of 2000 days may still be practicable. Note however, that the bounds on the leucocyte stem cells are violated up to 0.5. So for a optimization with real values perhaps a threshold should be added to the leucocyte bound.

We finally have a look at a comparison of the tumor without therapy, with optimal controlled therapy, and with a standard treatment in figure 5.60. Without any treatment the tumor grows to more than its double initial size, to about 760. The standard treatment pushes the tumor down to 26.75 (3.5% of the no treatment size), with a usage of 420 units of the chemotherapeutic drug and 504 of the immunotherapeutic drug, whereas the optimization results with $x_1(t) \geq 2.0$ and $u_0(t) \leq 2.0$ do almost not use the rescue package but about 1109 units (164% more) of the chemotherapeutic drug and get the tumor down to about $3.3 \cdot 10^{-3}$ (0.01% of the standard treatment size).

A comparison between a minimization and a maximization could not be completed due to computational problems and time limitation, but will be done in future, as soon as the fitted parameter set is complete.
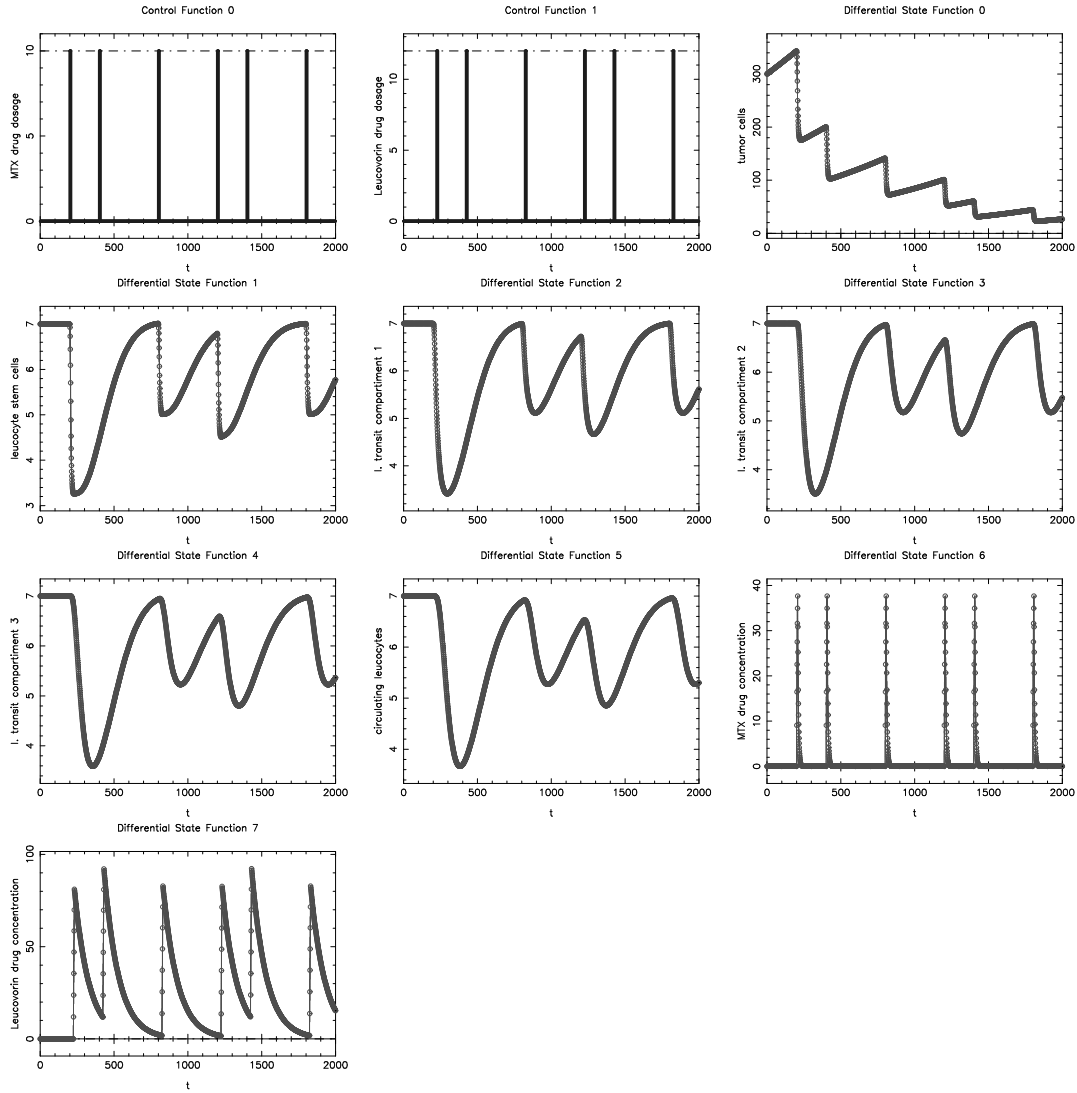
Figure 5.50: Simulation result of a standard therapy for *AG Lebiedz* model.
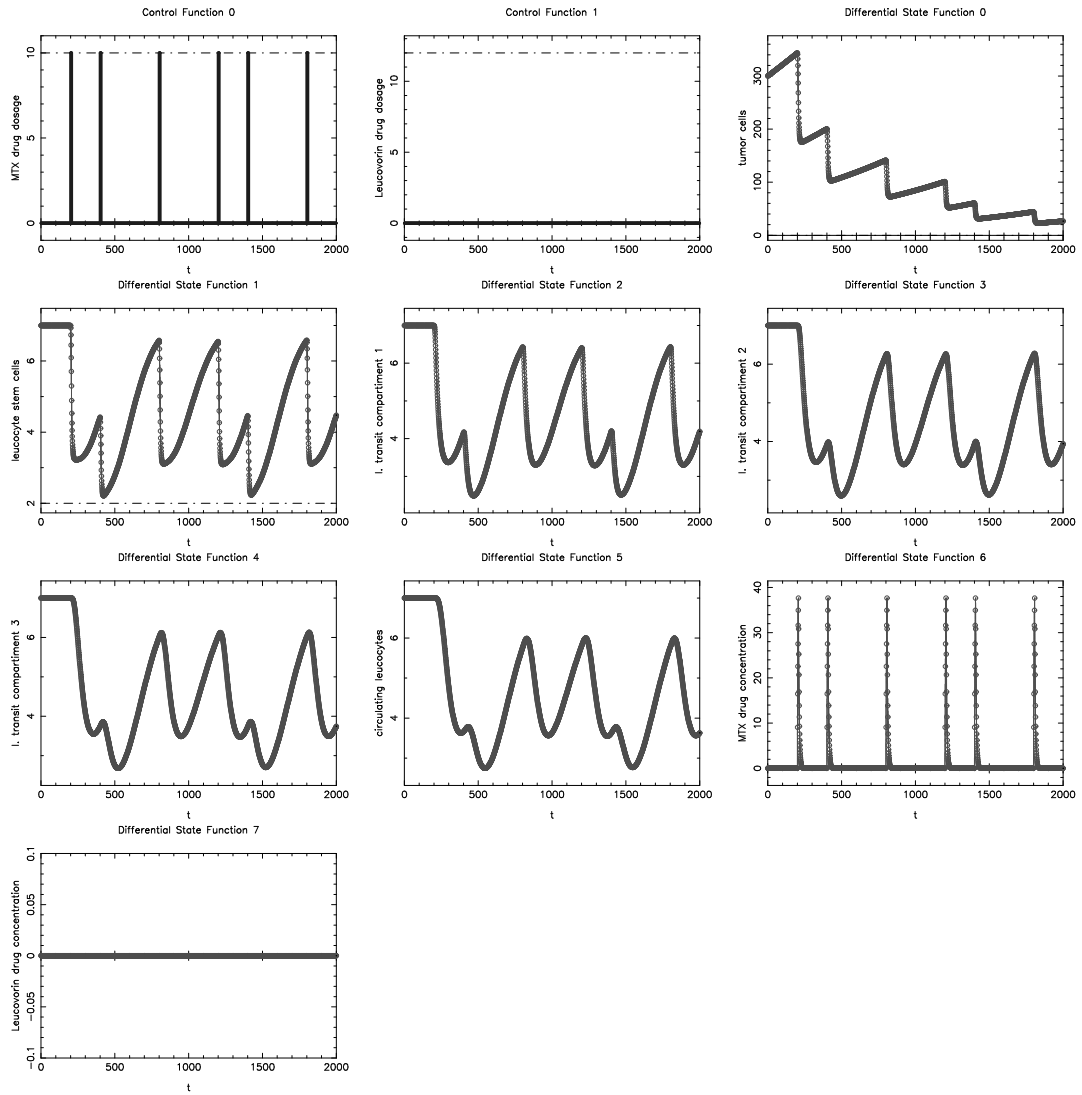
Figure 5.51: Simulation result of a standard therapy without rescue package for *AG Lebiedz* model.
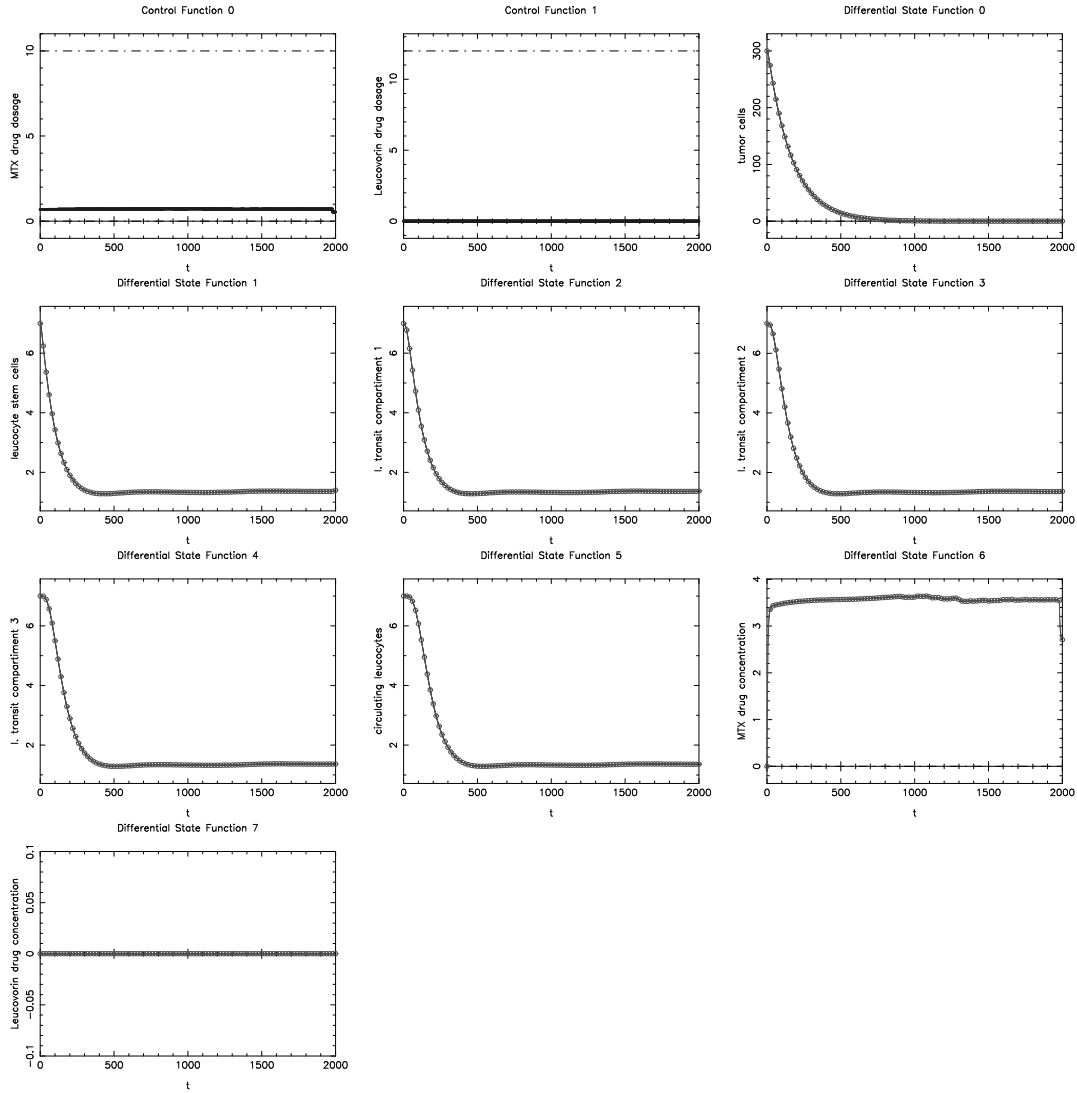
Figure 5.52: Optimal control result for *AG Lebiedz* model without additional bounds.
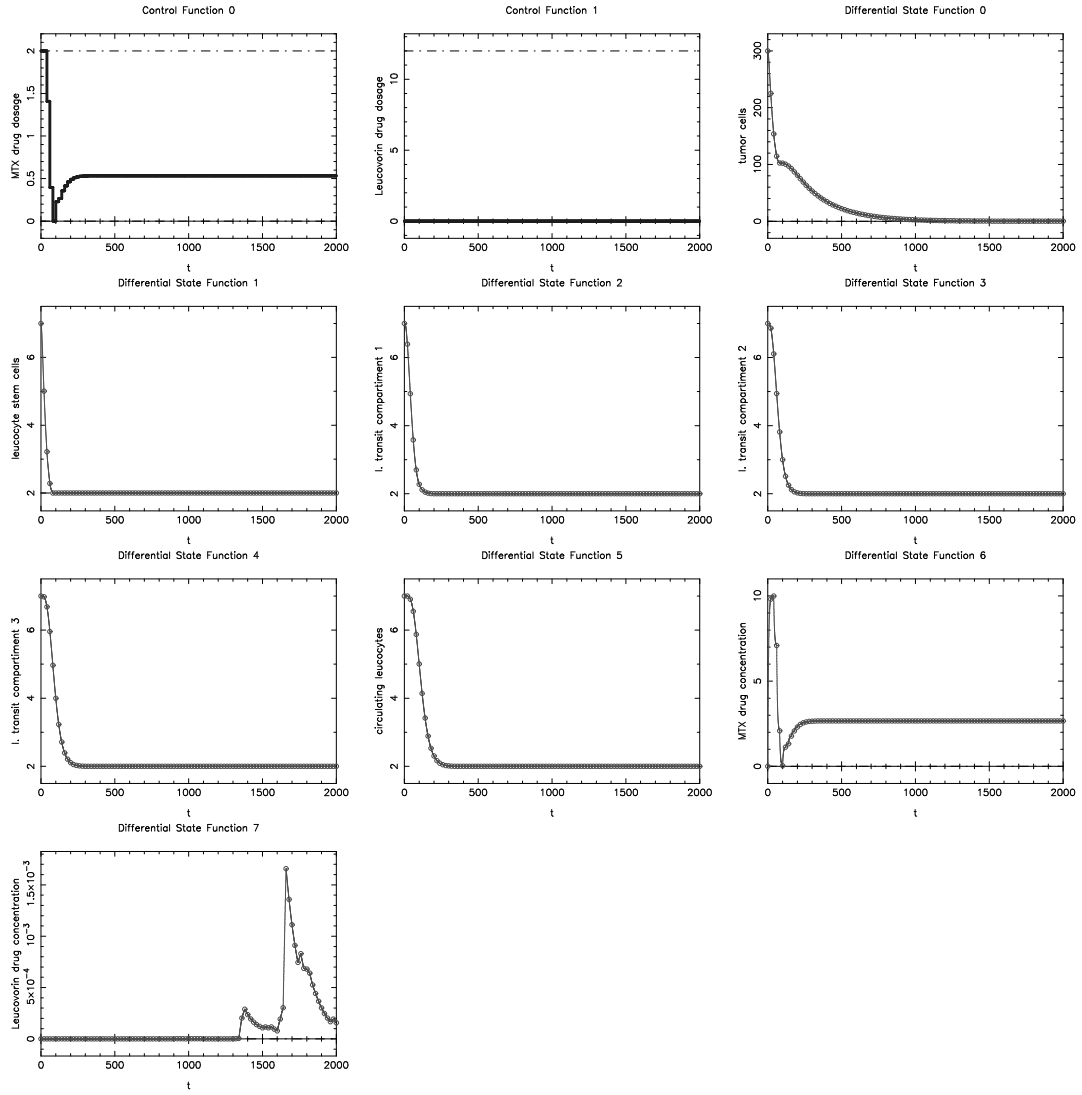
Figure 5.53: Optimal control result for *AG Lebiedz* model with $x_1(t) \geq 2.0$, $u_0(t) \leq 2.0$.
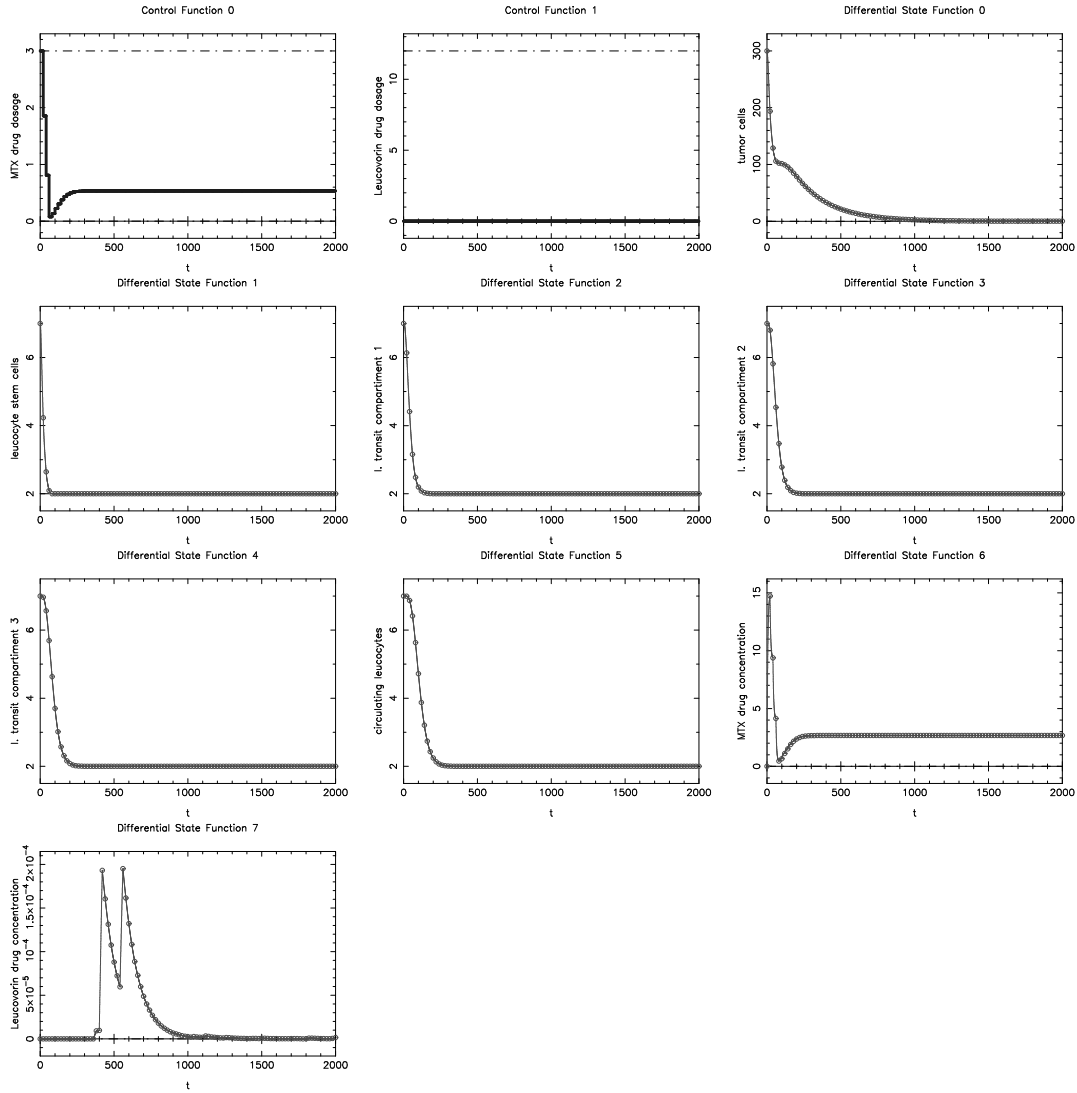
Figure 5.54: Optimal control result for *AG Lebiedz* model with $x_1(t) \geq 2.0$, $u_0(t) \leq 3.0$.
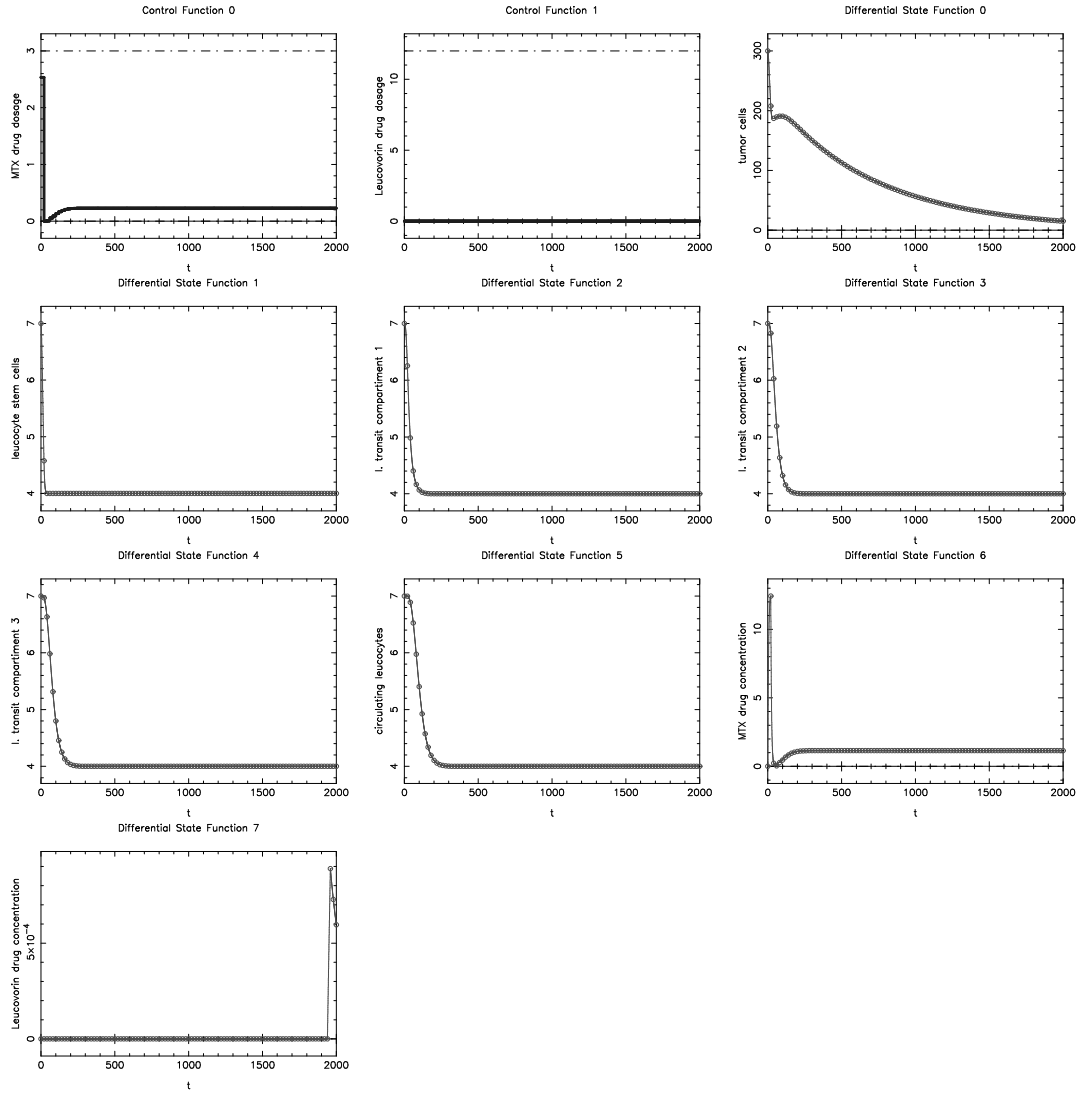
Figure 5.55: Optimal control result for *AG Lebiedz* model with $x_1(t) \geq 4.0$, $u_0(t) \leq 3.0$.
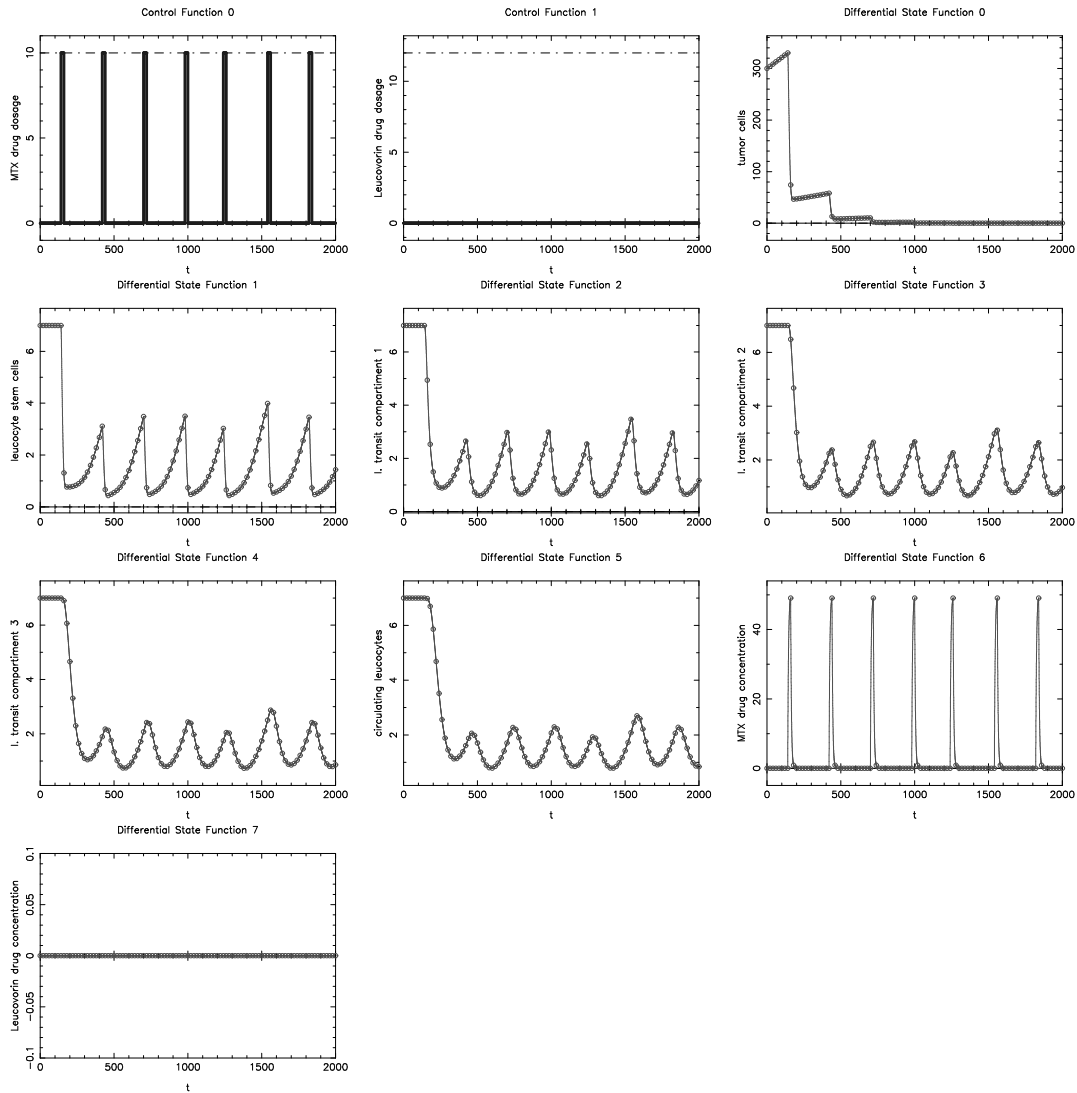
Figure 5.56: Sum up rounding result for *AG Lebiedz* model for original continuous control without additional bounds.
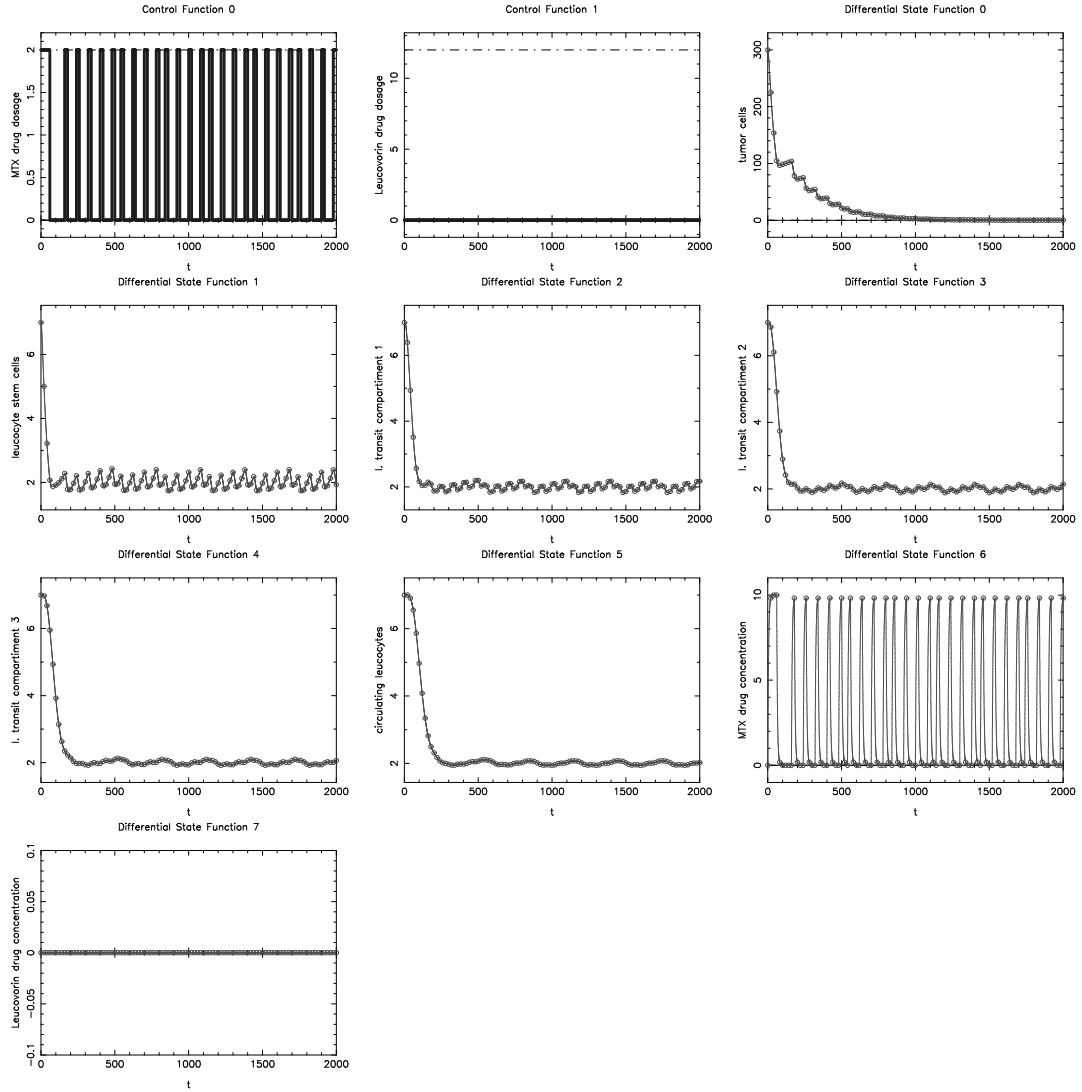
Figure 5.57: Sum up rounding result for *AG Lebiedz* model for original continuous control with $x_1(t) \geq 2.0$, $u_0(t) \leq 2.0$.
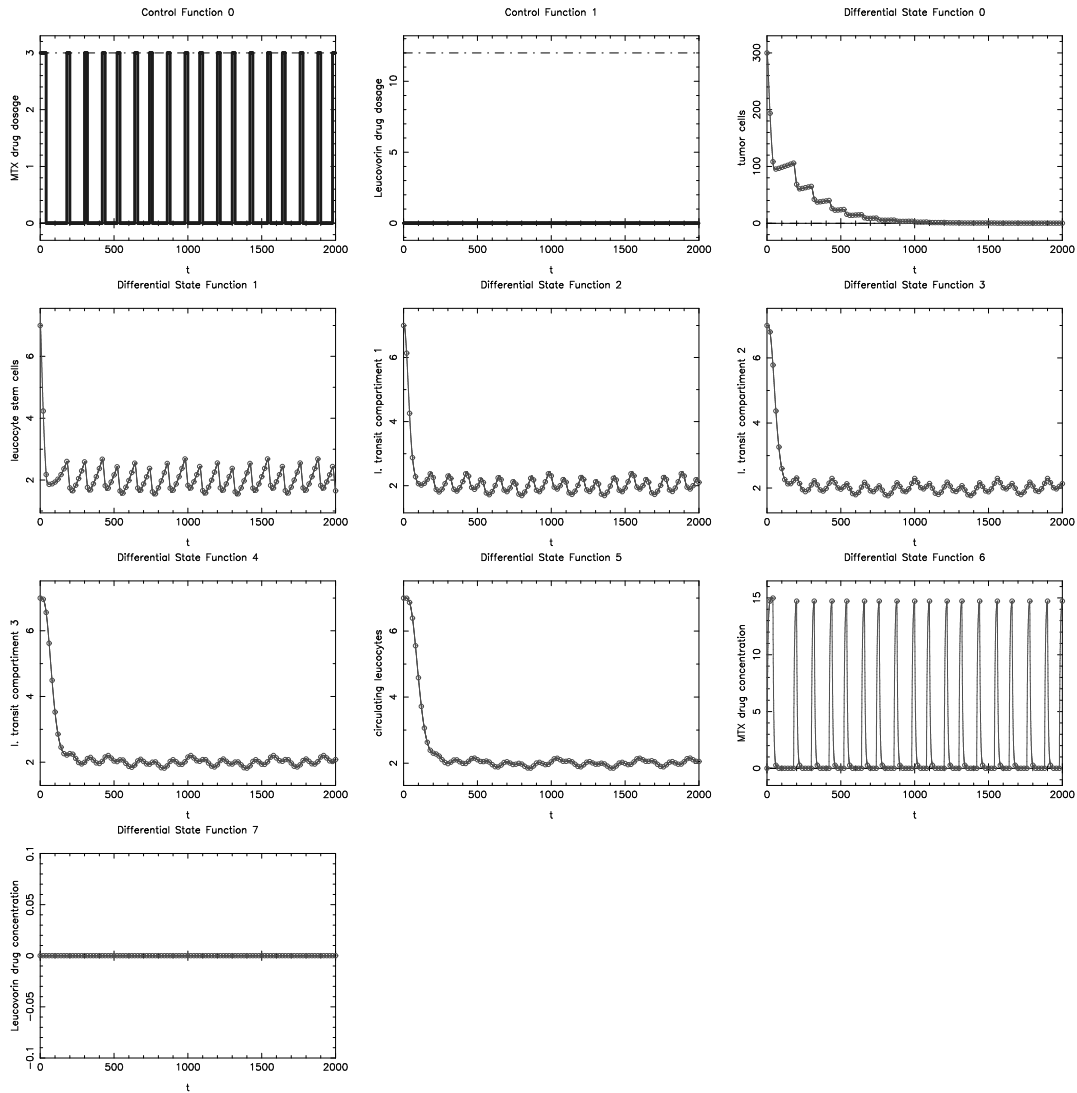
Figure 5.58: Sum up rounding result for *AG Lebiedz* model for original continuous control with $x_1(t) \geq 2.0$, $u_0(t) \leq 3.0$.
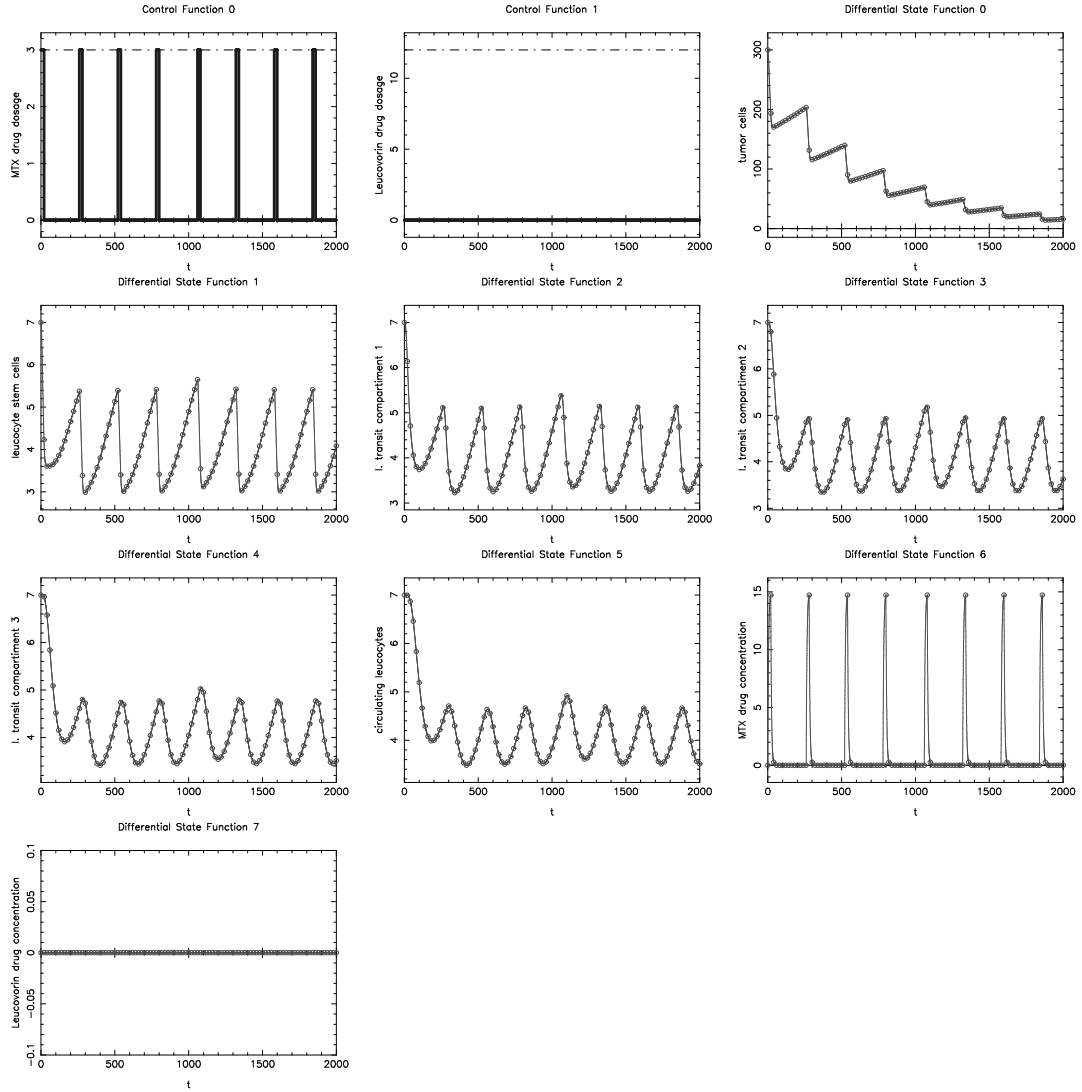
Figure 5.59: Sum up rounding result for *AG Lebiedz* model for original continuous control with $x_1(t) \geq 4.0$, $u_0(t) \leq 3.0$.
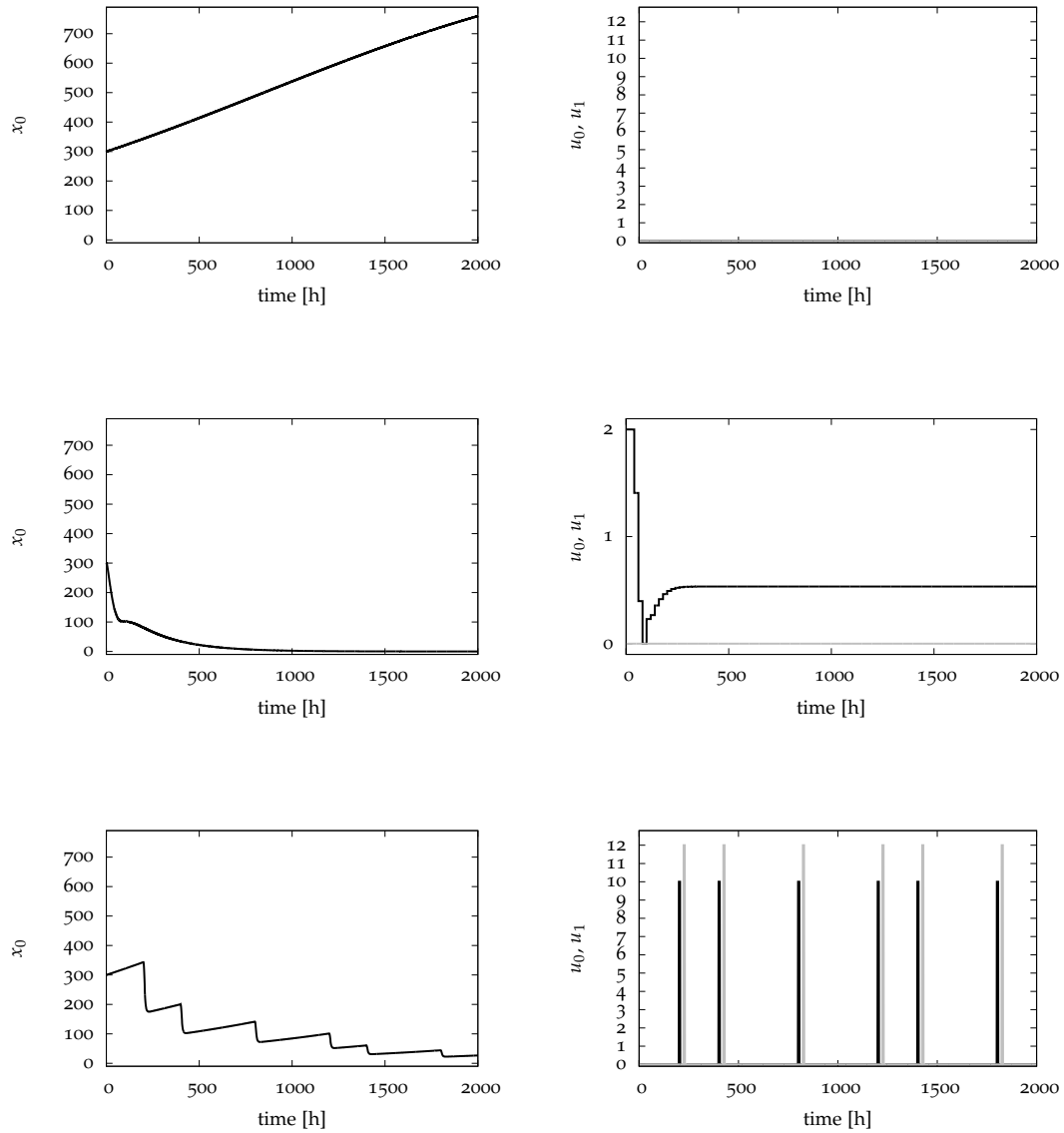
Figure 5.60: Comparison between no therapy, optimal control and standard treatment of *AG Lebiedz* model. Top: no treatment, middle: optimal controlled treatment for $x_1(t) \geq 2.0$ and $u_0(t) \leq 2.0$, bottom: standard treatment. Tumor volume is shown on the left side, chemotherapy (dark) and rescue package (bright) on the right side.

5.8 AG Lebiedz Fitted

This parameter set is based on real human proband data, but there are still parameters which—until the completion of this work—could not be fitted due to a lack of data. Additionally, as already mentioned in the section above, a bound on the leucocyte stem cells for the measurement of the patient's health is required, but reasonable values for this bound have not yet been known and initial values were not available either. Although this model may be one of the most promising approaches, with this enormous lack of required data, applying optimal control techniques to partly fitted and partly guessed values does not seem to make any sense. Therefore, we cannot present optimal control results for this parameter set so far.

Chapter 6

Conclusion and Outlook

In this final chapter, we summarize the results of this work and give an outlook on possible directions of future work.

Cancer Chemotherapy Models

We presented five models for cancer chemotherapy with eight different parameter sets. Four of these sets have been solved to optimality for the first time to the best of our knowledge.

The first model was the one of *Hahnfeldt et al.* [24] with two states, tumor volume and vasculature volume. It featured different *anti-angiogenic* treatments with one control for the dosage and a parameter set dervied by experiments with *Lewis lung carcinoma* in mice. Kind of a descendant of this model was the one in *d'Onofrio et al.* [17], which is based on a modification of the *Hahnfeldt* model by *d'Onofrio and Gandolfi*. This model contained an additional control for *chemotherapy* and identified dosage and drug concentration. Parameters have been taken from [24], while the tumor growth parameter has been adjusted erroneously and missing parameters are mainly test values for the numerical computations. An optimal control problem with free end time has been formulated and solved with different initial values and parameters in the article.

In the next part, we introduced a model by *de Pillis et al.* [10] which was based on multiple previous articles of the same or similar authors. In contrast to the first two models, this one contained three immune cell populations instead of the vasculature: *NK cells*, *CD8+ T cells* and *circulating lymphocytes*. Accordingly, it contained two immunotherapeutic treatments, *Interleukin-2* (*IL-2*) and *tumor infiltrating lymphocytes* (*TIL*), which formed the three controls together with *chemotherapy*. With tumor population and drug concentrations for chemotherapy and IL-2, the model had up to 6 states. Three parameter sets for this model, *mouse*, *human 9*, and *human 10*, were presented. They were based on different experimental works with different types of cancer. Especially, for the *human* sets, there was only one reference with human data so that about one third of the parameter values came from *murine* experiments. Therefore the model served for more or less general qualitative investigations. Many different scenarios with different therapies were tested by the authors, whereas optimal control has not been done for the model until now.

For a derived model however, optimal control was done by *de Pillis et al.* [9]. This model also was described and the differences to the previous model were highlighted. There were six states and three controls as in the model above. This work already contained three different optimal control problems with two different initial value sets.

Finally, we presented a model of our cooperation partners *Lebiedz et al.* which was based on human data for *non-hodgkin lymphoma of CNS*. This model contained leucocyte dynamics based on work by *Friberg et al.* [22] with states for *leucocyte stem cells*, *circulating leucocytes*, and three *transit compartments*. Together with a tumor state and two states for drug concentrations,

it had a total of eight states. The dosages of the two drugs applied, *Methotrexat* (*MTX*) as chemotherapy and *Leucovorin* as immunotherapy, were the two controls. We presented two parameter sets: one with test values and one with fitted values from experimental data, though not all parameters could be fitted until the completion of this work. As this model has not been published yet, optimal control was not done before.

Optimal Control Methods

In the next two chapters, we explained the optimal control methods which were applied to the different cancer chemotherapy models. *Direct multiple shooting* by *Bock and Plitt* [6] was applied to solve optimal control problems with continuous controls. We formulated the abstract problem class and discretized the infinite-dimensional problem in states and controls with *multiple shooting*. The resulting *nonlinear programming problem* was solved with a *structured SQP* method. The software package `MUSCOD-II`, which contains these methods, was used in this work.

We gave a motivation for the application of mixed-integer optimal control methods to the models. Continuous optimal controls with singular arcs might be unsuitable for treatments in medical practice. The *outer convexification* approach by *Sager et al.* [39] was explained and the *MS MINTOC* algorithm with *grid adaptivity*, *sum up rounding* and *switching-time optimization* was described.

With the *decomposed MILP* respectively *integral approximation*, we introduced a new rounding heuristic where a *mixed-integer linear program* with a limit on the number of switches is solved to approximate the continuous control. This algorithm was implemented in the `MUSCOD-II` framework and applied to some of the models as a part of this work.

Our results can be considered as a proof of concept: the methods work for all presented models and parameter sets. When medical understanding yields better models, optimization methods will be ready for optimal control of them.

Numerical Results

We reproduced different results of *Hahnfeldt et al.* by simulations with our implementation of the model in `MUSCOD-II`. Our optimal control solutions of the *d'Onofrio* model mostly matched the ones in the article. Though there was a difference in the end time up to 10.8%. As all results mainly consist of singular arcs, *sum up rounding* and *decomposed MILP* were applied to one of the four scenarios. The *sum up rounding* tumor value was very close to the continuous one, but the solution showed some *chattering*, which made it not that much more useful than the continuous singular solution. For *decomposed MILP*, we limited the number of switches to 4, 6, and 8 while the 6 switches result was higher than the 4 and 8 switches ones and in general the results were about 10% higher than the continuous ones. A comparison to a (continuous) maximization of the tumor at the end time with fixed drug amounts showed that we gained about 15% with the optimal control whereas without any treatment, the tumor would have been about 40% bigger.

For the different parameter sets *mouse*, *human 9*, and *human 10* for the model by *de Pillis et al.*, we introduced three different objective functions: tumor population at the end time, additionally with a penalty on chemotherapy, and a weighted sum of the tumor population over the whole time, at the end time and a penalty on the chemotherapeutic control. Three time horizons ($t_f = 40$, $t_f = 120$, and t_f free) together with 7 initial value sets were considered.

The many different scenarios showed many different continuous optimal control structures. However, in the *human* models immunotherapy was never used significantly. We showed that in this model, immunotherapy has almost no influence. So we could not reproduce the results with immunotherapy of *de Pillis et al.*, whereas the scenarios with pure chemotherapy or no therapy at all could be verified.

Sum up rounding was applied to the different scenarios and for the ones which almost had a bang-bang structure the results were obvious. A part of the singular solutions resulted in a rounded result with *chattering*. We also applied *decomposed MILP* with a maximum of 4, 6, and 8 switches to some problems. On the short time scale, the results looked good with an acceptable deviation from the continuous optimal control. For the long scale, the number of switches may have been too low though the calculation times even for an 8 switches solution would have been several hours, so this has not been tried. A maximization of the tumor population in some exemplary scenarios showed that the difference between minimal and maximal value can be some orders of magnitude. The performance of the standard treatments was always bad, however, the drug amounts were much lower. The authors of the article stated that *circulating lymphocytes* can be considered a measure for the health of the patient, but a bound was not given as well as reasons for the dosages chosen for the controls. Such values would be necessary for the computation of useful optimal controls.

The results of the optimal control paper [9] by *de Pillis et al.* could not be reproduced with the equations and the parameter set given in the article. However, with a modified tumor growth parameter (4.0 instead of $2.0 \cdot 10^{-3}$) we succeeded in the reproduction of the optimal controls result of a first scenario. For a second scenario, we could mostly reproduce the result with again a different tumor growth parameter (2.0). Our attempts to contact the authors to resolve these deviations have not been successful until now. Therefore no further optimal control computations were done with this model.

Eventually, we presented optimal controls for the model by *Lebiedz et al.* Only the test parameter set was considered since the fitted set still contains some unfitted parameters and initial values were not available. This could be an interesting point for future investigations. Again, a state is said to be a measure for the health of the patient but no reasonable bound was known. We tested two different lower bounds with two maximal dosages for chemotherapy. The optimal controls did not significantly contain the rescue package, but we showed that it has an observable influence in this model. In future work it could be interesting to try different objectives, e.g. like proposed by *Chareyron and Alamir* [8]. *Sum up rounding* was applied to this model, too, and because of the low level constant treatments in the optimal controls and the long time scale the solutions looked practicable.

Outlook

We showed that with our methods optimal control can be successfully done for several existing models. In particular, we presented mixed-integer algorithms for computing therapies which may be applicable in medical practice. The results look promising for improvements of real treatments in future.

However, there is only little data for parameter sets particularly for human models, but there is a partly big variation from cancer type to cancer type and even from patient to patient. Therefore, our current solutions are of no practical relevance for medical applications, but show what could be possible. It seems that a lot more cooperation between mathematicians, biologists and physicians will be needed to fill this gap and to bring optimal control

techniques into medical practice. The model by *Lebiedz et al.* could be a first step in this direction.

Bibliography

[1] COIN-OR homepage. http://www.coin-or.org/.

[2] Cbc homepage. http://projects.coin-or.org/Cbc.

[3] A. Abbas, A. Lichtman, and S. Pillai. *Cellular and Molecular Immunology*. Elsevier Saunders, 2007.

[4] K. Abhishek, S. Leyffer, and J. Linderoth. Filmint: An outer-approximation-based solver for nonlinear mixed integer programs. Preprint ANL/MCS-P1374-0906, Argonne National Laboratory, Mathematics and Computer Science Division, September 2006.

[5] I. Bauer. *Numerische Verfahren zur Lösung von Anfangswertaufgaben und zur Generierung von ersten und zweiten Ableitungen mit Anwendungen bei Optimierungsaufgaben in Chemie und Verfahrenstechnik*. PhD thesis, Universität Heidelberg, 1999.

[6] H. G. Bock and K. Plitt. A multiple shooting algorithm for direct solution of optimal control problems. In *Proceedings 9th IFAC World Congress Budapest*, pages 243–247. Pergamon Press, 1984. Available at http://www.iwr.uni-heidelberg.de/groups/agbock/FILES/Bock1984.pdf.

[7] P. Bonami, L. Biegler, A. Conn, G. Cornuéjols, I. Grossmann, C. Laird, J. Lee, A. Lodi, F. Margot, N. Sawaya, and A. Wächter. An algorithmic framework for convex mixed integer nonlinear programs. *Discrete Optimization*, 5(2):186–204, 2009. (in press).

[8] S. Chareyron and M. Alamir. Mixed immunotherapy and chemotherapy of tumors: Feedback design and model updating schemes. *Journal of Theoretical Biology*, 45:1052–1057, 2009.

[9] L. de Pillis, K. Fister, W. Gu, T. Head, K. Maples, T. Neal, A. Murugan, and K. Kozai. Optimal control of mixed immunotherapy and chemotherapy of tumors. *Journal of Biological Systems*, 16(1):51–80, 2008.

[10] L. de Pillis, W. Gu, and A. Radunskaya. Mixed immunotherapy and chemotherapy of tumors: modeling, applications and biological interpretations. *Journal of Theoretical Biology*, 238(4):841–862, 2006.

[11] L. de Pillis and A. Radunskaya. A mathematical tumor model with immune resistance and drug therapy: an optimal control approach. *Journal of Theoretical Medicine*, 3:79–100, 2001.

[12] L. de Pillis and A. Radunskaya. The dynamics of an optimally controlled tumor model: A case study. *Mathematical and Computer Modelling*, 37:1221–1244, 2003.

[13] L. G. de Pillis, A. E. Radunskaya, and C. L. Wiseman. A validated mathematical model of cell-mediated immune response to tumor growth. *Cancer Research*, 65:7950–7958, 2005.

[14] A. Diefenbach, E. R. Jensen, A. M. Jamieson, and D. H. Raulet. Rae1 and H60 ligands of the NKG2D receptor stimulate tumour immunity. *Nature*, 413:165–171, 2001.

[15] A. d'Onofrio and A. Gandolfi. Tumour eradication by antiangiogenic therapy: analysis and extensions of the model by Hahnfeldt et al. *Mathematical Biosciences*, 191:159–184, 2004.

[16] A. d'Onofrio and A. Gandolfi. The response to antiangiogenic anticancer drugs that inhibit endothelial cell proliferation. *Applied Mathematics and Computation*, 181:1155–1162, 2006.

[17] A. d'Onofrio, U. Ledzewicz, H. Maurer, and H. Schaettler. On optimal delivery of combination therapy for tumors. *Mathematical Biosciences*, (in press), 2009.

[18] M. E. Dudley, J. R. Wunderlich, P. F. Robbins, J. C. Yang, P. Hwu, D. J. Schwartzentruber, S. L. Topalian, R. Sherry, N. P. Restifo, A. M. Hubicki, M. R. Robinson, M. Raffeld, P. Duray, C. A. Seipp, L. Rogers-Freezer, K. E. Morton, S. A. Mavroukakis, D. E. White, and S. A. Rosenberg. Cancer regression and autoimmunity in patients after clonal repopulation with antitumor lymphocytes. *Science*, 298:850–854, 2002.

[19] A. Ergun, K. Camphausen, and L. M. Wein. Optimal scheduling of radiotherapy and angiogenic inhibitors. *Bulletin of Mathematical Biology*, 65:407–424, 2003.

[20] J. Folkman. Anti-angiogenesis: New concept for therapy of solid tumors. *Annals of Surgery*, 175:409–416, 1972.

[21] R. Fourer, D. Gay, and B. Kernighan. *AMPL: A Modeling Language for Mathematical Programming*. Duxbury Press, 2002.

[22] L. Friberg, A. Henningsson, H. Maas, L. Nguyen, and M. Karlsson. Model of chemotherapy-induced myelosuppression with parameter consistency across drugs. *Journal of Clinical Oncology*, 20:4713–4721, 2002.

[23] M. Gerdts. Solving mixed-integer optimal control problems by Branch&Bound: A case study from automobile test-driving with gear shift. *Optimal Control Applications and Methods*, 26:1–18, 2005.

[24] P. Hahnfeldt, D. Panigraphy, J. Folkman, and L. Hlatky. Tumor development under angiogenic signaling: A dynamical theory of tumor growth, treatment response, and postvascular dormancy. *Cancer Research*, 59:4770 – 4775, 1999.

[25] O. Isaeva and V. Osipov. Different strategies for cancer treatment: mathematical modeling. *arXiv.org*, 2006. Available at http://arxiv.org/abs/q-bio/0506006v4.

[26] C. Kirches, S. Sager, H. G. Bock, and J. P. Schlöder. Time-optimal control of automobile test drives with gear shifts. *Optimal Control Applications and Methods*, 30(5), September/October 2009. DOI 10.1002/oca.892.

[27] D. Kirschner and J. C. Panetta. Modeling immunotherapy of the tumor - immune interaction. *Journal of Mathematical Biology*, 37:235–252, 1998.

[28] V. A. Kuznetsov, I. A. Makalkin, M. A. Taylor, and A. S. Perelson. Nonlinear dynamics of immunogenic tumors: Parameter estimation and global bifurcation analysis. *Bulletin of Mathematical Biology*, 56:295–321, 1994.

[29] U. Ledzewicz, J. Marriott, H. Maurer, and H. Schättler. Realizable protocols for optimal administration of drugs in mathematical models for novel cancer treatments. *Journal of Medical Informatics and Technologies*, 2008.

[30] D. Leineweber. *Efficient reduced SQP methods for the optimization of chemical processes described by large sparse DAE models*, volume 613 of *Fortschritt-Berichte VDI Reihe 3, Verfahrenstechnik*. VDI Verlag, Düsseldorf, 1999.

[31] F. Lévi and U. Schibler. Circadian rhythms: Mechanisms and therapeutic implications. *Annual Review of Pharmacology and Toxicology*, 47:593–628, 2007.

[32] A. Martin, M. Möller, and S. Moritz. Mixed integer models for the stationary case of gas network optimization. *Mathematical Programming*, 105:563–582, 2006.

[33] J. Nocedal and S. Wright. *Numerical Optimization*. Springer Verlag, Berlin Heidelberg New York, 2nd edition, 2006. ISBN 0-387-30303-0.

[34] M. Powell. A fast algorithm for nonlinearly constrained optimization calculations. In G. Watson, editor, *Numerical Analysis, Dundee 1977*, volume 630 of *Lecture Notes in Mathematics*, Berlin, 1978. Springer.

[35] S. Sager. MIOCP benchmark site. http://mintoc.de.

[36] S. Sager. *Numerical methods for mixed–integer optimal control problems*. Der andere Verlag, Tönning, Lübeck, Marburg, 2005. ISBN 3-89959-416-9. Available at http://sager1.de/sebastian/downloads/Sager2005.pdf.

[37] S. Sager. Reformulations and algorithms for the optimization of switching decisions in nonlinear optimal control. *Journal of Process Control*, 2009. DOI 10.1016/j.jprocont.2009.03.008.

[38] S. Sager, C. Kirches, and H. G. Bock. Fast solution of periodic optimal control problems in automobile test-driving with gear shifts. In *Proceedings of the 47th IEEE Conference on Decision and Control (CDC 2008), Cancun, Mexico*, pages 1563–1568, 2008. ISBN: 978-1-4244-3124-3.

[39] S. Sager, G. Reinelt, and H. G. Bock. Direct methods with maximal lower bound for mixed-integer optimal control problems. *Mathematical Programming*, 118(1):109–149, 2009.

[40] J. Till, S. Engell, S. Panek, and O. Stursberg. Applied hybrid system optimization: An empirical investigation of complexity. *Control Engineering Practice*, 12:1291–1303, 2004.

[41] R. Wilson. *A simplicial algorithm for concave programming*. PhD thesis, Harvard University, 1963.

[42] M. Zelikin and V. Borisov. *Theory of chattering control with applications to astronautics, robotics, economics and engineering*. Birkhäuser, Basel Boston Berlin, 1994.

[43] J. Zhang, K. Johansson, J. Lygeros, and S. Sastry. Zeno hybrid systems. *International Journal of Robust and Nonlinear Control*, 11:435–451, 2001.

List of Figures

List of Tables

Index

Erklärung

Hiermit versichere ich, dass ich meine Arbeit selbständig unter Anleitung verfasst habe, dass ich keine anderen als die angegebenen Quellen und Hilfsmittel benutzt habe, und dass ich alle Stellen, die dem Wortlaut oder dem Sinne nach anderen Werken entlehnt sind, durch die Angabe der Quellen als Entlehnungen kenntlich gemacht habe.

Heidelberg, den 10. September 2009.